Guided Spontaneous-Emission Circuit Technique with Improved Optical Power Resolution

Doctor of Philosophy in Engineering

By

MD GOLAM BARKATUL ABRAR

Principal Supervisor:

Professor Dr. Hiroji Masuda

Assistant Supervisors:

Professor Dr. Yasuhisa Fujita

Professor Dr. Hiroyuki Kageshima

Associate Professor Dr. Toshiyuki Yoshida

Assistant Professor Dr. Kokoro Kitamura

Graduate School of Natural Science and Technology

Shimane University, Japan

March 2026

Acknowledgments

First of all, I would like to sincerely extend my appreciation to my beloved supervisor, Professor Dr. Hiroji Masuda, for the opportunities he gave me for this study. I truly could not have asked for a better mentor. I extend my cordial thanks for his guidance, support, and belief in me shaped not only this research but the person I have become through it. His invaluable insights, constructive feedback, and unrelenting encouragement have been crucial in developing and enhancing the quality and integrity of this thesis. I would also like to express my heartfelt gratitude to my co-supervisor, Assistant Professor Dr. Kokoro Kitamura, for her valuable time, insight, and encouragement.

I would like to express my gratitude to all co-authors for their valuable time, experience, and willingness to share their insights into this study. Their contributions were crucial in collecting the necessary data and achieving the objectives of this study.

I express my deep gratitude for the valuable financial support provided by JSPS KAKENHI Grant-in-Aid for Scientific Research 19K004410, 22K04140, and JST (Japan Science and Technology). Without their financial assistance, this research could not have been conducted.

Finally, I will be forever grateful for the love and support of my friends, family, and those who stood by me through this long and challenging road. Their steadfast love, patience, and understanding have laid the foundations of my academic career. Their constant support has given me the strength to overcome obstacles and achieve this success. In conclusion, I express my deep gratitude to Professor Dr. Hiroji Masuda and all members for their invaluable suggestions and help.

ABRAR MD GOLAM BARKATUL

List of Figures

1. Introduction

Figure 1.1 System Configuration

2. Guided Spontaneous-Emission Circuit

Figure 2.1 Name and classification of proposal method

Figure 2.2 Basic system configuration for optical detection

Figure 2.3 EDF propagated and spontaneously emitted light

Figure 2.4 Basic configuration of Guided Spontaneous-Emission Circuit

Figure 2.5 Output power vs. input power (Conventional techniques with Optical Amplifier

Figure 2.6 Output power vs. input power (Conventional techniques with Guided Spontaneous-Emission Circuit

3. Improved Optical Performance Evaluation Based on Numerical Simulation of Guided Spontaneous-Emission Circuit

Figure 3.1 Schematics of the (a) experimental setup and configurations of (b) single-stage GSEC (c) dual-stage GSEC

Figure 3.2 Characteristics of the GSEC with 15.9-m EDF in forward pumping (a) GSE power and (b) slope spectra

Figure 3.3 Characteristics of the GSEC with 15.9-m EDF in forward pumping (a) output power and (b) slope as a function of the input power

Figure 3.4 Characteristics of the GSEC with 15.9-m EDF in forward pumping (a) input power and (b) slope as a function of the output power for three-times measurements

Figure 3.5 Characteristics of the GSEC with 15.9-m EDF in backward pumping (a) GSE power and (b) slope spectra, (c) output powers, and (d) slope as a function of the input power

Figure 3.6 Characteristics of the GSEC with 20.4-m EDF in (a) forward (b) backward pumping

Figure 3.7 Characteristics of the dual-stage GSEC (a) GSE power and (b) slope spectra, (c) output powers, and (d) slope as a function of input power

Figure 3.8 Characteristics of the dual-stage GSEC without the short-wavelength pass Filter (a) GSE spectra and (b) slope as a function of input power

4. Performance Evaluation Based on Numerical Simulation of Guided Spontaneous-Emission Circuit

Figure 4.1 Schematic configuration of (a) measurement system and GSEC with (b) forward (c) backward pumping

Figure 4.2 Characteristics of GSEC with forward pumping (a) output power and (b) slope spectra

Figure 4.3 Input/output power characteristics of GSEC with forward pumping (a) output optical power and (b) slope according to input optical power

Figure 4.4 Characteristic of GSEC with backward pumping (a) output power and (b) slope spectra

Figure 4.5 Input/output power characteristics of GSEC with backward pumping (a) output optical power and (b) slope according to input optical power

Figure 4.6 Mode Field Diameter dependence results at wavelengths of (a) 1533, (b) 1540 nm for forward pumping. The figures in the left and right columns show the output powers and slopes according to input optical power

Figure 4.7 Mode Field Diameter dependence results at wavelengths of (a) 1550, (b) 1560 nm for forward pumping. The figures in the left and right columns show the output powers and slopes according to input optical power

5. High-Resolution Optical Power Variation Measurement to Improve the Optical Power Resolution of the Guided Spontaneous-Emission Circuit Techniques

Figure 5.1 (a) System configuration of the GSEC technique (b) basic configuration of the multistage GSEC

Figure 5.2 Schematics of the experimental setup (a) The measurement system, (b) single-stage GSEC, (c) two-stage GSEC, and (d) emulator

Figure 5.3 Input-output characteristics of the SS-GSEC with a 15.9-m EDF at the output wavelengths of 1532.5, 1540, 1550, and 1560 nm, (a) Input powers and (b) slopes as a function of the output power

Figure 5.4 (a) Input powers and (b) slope as a function of the output power for TS-3 and -4

Figure 5.5 Output powers of the pump as a function of the input power

Figure 5.6 Output spectra at Points F, G, B, and C of TS-4 in (a), (b), (c), and (d), respectively. (e) Output spectra at operating point P3, and (f) detailed parts of (e) around 1532.5 nm

Figure 5.7 (a) Variations in the output power from the emulator (ΔPe) as a function of the loss of VOA-E (L), and (b) the measured power variation (ΔPe-m) as a function of the calculated power variation (ΔPe-c)

6. Investigation of the Guided Spontaneous-Emission Circuit Using Numerical Simulation

Figure 6.1 Basic configuration of guided spontaneous emission optical circuits (a) single-stage EDF configuration (b) dual-stage configuration

Figure 6.2 Input/output optical power characteristics at λ_{out} = 1560 nm and λ_{in} = (a) 1470 nm, (b) 1480 nm. The figures in the left and right columns show the output powers and slopes according to the input optical power

Figure 6.3 Input/output optical power characteristics at λ_{out} = 1560 nm and λ_{in} = (a) 1490 nm, (b) 1510 nm, and (c) 1520 nm. The figures in the left and right columns show the output powers and slopes according to the input optical power

Figure 6.4 Input/output optical power characteristics at λ_{out} = 1560 nm and λ_{in} = (a) 1530 nm, (b) 1540 nm, and (c) 1550 nm. The figures in the left and right columns show the output powers and slopes according to the input optical power

Figure 6.5 Input/output optical power characteristics at λ_{out} = 1565 nm and λ_{in} = (a) 1470 nm, (b) 1480 nm. The figures in the left and right columns show the output powers and slopes according to the input optical power

Figure 6.6 Input/output optical power characteristics at λ_{out} = 1565 nm and λ_{in} = (a) 1490 nm, (b) 1510 nm, and (c) 1520 nm. The figures in the left and right columns show the output powers and slopes according to the input optical power

Figure 6.7 Input/output optical power characteristics at λ_{out} = 1565 nm and λ_{in} = (a) 1530 nm, (b) 1540 nm, and (c) 1550 nm. The figures in the left and right columns show the output powers and slopes according to the input optical power

Figure 6.8 Peak loss dependence of maximum slope condition (a) λ_{out} = 1560 nm (b) λ_{out} = 1565 nm

Figure 6.9 Peak loss dependence on input wavelength under the maximum slope condition (a) λ_{out} = 1560 nm (b) λ_{out} = 1565 nm

7. Pumping Direction Dependence in Guided Spontaneous-Emission Circuit

Figure 7.1 Schematics of experimental setup for (a) the forward pumping and (b) backward pumping

Figure 7.2 Input and output characteristics of the GSEC with 15.9-m EDF in the forward pumping configuration. (a) GSE power and (b) slope spectra, (c) input and output power characteristics, and (d) slope characteristics

Figure 7.3 Input and output characteristics of the GSEC with 15.9-m EDF in the backward pumping configuration. (a) GSE power and (b) slope spectra, (c) input and output power characteristics, and (d) slope characteristics

Figure 7.4 Calculated input and output characteristics at the peak loss of (a) 50, (b) 150, and (c) 200 dB for the forward pumping. Left and right-side figures show the output powers and slopes as a function of the input power

Figure 7.5 Calculated input and output characteristics at the peak loss of (a) 50, (b) 150, and (c) 200 dB for the backward pumping. Left and right-side figures show the output powers and slopes as a function of the input power

Figure 7.6 Calculated input and output characteristics at the peak loss of (a) 50, (b) 150, and (c) 200 dB for the backward pumping. Left and right-side figures show the output powers and slopes as a function of the input power

8. Application of Multicore-Fiber Sensing in Amplified Spontaneous Emission Feedback Circuit

Figure 8.1 System Configuration

Figure 8.2 Experimental Setup

Figure 8.3 (a) The input power and (b) the slope as a function of the output power

List of Publications

Journal Articles

As the Co-author

[1] Kokoro Kitamura, **Md Golam Barkatul Abrar**, Kunihiro Tanaka, Ryuga Harada, and Hiroji Masuda, "Guided spontaneous emission circuit technique with improved optical power resolutions for optical power variation measurement", **IEICE Electronics Express** (**2025**), Vol.22, No.10, p.1-6. https://doi.org/10.1587/elex.22.20250155.

[2] Hiroji Masuda, Yudai Takenouchi, Eiki Ueno, Yusuke Dokan, Seiji Uchida, and **Md Golam Barkatul Abrar**, "Dynamic guided spontaneous-emission circuit technique with an SNR enhancement factor of 22.5 dB for optical power variation measurement", **IEICE Electronics Express** (**2025**), Vol.22, No.24, p.1-6. https://doi.org/10.1587/elex.22.20250598.

[3] Biswajit Biswas, **MD Golam Barkatul Abrar**, Kunihiro Tanaka, Ryuga Harada, Kokoro Kitamura, and Hiroji Masuda, "High-resolution and Stable optical power measurement using a temperature controlled amplified-spontaneous-emission feedback circuit", **IEICE Communications Express** (**2023**), Vol. 12, No. 5, pp. 230-235. https://doi.org/10.1587/comex.2023XBL0014.

[4] Biswajit Biswas, **MD Golam Barkatul Abrar**, Kunihiro Tanaka, Ryuga Harada, Kokoro Kitamura, and Hiroji Masuda, "Amplified-spontaneous-emission feedback circuit with wide operating bandwidth and dynamic range", **IEICE Electronics Express** (**2023**), Vol. 20, No. 17, pp. 1-6. https://doi.org/10.1587/elex.20.20230229.

Technical Report

As the Co-author

[1] Hiroji Masuda, **Md Golam Barkatul Abrar**, Kokoro Kitamura, and Ryuga Harada, "Design and Performance of an Amplified-Spontaneous-Emission Feedback Circuit for Fiber-Optic Temperature Sensing", **IEICE Tech. Rep**., vol. 122, no. 162, **OFT 2022-16**, pp. 50-55, **Aug. 2022**. https://ken.ieice.org/ken/paper/20220826AClL/eng/.

[2] Hiroji Masuda, **Md Golam Barkatul Abrar**, Kokoro Kitamura, and Ryuga Harada, "A study on the system configuration of an amplified-spontaneous emission nonlinear

circuit technique", **IEICE Tech. Rep**., vol. 122, no. 344, **OFT 2022-43**, pp. 1-6, **Jan. 2023 (in Japanese)**. https://ken.ieice.org/ken/paper/202301197CpQ/eng/.

[3] Kokoro Kitamura, **Md Golam Barkatul Abrar**, Kunihiro Tanaka, Ryuga Harada, and Hiroji Masuda, "Proposal of an optical input and output nonlinear circuit technique and investigation of the characteristics of improvements in the optical power resolution", **IEICE Tech. Rep**., vol. 123, no. 210, **OFT 2023-45**, pp. 115-118, **Oct. 2023 (in Japanese)**. https://ken.ieice.org/ken/paper/20231013ZCX5/eng/.

[4] Hiroji Masuda, **Md Golam Barkatul Abrar**, Kokoro Kitamura, and Ryuga Harada, "Temperature sensing technique using a guided-spontaneous-emission circuit in fiber-optic measurement systems", **IEICE Tech. Rep**., vol. 124, no. 15, **OFT 2024-7**, pp. 28-33, **May 2024 (in Japanese)**. https://ken.ieice.org/ken/paper/20240509Ic22/eng/.

[5] Hiroji Masuda, Kokoro Kitamura, Kunihiro Tanaka, **Md Golam Barkatul Abrar**, and Ryuga Harada, "Design and applications of an amplified-spontaneous-emission feedback circuit technique", **IEICE Tech. Rep**., vol. 123, no. 210, **OFT 2023-46**, pp. 192-122, **Oct. 2023 (in Japanese)**. https://ken.ieice.org/ken/paper/20231013oCXN/eng/

[6] Hiroji Masuda, Kokoro Kitamura, Kunihiro Tanaka, Md Golam Barkatul Abrar, and Ryuga Harada, "Design and applications of an amplified-spontaneous-emission feedback circuit technique", **IEICE Tech. Rep**., vol. 123, no. 210, **OFT 2023-46**, pp. 119-122, Oct. 2023 (in Japanese). https://ken.ieice.org/ken/paper/20231013oCXN/eng/.

[7] Hiroji Masuda, Kokoro Kitamura, **Md Golam Barkatul Abrar**, Kunihiro Tanaka, and Ryuga Harada, "Design of a guided spontaneous-emission type of the optical input-output nonlinear circuit technique", **IEICE Tech. Rep**., vol. 123, no. 244, **OFT 2023-50**, pp. 13-18, **Nov. 2023** (in Japanese). https://ken.ieice.org/ken/paper/20231109fCyc/eng.

[8] Hiroji Masuda, Ryuga Harada, Yudai Takenouchi, Kokoro Kitamura, Yuusuke Doukan, and **Md Golam Barkatul Abrar**, "Theory and applications of an optical input-output nonlinear circuit technique to enable improving the optical power resolution", IEICE

Tech. Rep., vol. 124, no. 238, **OFT 2024-73**, pp. 23-28, **Nov. 2024 (in Japanese)**. https://ken.ieice.org/ken/paper/20241108YcfV/eng/.

[9] Ryuga Harada, Hiroji Masuda, Yudai Takenouchi, Yusuke Dokan, **Md Golam Barkatul Abrar**, and Kokoro Kitamura, "Characteristics of improvements in the optical power resolution of an optical input and output nonlinear circuit", IEICE Tech. Rep., vol. 124, no. 238, **OFT 2024-72**, pp. 19-22, **Nov. 2024 (in Japanese)**. https://ken.ieice.org/ken/paper/20241108QcFT/eng/.

Conference Papers

As the first author.

[1] **Md Golam Barkatul Abrar,** Kokoro Kitamura, and Hiroji Masuda "Performance Evaluation Based on Numerical Simulation of Novel Guided Spontaneous Emission Circuit for Improved Optical Power Resolution", **IEEE ICCT-Pacific**, P2-4, **30 May 2025**), (**International conference with review**). 10.1109/ICCT-pacific63901.2025.11012822.

[2] **Md Golam Barkatul Abrar**, Kunihiro Tanaka, Ryuga Harada, Kokoro Kitamura, and Hiroji Masuda, "Pumping Direction Dependence of the performance of Amplified-Spontaneous-Emission Nonlinear Circuit", **HISS 2023**, TP-B-8, pp. 184-187, **Nov. 2023,** (**Domestic conference (symposium) with review**), (**HISS Excellent Research Award**).

[3] **Md Golam Barkatul Abrar,** Biswajit Biswas, Kunihiro Tanaka, Ryuga Harada, Kokoro Kitamura, and Hiroji Masuda, "Amplified-spontaneous-emission feedback circuit technique with high optical power resolutions for multicore-fiber sensing", 7th International Symposium on Extremely Advanced Transmission Technologies- **EXAT** (**2023**), P-27, (**International conference symposium with review**).

[4] **MD Golam Barkatul Abrar,** Hiroji Masuda, Kunihiro Tanaka, and Ryuga Harada, "Wavelength-division-multiplexing characteristics of an amplified-spontaneous-emission circuit technique for multipoint sensing applications", **IEICE Society Conference**, B-13-20 (**2022**).

[5] **MD Golam Barkatul Abrar,** Kunihiro Tanaka, Ryuga Harada, Biswajit Biswas, and Hiroji Masuda "Parameter Dependence of the Performance of an Amplified - Spontaneous Emission Feedback Circuit", **IEICE General Conference 2023**, B-13-17

As the Co-author.

[1] Kokoro Kitamura, **Md Golam Barkatul Abrar**, Kunihiro Tanaka, Ryuga Harada, and Hiroji Masuda, "Amplified-spontaneous-emission nonlinear circuit technique with improved optical power resolution", **ICETC (2023), O1-4**, **11 November 2023**, (**International conference symposium with review**). https://doi.org/10.34385/proc.79.O1-4.

[2] Kokoro Kitamura, **Md Golam Barkatul Abrar**, Ryuga Harada, Yuusuke Doukan, and Hiroji Masuda, "Erbium-doped Fiber Nonlinear Transmission Circuit Technique for Improving the Optical Power Resolution in Fiber-optic Measurements", **ICETC (2024)**, **O2-01**, **11 November 2024, (International conference symposium with review**). https://doi.org/10.34385/proc.85.O2-01.

[3] Kunihiro Tanaka, **MD Golam Barkatul Abrar**, Ryuga Harada, and Hiroji Masuda, "High resolution optical power measurement using an amplified-spontaneous-emission circuit", **IEICE General Conference**, B-13-15 (**2023**), **(In Japanese)**.

[4] Ryuga Harada, **MD Golam Barkatul Abrar**, Kunihiro Tanaka, and Hiroji Masuda, "Characteristics of the optical power spectra of an amplified-spontaneous-emission feedback circuit", **IEICE General Conference**, B-13-16 (**2023**) **(in Japanese)**.

[5] Kunihiro Tanaka, Hiroji Masuda, Ryuga Harada, and **MD Golam Barkatul Abrar**, "Amplified spontaneous emission optical circuit optimization in fiber optic temperature sensing applications", **IEICE Society Conference**, B-13-18 (**2022**) **(in Japanese)**.

[6] Ryuga Harada, Hiroji Masuda, Kunihiro Tanaka, and **MD Golam Barkatul Abrar**, "Characteristics of High Sensitivity Temperature Sensing Using Amplified Spontaneous-Emission Feedback", **IEICE Society Conference**, B-13-19 (**2022**) **(in Japanese)**.

[7] Ryuga Harada, Kunihiro Tanaka, **MD Golam Barkatul Abrar**, Hiroji Masuda, and Kokoro Kitamura, "A study on the configuration of an amplified-spontaneous-emission nonlinear circuit", **HISS 2023**, TP-B-7, pp. 181-183, **Nov. 2023 (in Japanese)**.

[8] Kunihiro Tanaka, Ryuga Harada, **MD Golam Barkatul Abrar**, Kokoro Kitamura, and Hiroji Masuda "Proposal and Simulation Characteristics of an Amplified Spontaneous Emission Nonlinear Circuit Method for High-Resolution Optical Power Measurement", **HISS 2023**, TP-A-7, pp. 27-30, **Nov. 2023 (in Japanese)**.

[9] Hiroji Masuda, Kunihiro Tanaka, Ryuga Harada, **MD Golam Barkatul Abrar**, Kokoro Kitamura, "Performance optimization of guided spontaneous emission optical circuit systems", **IEICE General Conference**, B-10A_B-13-02 (**2024**) **(in Japanese)**.

[10] Kunihiro Tanaka, Hiroji Masuda, Ryuga Harada, **MD Golam Barkatul Abrar**, and Kokoro Kitamura, "Design technology for guided spontaneous emission optical circuit systems", **IEICE General Conference**, B-10A_B-13-01(**2024**) **(in Japanese)**.

Abstract

Optical fiber sensing (OFS) has attracted considerable attention for a wide range of applications. These include industrial and environmental monitoring, long-distance transmission, and wide-area distributed sensing**.** Conventional optical power measurement approaches are often limited by gain saturation and nonlinear effects, which degrade measurement accuracy and stability. To overcome these limitations, this study proposes and investigates a novel nonlinear EDF-based optical circuit technique designed to significantly improve optical power resolution (OPR). The proposed circuit was previously referred to as the amplified-spontaneous-emission nonlinear circuit (ASENLC) and is hereafter referred to as the guided spontaneous- emission circuit (GSEC).

In recent years, a high OPR technique using an amplified spontaneous emission feedback circuit (ASEFC) has been reported to significantly improve OPR. ASEFC is a feedback fiber loop that consists of a gain medium that operates at the lasing threshold. Furthermore, the pumping direction dependence of the GSEC technique was investigated, thereby significantly improving the OPR in optical measurement systems. The results showed that forward pumping provides significantly higher OPR improvement than backward pumping.

Furthermore, numerical simulations were conducted to evaluate the performance of a GSEC technique in improving OPR. Experimental results demonstrated maximum slope values of 9.5 and 4.4 for forward and backward pumping, respectively, at an output wavelength of 1532.5 nm. The maximum slope of forward pumping was more than twice that of backward pumping. Numerical simulations of the mode field diameter (MFD) dependence revealed that the maximum slope increased with increasing MFD and reached a maximum value of 12.6 at the wavelength of 1533 nm.

Additionally, the basic characteristics of the GSEC technique were experimentally investigated using both single-stage (SS-GSEC) and dual-stage (TS-GSEC) configurations

were experimentally investigated. The SS-GSEC achieved a maximum slope (S_{max}) of 22.8 using a 20.4-m EDF for forward pumping at 1532.5 nm.

Finally, in the dual-stage GSEC (TS-GSEC) configuration achieved, a maximum slope of approximately 30.6 the TS-4, which consisted of two EDFs with a total length L_{tot} ＝36.3 m at an output wavelength of 1532.5 nm. Therefore, these results demonstrate that the proposed GSEC technique enables high-resolution optical power measurement and significantly improves OPR, representing a significant contribution to optical fiber sensing technology.

Table of Contents

Acknowledgement ii

List of Figures iii

List of Publications vi

Abstract xi

Table of Contents xiii

1. Introduction 1

1.1 Background 1

1.2 Conventional Techniques 2

1.3 Motivation 4

2. Guided Spontaneous-Emission Circuit (GSEC) 5

2.1 Classification of the Proposal Techniques 5

2.2 System Configurations 6

2.3 Spontaneous-Emission Light Propagation in Erbium-Doped Fiber (EDF) 7

2.4 Basic Configuration of Guided Spontaneous-Emission Circuit 7

2.5 Output Power vs. Input Power (Conventional Techniques with Optical Amplifier) 8

2.6 Output Power vs. Input Power (Conventional Techniques with Guided Spontaneous-Emission Circuit) 9

3. Improved Optical Power Resolution of Guided Spontaneous-Emission Circuit 10

3.1 Introduction 10

3.2 Experimental Setup of GSEC-Based Optical Measurement System 11

3.3 Experimental Results 13

3.3.1 Characteristics of the GSEC with 15.9-m EDF in Forward Pumping 13

3.3.2 Characteristics of the GSEC with 15.9-m EDF in Backward Pumping 17

3.3.3 Characteristics of the GSEC with 20.4-m EDF in Forward Pumping 18

3.4 Characteristics of Dual-Stage GSEC 19

3.5 Characteristics of Dual-Stage GSEC without Short Wavelength Pass Filter 20

3.6 Conclusion of the Study 21

4. Performance Evaluation Based on Numerical Simulation of Guided Spontaneous-Emission Circuit 22

4.1 Introduction 22

4.2 System Configurations 23

4.3 Comparison Between Experiment and Numerical Simulation 25

4.3.1 Characteristics of GSEC with Forward Pumping 25

4.3.2 Characteristics of GSEC with Backward Pumping 28

4.4 Mode Field Diameter Dependence Results of Forward Pumping Based on Numerical Simulation System Configurations 30

4.5 Conclusion of Study 32

5. High Resolution Optical Power Variation Measurement to improve the Optical Power Resolution of the Guided Spontaneous-Emission Circuit Technique 33

5.1 Introduction 33

5.2 Guided Spontaneous-Emission Circuit Technique 35

5.3 Experimental Setup 36

5.4 Characteristics of Single-Stage GSEC 40

5.5 Characteristics of Two-Stage GSEC 42

5.6 Improvement Characteristics of Optical Power Resolution 46

5.7 Conclusion of the Study 49

6. Investigation of the Guided Spontaneous-Emission Circuit Using Numerical Simulation 50

6.1 Theory of the GSEC 50

6.2 Numerical Simulation Result of the 1st Study 51

6.3 Numerical Simulation Result of the 2nd Study 54

6.4 Wavelength-Dependence Performance Characteristics of the GSEC 57

6.5 Conclusion of the Study 58

7. Pumping Direction Dependence in the Guided Spontaneous-Emission Circuit 60

7.1 Introduction 60

7.2 System Configurations 61

7.3 Numerical Simulation Modeling of the GSEC 62

7.4 Comparison Between the Experimental and Theoretical Results 64

7.5 Numerical Simulation 66

7.6 Conclusion of the Study 69

8. Application of Multicore-Fiber Sensing in Amplified Spontaneous Emission Feedback Circuit 70

8.1 Introduction 70

8.2 Multicore-Fiber Sensing System 70

8.3 Experimental Setup 71

8.4 Conclusion of the Study 72

9. Summary 73

References

1. Introduction

1.1 Background

Optical fiber sensing (OFS) has attracted attention for a wide range of applications, especially monitoring of industrial and environmental systems, long-distance transmission, and wide-area distributed sensing. Optical fiber communication is critical for the measurement of optical signals in fiber systems applications as well as optical communications, because the frequency of light is larger than 100 THz in the near-infrared wavelength region used in the application [4-7]. An optical power meter (PM) is a major component in an OFS. PMs that use photodiodes (PDs) as light detectors have excellent resolution, sensitivity, and response speed, and they are widely used in OFS systems [4, 5, 6, 7, 8, 9, 10, 11]. PM is an important parameter that influences OFS accuracy through optical power resolution. However, the optical power resolution of a PM, also referred to as uncertainty expressed in decibels or percentages, is very small values on the order of about 0.01 dB (or 0.23%) [19, 36, 37]. Interference noise and polarization dependence occur in a large proportion of the OPR in state-of-the-art PMs. In a previous study, we proposed a circuit, an amplified spontaneous emission feedback circuit that can significantly enhance the OPR by 10-100 times when placed in front of the PM [13, 14, 18, 20, 23, 24, 25]. We propose a fiber-optic sensing technique with high optical power resolutions (OPRs) using an amplified-spontaneous-emission feedback circuit (ASEFC) for multicore-fiber sensing applications. ASEFC is a feedback fiber loop that consists of a gain medium (EDF or optical semiconductor amplifier) that operates at the lasing threshold.

This study investigates nonlinear EDF-based circuit techniques: that is, identical throughout this study, initially known as the amplified-spontaneous-emission nonlinear circuit (ASENLC) and subsequently referred to as the guided spontaneous emission circuit (GSEC) [30, 31, 33]. By exploiting the nonlinear input-output characteristics of EDF structures, these

circuit techniques dramatically improve the OPR. The improvement factor (IF), defined as the maximum slope (S_{max}) of the nonlinear transmission curve in dBm, is used to quantify the enhancement of the optical power resolution (OPR) [30].

After that, we propose a novel circuit known as a guided-spontaneous emission circuit that can significantly improve the improvement factor of optical measurement systems [26, 28, 29, 30]. Next, we investigated another novel technique, a guided spontaneous-emission circuit (GSEC), employing forward and backward pumping cases, both experimentally and numerically [31]. We observed OPR enhancement factors of 9.5 and 4.4, corresponding to maximum slope (S_{max}) values at 1533 nm for the forward and backward pumping cases, respectively. Numerical simulation of the mode field diameter (MFD) dependence reveals that S_{max} increases with increasing MFD, reaching 12.6 at a wavelength of 1533 nm. Furthermore, a two-stage GSEC configuration using EDFs and optical filters optimized the IF to approximately 30.6, which consisted of two EDFs with a total length L_{tot} = 36.3 m at an output wavelength of 1532.5 nm. The proposed two-stage GSEC configuration can significantly improve OPR [33].

1.2 Conventional Technique vs GSEC Techniques

High-resolution optical power sensing plays a key role in photonics systems, such as optical communication and measurement systems. To measure the gain or loss of optical components, optical amplifiers, laser light sources, and passive components of the system, a measurement device/instrument is used, including an optical power meter and an optical spectrum analyzer with high optical power resolution. [13-33]. In a conventional method, the photo-detection efficiency of a photodiode-utilizing optoelectronic circuit is employed to determine and limit the resolution in the system. Typical values of the resolution in dB units are in the order of 0.1 dB or 0.01 dB [19, 36, 37]. In this study of optical power sensing, three system configurations are shown in **Figure 1.1.**

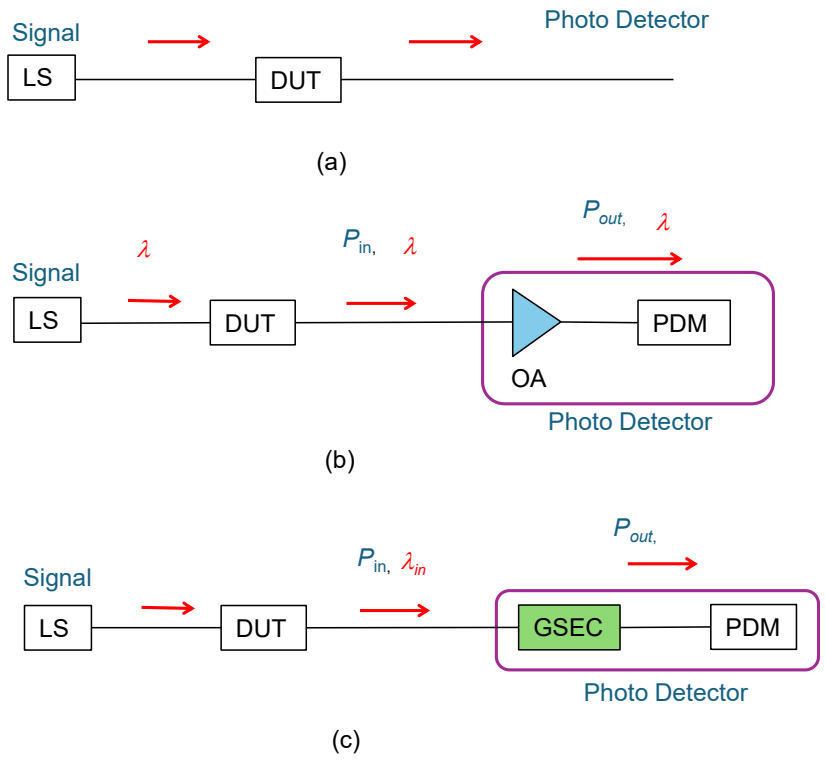

Figure 1.1. System configurations **(a)** Conventional technique, **(b)** Optical Amplifier technique (c) GSEC technique. Referring [26-33].

Figure 1.1 (a), **(b),** and **(c)** show the system configuration of optical power measurement in a conventional scheme, the conventional method utilizing an optical amplifier (OA) scheme, and the guided spontaneous-emission circuit (GSEC) scheme, respectively [26-33].

The three schemes individually use the laser light source (LS), a photo-diode module (PDM), and a device under test (DUT). The PDM has a photodiode, and an electrical circuit follows the PDM. The device under test (DUT) is either an optical gain medium or a loss medium, such as an optical amplifier or a passive optical component, respectively. On the other hand, the PD comprises an OA and GSEC, followed by a PDM in the case of the optical amplifier (OA) scheme and guided spontaneous-emission circuit (GSEC) scheme. The input wavelengths and output wavelengths of the lights are labeled λ_{in} and λ_{out}, respectively, because λ_{out} is different from λ_{in}. The input power and output power for the GSEC are labeled P_{in} and P_{out} in dBm units, respectively [26-33].

1.3 Motivation

Optical power measurement is crucial for various applications in optical communication and sensing systems. An optical power meter (PM) is a major component in fiber optic measurement and optical communication systems. Optical power measurement in conventional technology and optical amplifier-based configuration has faced some drawbacks in sensitivity and optical power resolution due to interference noise and fluctuation of the signal.

We previously proposed an amplified spontaneous emission feedback circuit that can significantly improve the OPR by 10-100 times when placed in front of the PM [13, 14, 18, 20, 23, 24, 25]. The ASEFC comprises a gain medium, an erbium-doped fiber (EDF) (or an optical semiconductor amplifier), and a feedback fiber loop that operates at a lasing threshold. This ASEFC has significantly improved the improvement factor (IF) in the optical power resolution [13, 14, 18, 20, 23, 24, 25].

In this research, we investigated the erbium-doped fiber-based circuit technique for enhancing the performance of low noise and high optical power resolution (OPR) by a guided spontaneous-emission circuit (GSEC) [30, 31, 32, 33, 37]. Improving optical power resolution (OPR) is a critical requirement for high-precision fiber-optic sensing (OFS) measurement systems.

First, we proposed a nonlinear EDF-based optical circuit technique that is identical throughout this study, initially known as the amplified-spontaneous-emission nonlinear circuit (ASENLC) and subsequently referred to as the guided spontaneous-emission circuit (GSEC). [26, 28, 29, 30]. Next, we experimentally and numerically investigated a GSEC technique in both forward and backward pumping cases. We observed OPR enhancement factors of 9.5 and 4.4, corresponding to maximum slope (S_{max}) values at 1533 nm for the forward and backward pumping cases, respectively. Numerical simulation of the mode field diameter

(MFD) dependence reveals that S_{max} increases with increasing MFD, reaching 12.6 at a wavelength of 1533 nm. Furthermore, we observed the OPR enhancement factors of both stages, with the maximum slope (S_{max}) values of 22.8 for the forward pumping case of wavelength at 1532.5 nm. In the dual-stage GSEC, the maximum slope value (S_{max}) is 2.4 times larger than that in the case of the single-stage GSEC with 15.9 m EDF.

Finally, a two-stage GSEC configuration using EDFs and optical filters optimized the IF to approximately 30.6, which consisted of two EDFs with a total length $L_{tot} = 36.3$ m at an output wavelength of 1532.5 nm. The proposed two-stage GSEC configuration can significantly improve OPR [33].

2. Guided Spontaneous-Emission Circuit (GSEC)

2.1 Classification of Proposal Techniques

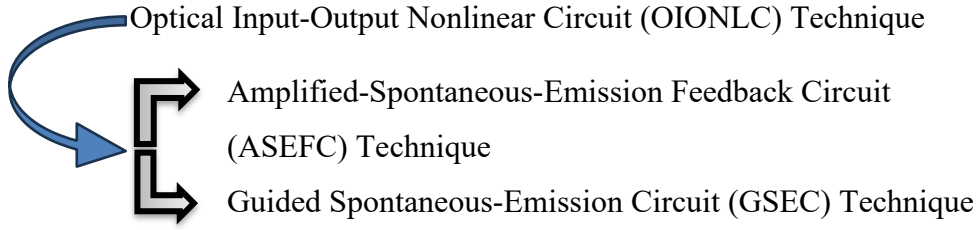

Figure 2.1. Name and classification of the proposal techniques.

Figure 2.1 shows the name and classification of our proposed methods. This figure shows that previously we proposed a technique, an amplified spontaneous emission feedback circuit (ASEFC), and recently we proposed a guided spontaneous emission circuit (GSEC) as optical input-output nonlinear circuits (OIONLCs). It was initially referred to as the amplified-spontaneous-emission nonlinear circuit (ASENLC) and was subsequently renamed the guided spontaneous emission circuit (GSEC). In this study, these terms (ASENLC and GSEC) are used to denote the same circuit, respectively.

2.2 System Configurations

Figure 2.2 shows the basic configuration of an optical power detection system. **Figure 2.2 (a)** shows the basic configuration of conventional technology, which includes a light source, a photodetector, and the sensor to be measured. For example, it measures the change in optical loss of the sensor. Without the sensor, the system measures the optical power of the light source. The light source used is a laser or a guided spontaneous-emission light source (GSE light source). The OPR of this PDM-type photodetector is typically limited by the known OPR interference noise and polarization dependence, which is calculated to be about 0.01 dB (relative accuracy of about 0.23%) [19, 36, 37]. The configurations of the OIONLC methods (GSEC methods) are shown in **Figure 2.2 (b)**.

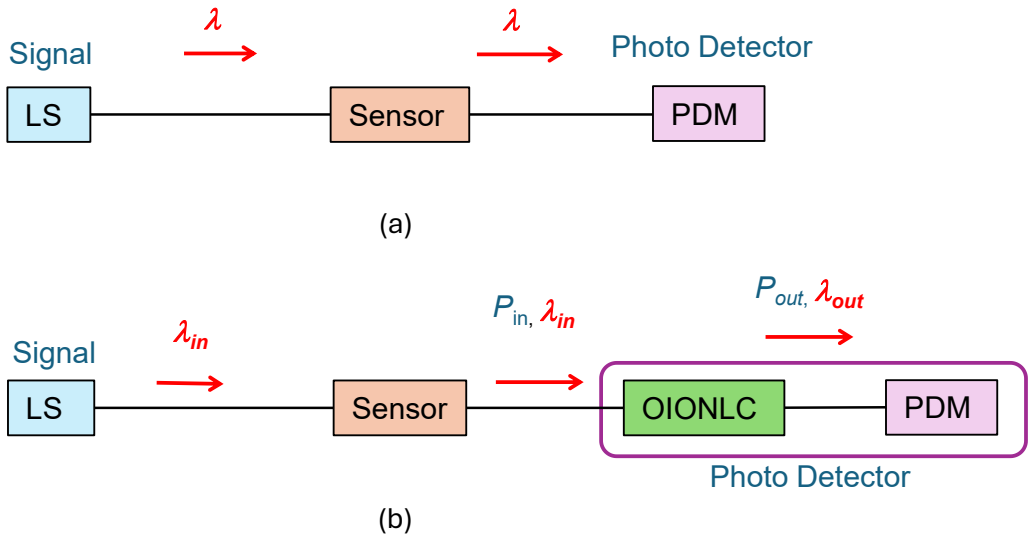

Figure 2.2. Basic system configuration for optical detection. Referring [26-33].

For example, the PDM set after the OIONLC. Since the input is different from the output, the output wavelength (λ_{out}) of the OIONLC is different. For simplicity, the following discussion will be on the case where the OIONLC is a GSEC. In GSEC, λ_{out} is larger than λ_{out} is typically a characteristic of the input/output optical power (P_{in} and P_{out} in dBm) of the OIONLC. The P_{out} vs. P_{in} curve has a large nonlinear response characteristic. The slope of the P_{out} vs. P_{in} curve (slope: $S = \Delta P_{out}/\Delta P_{in}$) gives the OPR improvement index.

2.3 Spontaneous-Emission Light Propagation in Erbium-Doped Fiber (EDF)

Figure 2.3 shows the amplitude of light through an EDF when amplifying the signal light. The direction input, the signal light is amplified by stimulated emission at the output of the EDF, while being attenuated by absorption of the pump light. Since spontaneous-emission is emitted equally in all directions, it is also emitted in directions other than the propagation direction as spontaneous-emission (SE). The SE light generated in the propagation direction is amplified by stimulated emission in the EDF, which converts the guided spontaneous-emission (GSE light) and the output into forward GSE light (F-GSE light) and backward GSE light (B-GSE light). SE light and GSE light are unpolarized and characterized by coherence. GSE light is considered a noise component.

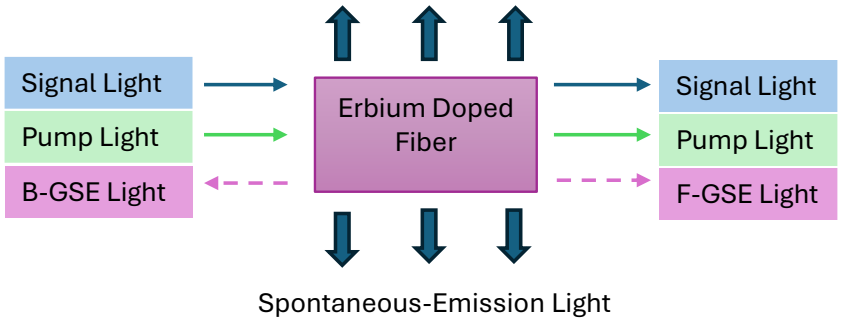

Figure 2.3. EDF propagated and spontaneously emitted light. Referring [26-33].

2.4 Basic Configuration of the Guided Spontaneous-Emission Circuit

Figure 2.4 shows the fundamental configuration of EDF-based GSEC [26-33]. The GSEC consisted of an erbium-doped fiber as the gain medium and a wavelength-selective coupler WC-F as the input pump light. An additional coupler, WC-B was mounted at the output to remove unwanted transmitted pump light for forward pumping. Isolators (ISOs) were set on the right and left sides of EDF to reduce the effect of residual reflected light. The forward pumping (F-GSE) and backward-pumping (B-GSE) of them are formed throughout the EDF. The input pump light was transmitted to the EDF via the WC-F [30, 31, 32, 33] for forward pumping.

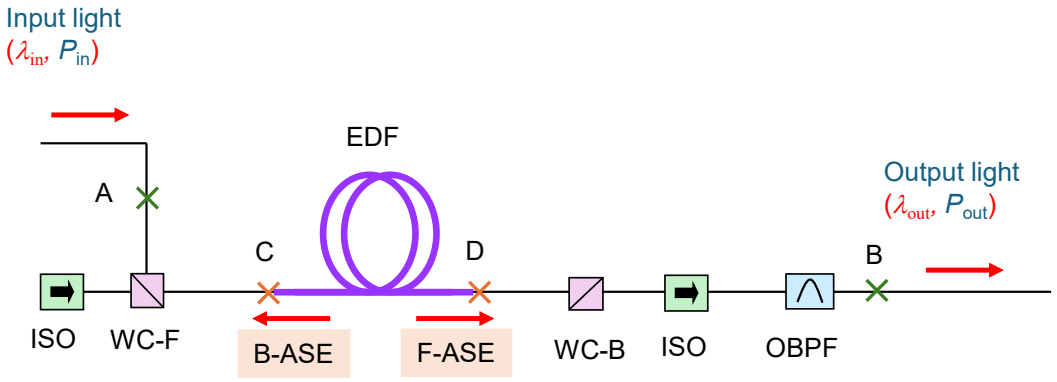

Figure 2.4. Basic configuration of Guided Spontaneous-Emission Circuit. Referring [26-33].

For backward pumping, the input pump light was transmitted backward to the EDF via the WC-B [30,31]. Forward GSE emitted from the EDF passes the optical bandpass filter (OBPF).

2.5 Output Power vs. Input Power (Conventional Techniques with Optical Amplifier)

Figure 2.5 shows the configuration for a conventional scheme using an optical amplifier [26-33].

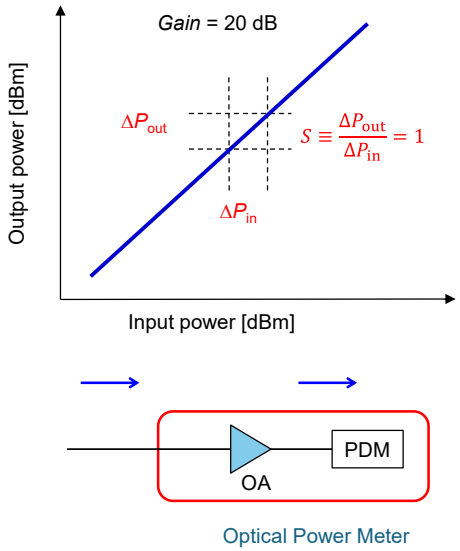

Figure 2.5. Output power vs. input power (conventional technique with optical amplifier). Referring [26-33].

The relative accuracy of the output power $\Delta P_{out}/P_{out}$ equals the relative accuracy of the input power $\Delta P_{in}/P_{in}$ because of the relations: $P_{out} = GP_{in}$ and $\Delta P_{out} = G\Delta P_{in}$, where G is the amplifier gain, so that $\Delta P_{out} = \Delta P_{in}$ [26-33].

$$S \equiv \frac{\Delta P_{\mathrm{out}}}{\Delta P_{\mathrm{in}}} = 0 \qquad (1)$$

If the improvement factor is the ratio slope $S = \Delta P_{out}/\Delta P_{in}$. Improvement factor slope (S) of the conventional configuration using the optical amplifier (OA) is 1.

2.6 Output Power vs. Input Power (Conventional Techniques with Guided Spontaneous-Emission)

Figure 2.6 shows the configuration of the GSEC scheme. However, the next relation when using the GSEC, $\Delta P_{out} >> \Delta P_{in}$ in the GSEC scheme [26-33].

$$S \equiv \frac{\Delta P_{\mathrm{out}}}{\Delta P_{\mathrm{in}}} \gg 1,\ S >> 1 \qquad (2)$$

Slope S indicated the value of an improvement in the optical power resolution (OPR).

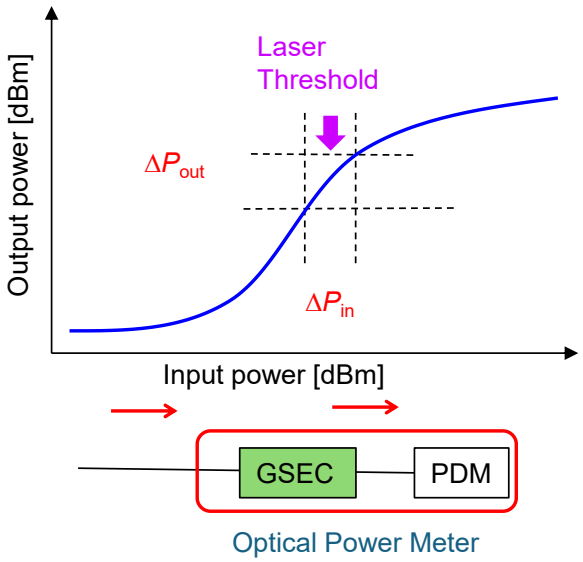

Figure 2.6. Output power vs. input power (Conventional Techniques with Guided Spontaneous-Emission). Referring [26-33]

3. Improved Optical Power Resolution of Guided Spontaneous-Emission Circuit Techniques

3.1 Introduction

Optical fiber sensing (OFS) is a key technology that provides notable advantages, including long-distance/wide area sensing, remote sensing, high stability, and high sensitivity [4-7]. We can measure various physical and chemical properties of the fiber, including temperature sensing, strain sensing, pressure sensing, displacement, and refractive index, in such applications [4, 11, 16]. In a previous study, we proposed a circuit, an amplified spontaneous emission feedback circuit (ASEFC), that can significantly enhance the OPR [13, 14, 18, 20, 23, 24, 25]. The ASEFC is a feedback fiber loop-based gain circuit used to improve the OPR.

In this study, we propose another technique that incorporates a novel optical circuit in front of the PM to improve the OPR [30]. This circuit was initially known as the amplified-spontaneous-emission nonlinear circuit (ASENLC) and subsequently referred to as the guided spontaneous-emission circuit (GSEC). Some basic features and characteristics of the GSEC technique are reported in the references. The circuit exhibits a nonlinear relationship between input and output power in dBm with two EDF gain blocks, whereas this circuit lacks a feedback loop. In contrast, the ASEFC circuit features a feedback loop. Further, the GSEC of the fictitious small internal signal gain in dB is estimated to be less than about 5 dB, while the gain medium of the ASE circuits used as a broadband light source in a fiber optic sensing system is greater than about 30-40 dB. GB(s) is pumped by input light of wavelength 1472 nm. We have developed an improved GSEC with two GBs pumped in the front and an intermediate short-wavelength pass filter (SF) in the C-band. The IF is successfully maximized, and the resulting OPR is minimized at the output wavelength of 1532.5 nm, so we have experimentally demonstrated the characteristics and performance of GSEC.

This chapter's content has already been published in the "International Conference on Emerging Technologies for Communications" (ICETC), as listed on the page of the Publications. Kokoro Kitamura, **Md Golam Barkatul Abrar**, Kunihiro Tanaka, Ryuga Harada, and Hiroji Masuda, "Amplified-spontaneous-emission nonlinear circuit technique with improved optical power resolution," **2023 International Conference on Emerging Technologies for Communications (ICETC 2023)**, O1-4, pp. 1-4, 11 **November 2023**, **(International Conference Symposium with Review)**. doi.org/10.34385/proc.79.O1-4.

3.2 Experimental Design of GSEC-Based Optical Measurement System

Figure 3.1(a) shows the experimental setup consisting of a light source (LS), GSEC, and a measurement section. We used a Fabry–Perot laser diode module as the light source. The pump light was emitted from the LS for the GSEC with a wavelength of 1472 nm. The optical output of the LS was coupled into the GSEC through the variable optical attenuator (VOA) and fiber coupler (FC_{in}) on the input side of the GSEC. The input light power (P_{in} in dBm) was measured using a photodiode module (PD_{in}), which is coupled to the 10% branching port of FCin. The optical output light from the GSEC, which was ASE light generated in the GSEC, was characterized by an additional PD module PD_{out}) and an optical spectrum analyzer (OSA) via another FC (FC_{out}).

Figure 3.1 (b) and **(c)** show the configuration of the single-stage and dual-stage GSEC, respectively. The single-stage GSEC circuit consists of an EDF employed as the gain medium and a wavelength-selective coupler for the input pump light (WC-F). Another coupler is set at the output point to remove the unwanted transmitted pump light (WC-B). The GSEC also comprises two isolators at the right and left sides of the EDF and a tunable optical bandpass filter (OBPF) with a center transmission wavelength of λ_c.

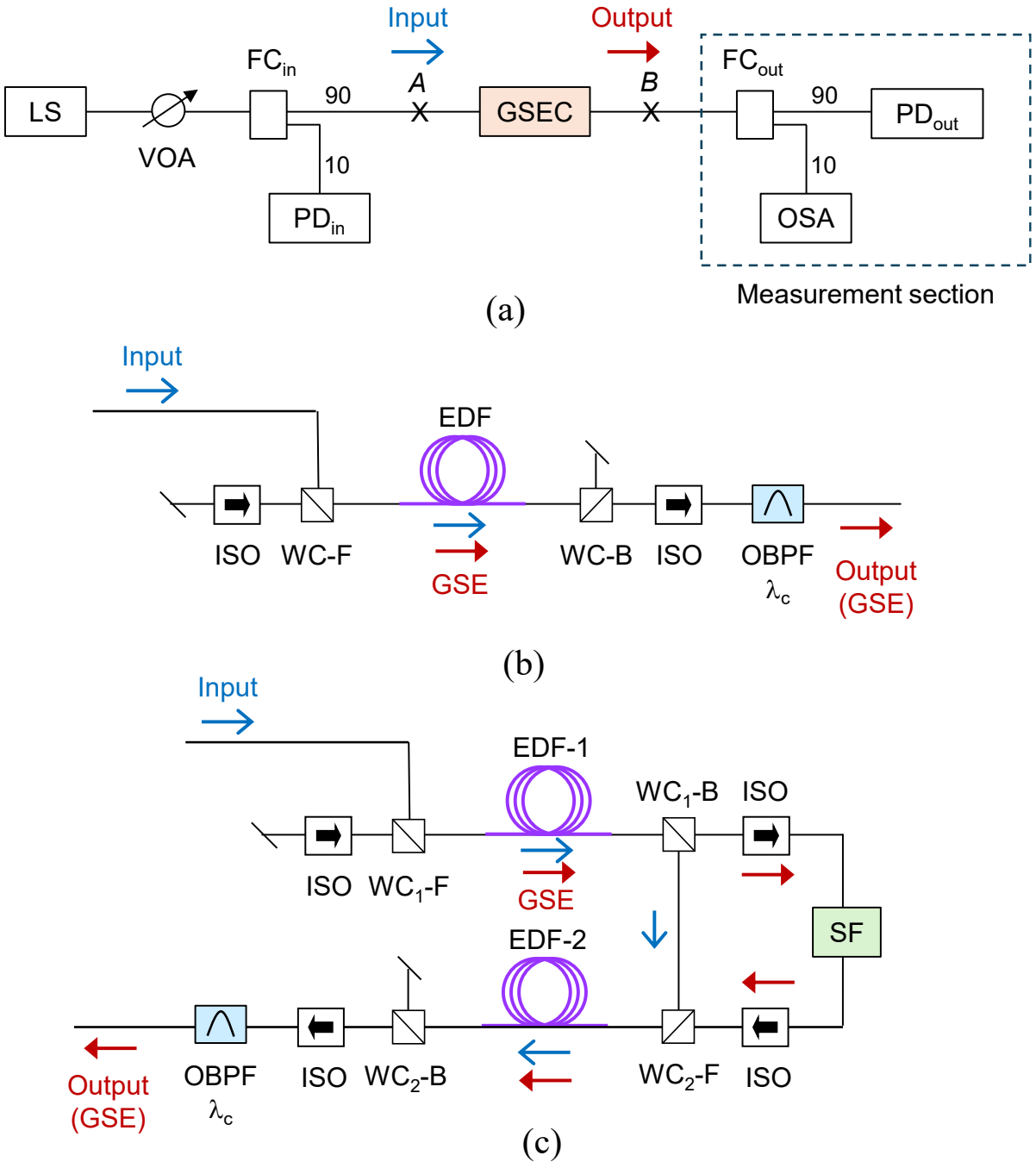

Figure 3.1. Schematics of the (a) experimental setup and configurations of (b) single-and (c) dual-stage GSEC. Referring [30].

We tested two pumping directions in terms of the F-GSE propagation direction: forward and backward pumping directions. **Figure 3.1 (b)** shows that the input pump light was coupled into the EDF through WC-F in the case of the forward pumping cases. In contrast, the input pump light is backward pumping cases launched into the EDF through WC-B. The

GSE light was emitted from the EDF output via the OBPF with an approximate bandwidth of about ~0.87 nm.

The dual-stage GSEC comprises two cascaded EDF modules (**Figure 3.1 (c)**). An SF was set between the EDF modules. The wavelength boundary of the SF was approximately 1544 nm. The residual pump light from the first EDF (EDF-1) was branched via WC1-B and launched into the second EDF (EDF-2) via WC2-F. Three EDF spools of different lengths (15.9, 18.0, and 20.4 m) were used in the experiments. Only an EDF of 15.9-m spool with a diameter of 9.5 cm was implemented within a temperature control module (T-Control). The ambient temperature was finely maintained at 23.0 ℃ by a temperature controller during the experiment.

3.3 Experimental Results

3.3.1 Characteristics of the GSEC with 15.9-m EDF in Forward Pumping

The experimental results of the GSEC with 15.9-m EDF in forward pumping are shown in **Figure 3.2 (a)** and **(b)**. We evaluated the basic characteristics of the GSEC using the single-stage configuration shown in **Figure 3.1 (b)**. The GSE power (P_{GSE}) was measured using an OSA with a resolution of 1.0 nm while the OBPF was removed. The spectra of the GSE output from the 15.9-m EDF in the forward pumping case are shown in **Figure. 3.2 (a)** at several input pump powers P_{in} from 3.9 to 6.9 dBm with a step of 0.5 dB. P_{in} and P_{out} values are defined at the input and output points of the EDF. **Figure. 3.2 (b)** shows the power differences per 0.5 dB (ΔP) for the data of **Figure 3.2 (a)**. From **Figure 3.2 (b)**, we can find that (ΔP) has maximum values around 1532.5 nm. The effective transmission bandwidth of the OBPF was estimated to be 1.0 nm.

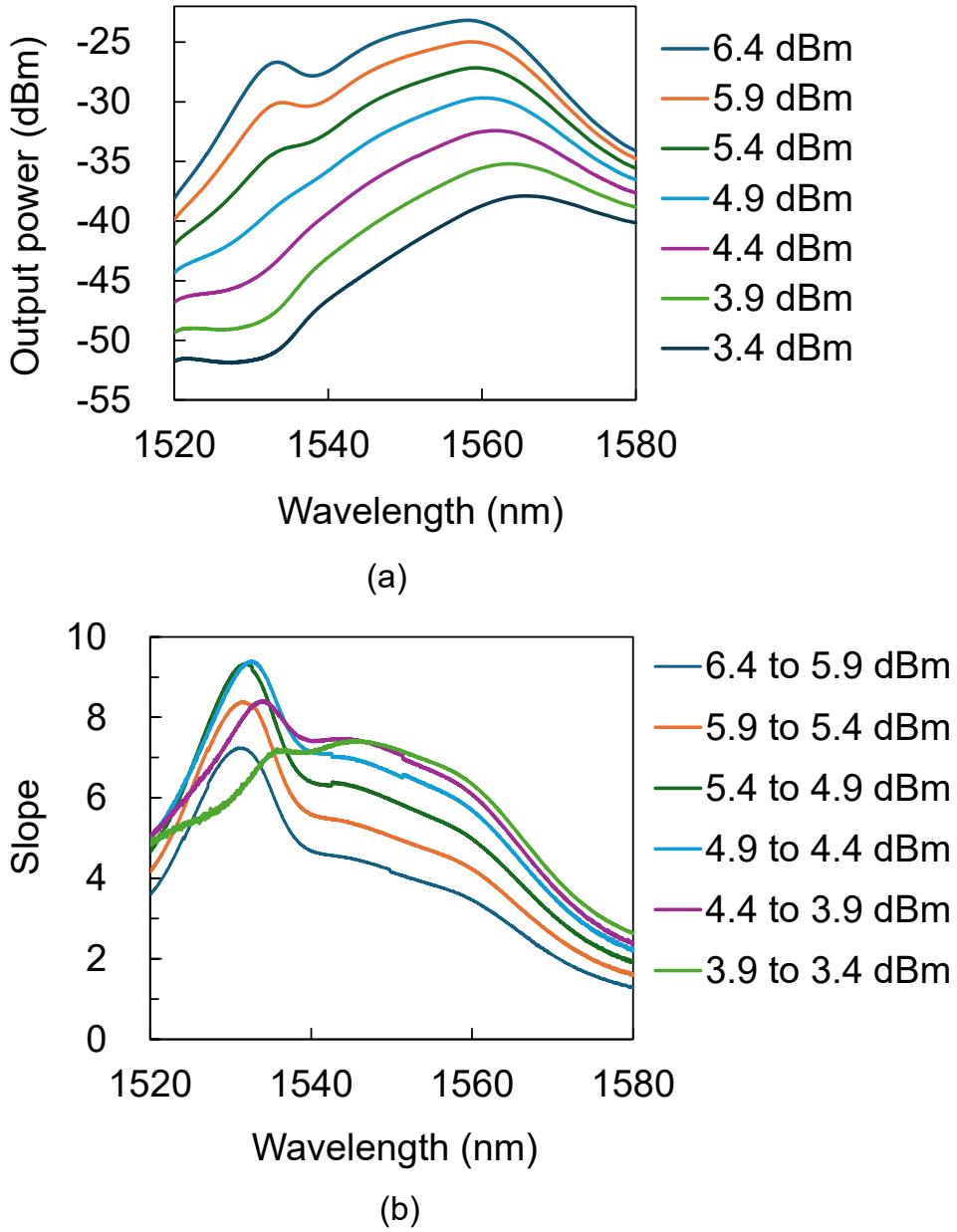

Figure 3.2. Characteristics of the GSEC with 15.9-m EDF in forward pumping (a) GSE power and (b) slope spectra. Referring [30]

Figure 3.3 (a) shows the input-output characteristics of the GSEC measured P_{out} as a function of P_{in} at the OBPF center wavelength λ_c of 1532.5, 1540, 1550, and 1560 nm.

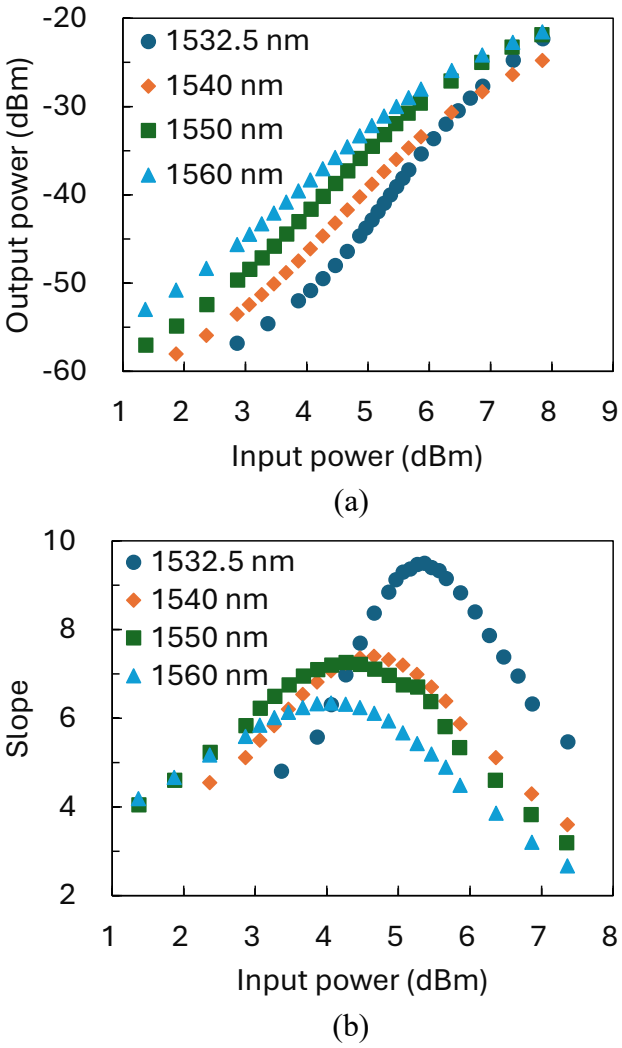

Figure 3.3. Characteristics of the GSEC with 15.9-m EDF in forward pumping (a) output power and (b) slope as a function of input power. Referring [30]

Moreover, **Figure 3.3 (b)** shows the slopes (*S*) of the input and output relations of **Figure 3.2 (a)**.

The slope is defined as,

$$S \equiv \frac{P_{\text{out}}}{P_{\text{in}}} \tag{3}$$

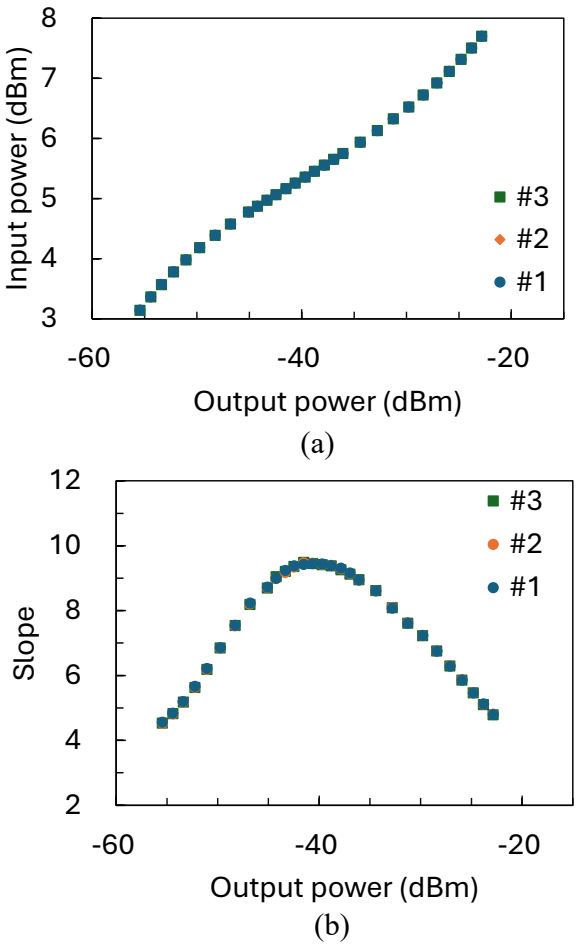

Figure 3.4. Characteristics of the GSEC with 15.9-m EDF in forward pumping (a) input power and (b) slope as a function of the output power for three-times measurements. Referring [30]

When the input power (P_{in}) increased, the slope (S) also increased. We derived the maximum slope (S_{max}) at each λ_c in **Figure 3.3 (b)**. The sets of values (P_{in} [dBm], P_{out} [dBm], S_{max}) at λ_c of 1532.5, 1540, 1550, and 1560 nm were (5.37, −40.01, 9.5), (4.66, −41.71, 7.4), (4.27, −40.17, 7.3), and (4.06, −38.30, 6.3), respectively.

In the proposed technique of the GSEC, the small changes in the equation were calculated in advance. The small changes in P_{in} were estimated from the measured changes in P_{out} using the fitting function. This is the fifth-order algebraic function,

$$P_{in} = \sum_{k=0}^{5} C^k P_{out}^k \tag{4}$$

3.3.2 Characteristics of the GSEC with 15.9-m EDF in Backward Pumping

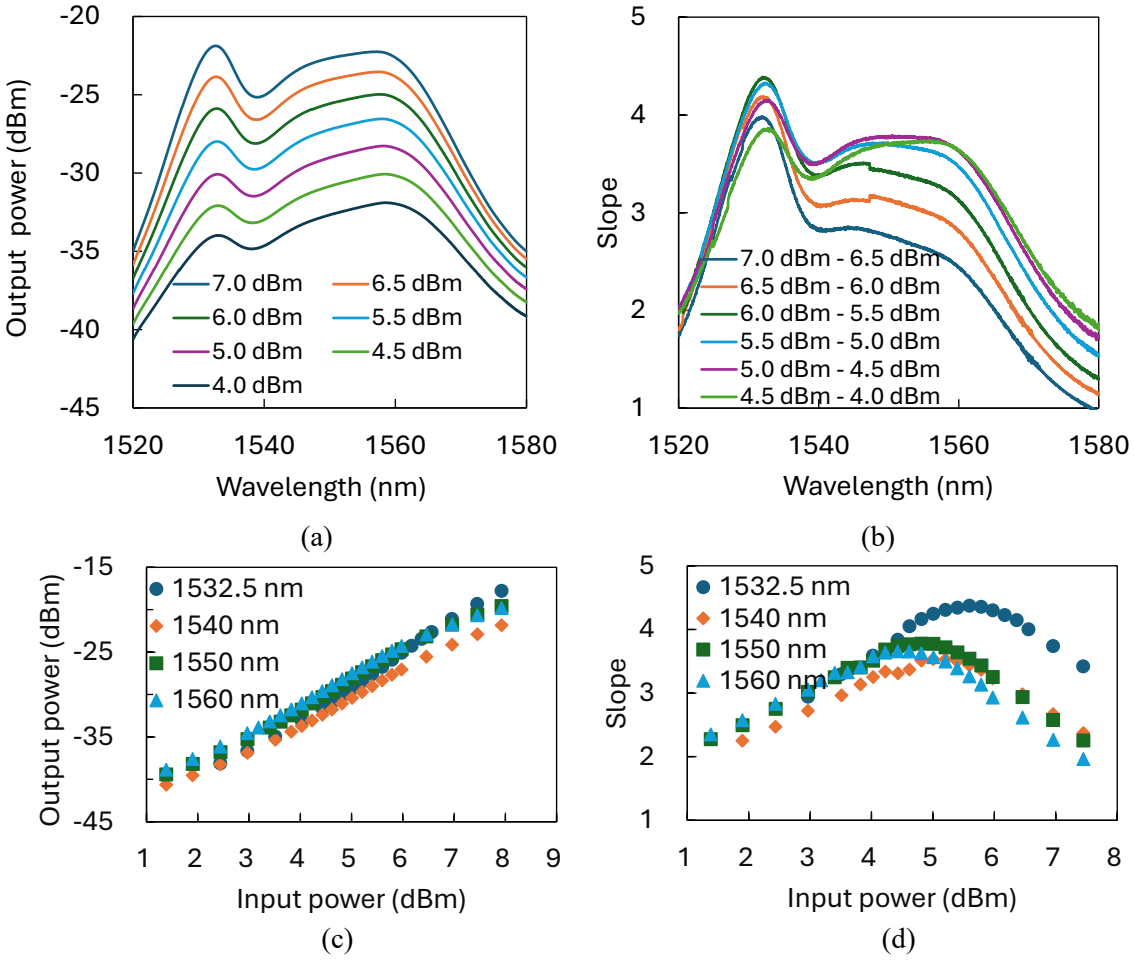

Figure 3.5. Characteristics of the GSEC with 15.9-m EDF in backward pumping GSE power and (b) slope spectra, (c) output power, and (d) slope as a function of the input power. Referring [30].

The measured values of P_{out} and S as a function of P_{in} for the backward pumping case are shown in **Figure 3.5**, as in the case of forward pumping. **Figures. 3 (a), (b), (c)**, and **(d)** show the GSE power spectra, slope spectra, input-output and slope characteristics, respectively. From **Figure 3.5 (d)**, we derived the maximum S (S_{max}) at each wavelength λ_c. The sets of values (P_{in} [dBm], P_{out} [dBm], S_{max}) at λ_c of 1532.5, 1540, 1550, 1560 nm were (5.60, −26.75,

4.4), (5.20, −29.71, 3.5), (4.81, −28.86, 3.8), and (4.43, −29.60, 3.7), respectively. Therefore, S_{max} for the forward and backward pumping cases are 9.5 and 4.4, respectively, at λ_c of 1532.5 nm: the former is more than two times larger than the latter.

3.3.3 Characteristics of the GSEC with 20.4-m EDF in Forward and Backward Pumping

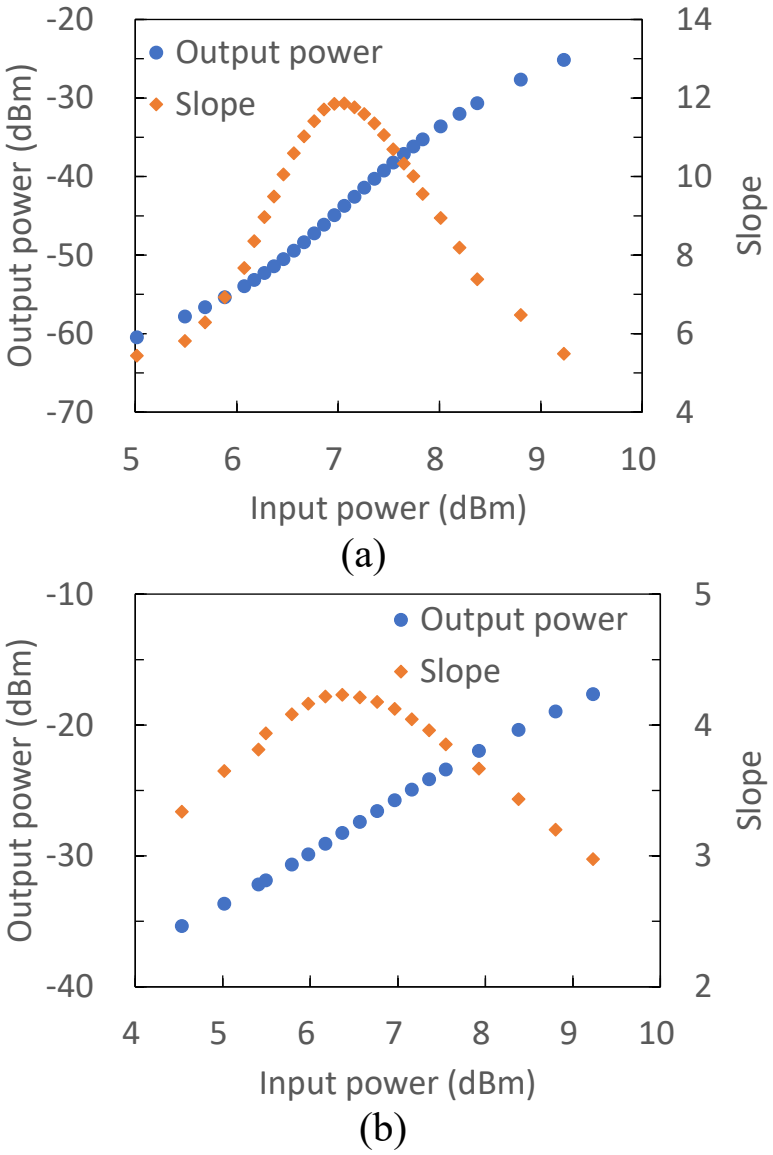

Figure 3.6. Characteristics of the GSEC with 20.4-m EDF (a) forward and (b) backward pumping. Referring [30].

Figure. 3.6 (a) and **(b)** show the characteristics of the GSEC 20.4-m EDF in forward and backward pumping, respectively. The wavelength λ_c was set at 1532.5 nm in these

measurements. The sets of values (P_{in} [dBm], P_{out} [dBm], S_{max}) in forward and backward pumping were (7.06, -43.75, 11.9) and (6.37, −28.25, 4.2), respectively. The maximum slope (S_{max}) in the case of forward pumping is larger than that of backward pumping, as in the case of 15.9-m EDF. Furthermore, in the case of forward pumping, S_{max} increased from 9.5 to 11.9 when the length of the EDF was increased from 15.9 to 20.4 m EDF.

3.4 Characteristics of Dual-Stage GSEC

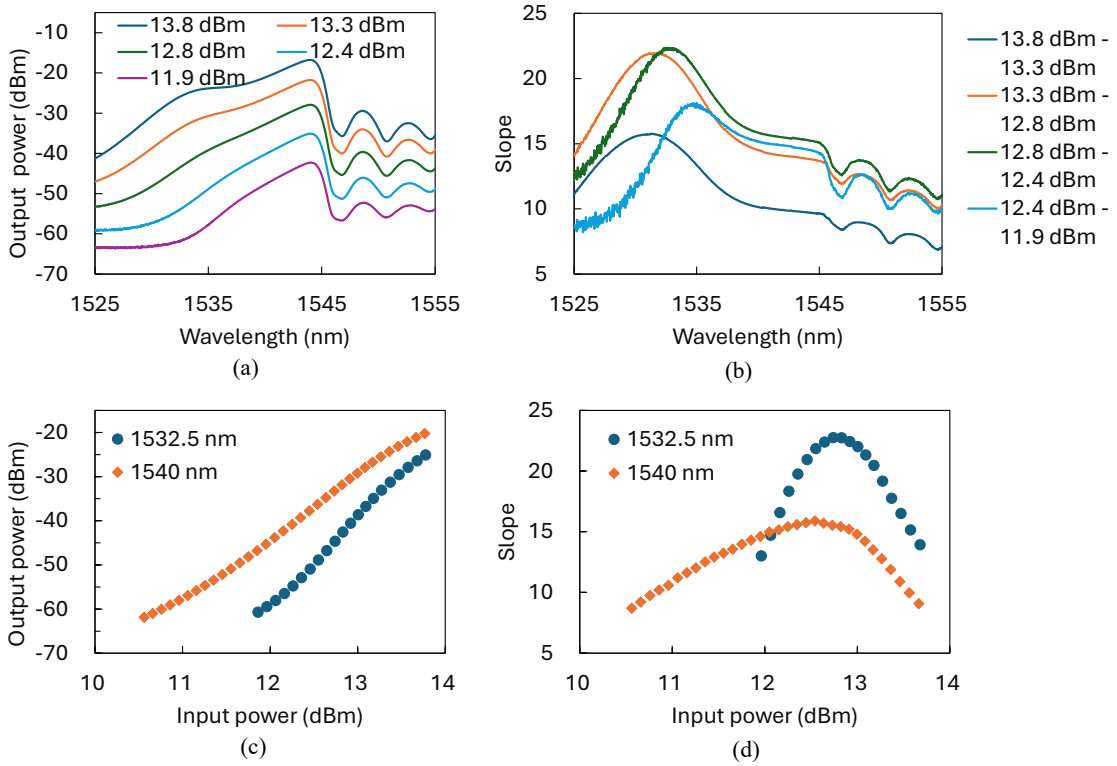

Figure 3.6. Characteristics of the dual-stage GSEC (a) ASE power and (b) slope spectra. (c) Output powers and (d) slope as a function of the power. Referring [30].

For further improvement, we investigated the dual-stage GSEC. The experimental results for the dual-stage GSEC are shown in Figure 3.7. The length of the dual-stage GSEC EDF module was 18.0 and 15.9 m, respectively. **Figures 3.7 (a-d)** show the GSE power and slope spectra, input-output, and slope as a function of input power, respectively. The GSE light with wavelengths longer than ~1544 nm was cut by the SF, and the slopes around 1532.5 nm are over 22.

Figure 3.7 (c) and **(d)** show the input-output and slope characteristics, where the wavelength λ_c was set at 1532.5 and 1540 nm in these measurements. The sets of values (P_{in} [dBm], P_{out} [dBm], S_{max}) at λ_c of 1532.5 and 1540 nm were (12.74, −44.63, 22.8) and (12.54, −36.25, 15.9), respectively. In the single-stage GSEC using a 15.9 m EDF under forward pumping, the maximum slope obtained was approximately 2.4 times greater at the dual-stage EDF.

3.5 Characteristics of Dual-Stage GSEC without Short Wavelength Pass Filter

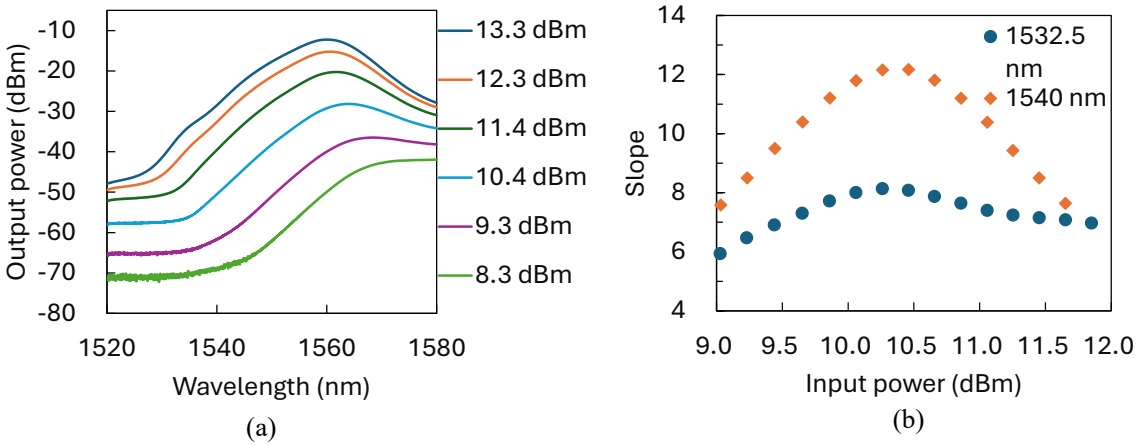

Figure 3.7. Characteristics of the dual-stage GSEC without the SF. (a) ASE spectra. (b) slopes as a function of the input power. Referring [30].

We constructed the effectiveness of the SF characteristics of a dual-stage GSEC without SF. Characteristics of the dual-stage GSEC without SF, the GSE spectra, and slope as a function of the input power are shown in **Figure 3.8 (a)** and **(b)**. Without SF, the GSE at long wavelengths became large, and the slopes were smaller than those obtained using SF. These results confirm the effectiveness of SF.

3.6 Conclusion of the Study

This study, we proposed a novel technique of GSEC that significantly improves the achievable optical power resolution (OPR) in optical power measurement systems. We experimentally demonstrated the single-stage configuration and investigated the basic characteristics of the GSEC technique. We achieved the maximum slope value (S_{max}) at λ_c 1532.5 nm. The S_{max} in forward pumping was higher than that in backward pumping. Furthermore, we experimentally demonstrated the dual-stage configuration and investigated the basic characteristics of the GSEC, and achieved the maximum slope (S_{max}) of 22.8. Therefore, we significantly achieve the improvement factor (IF) in the OPR using the proposed GSEC technique.

4. Performance Evaluation Based on Numerical Simulation of Guided Spontaneous-Emission Circuit

4.1 Introduction

Optical power meters (PMs) employing photodiodes are widely utilized due to their high sensitivity, fast response, and stable detection characteristics. However, the achievable sensing accuracy is strongly governed by the optical power resolution (OPR) of the measurement system. We conducted numerical simulations for the proposed GSEC [31]. Experimental results were compared with numerical simulation results were confirmed the good agreement. In addition, we found that the improvement factor (IF), which is the slope in the input-output optical power relation of the GSEC, was much higher for forward pumping than for backward pumping. Furthermore, numerical simulations were carried out on the mode field diameter (MFD) dependence, finding that the maximum slope (S_{max}) increased with the MFD, and the maximum IF in OPR was obtained at an output wavelength of 1533 nm.

This chapter's content has already been published in the "International Conference on Consumer Technology- Pacific 2025" (ICCT-Pacific 2025), as listed on the page of Publications. **Md Golam Barkatul Abrar**, Kokoro Kitamura, and Hiroji Masuda, "Performance Evaluation Based on Numerical Simulation of Novel Guided Spontaneous Emission Circuit for Improved Optical Power Resolution," **IEEE International Conference on Consumer Technology-Pacific 2025 (IEEE ICCT-Pacific 2025)**, P2-4, pp. 1-4, **30 May 2025, (International Conference with Review), (HISS Excellent Research Award)**. 10.1109/ICCT-Pacific63901.2025.11012822.

4.2 System Configuration

Figure 4.1(a) shows a schematic configuration of the experimental setup consisting of a light source (LS), GSEC, and measurement section. We used a Fabry–Perot pump diode module as the LS. The center wavelength of the pump light was approximately

1472.0 nm. The optical output of the LS was coupled into the GSEC through the variable optical attenuator (VOA) and fiber coupler (FC_{in}) on the input side of the GSEC. Points A and B in **Figure 4.1,** we can measure the values of input and output powers of the GSEC. The IF of the OPR using the GSEC is expressed by the slope (S) defined as,

$$S = \frac{dP_{out}}{dP_{in}} \tag{5}$$

where ΔP_{in} and ΔP_{out} are the increments in the input and output powers of the GSEC, respectively.

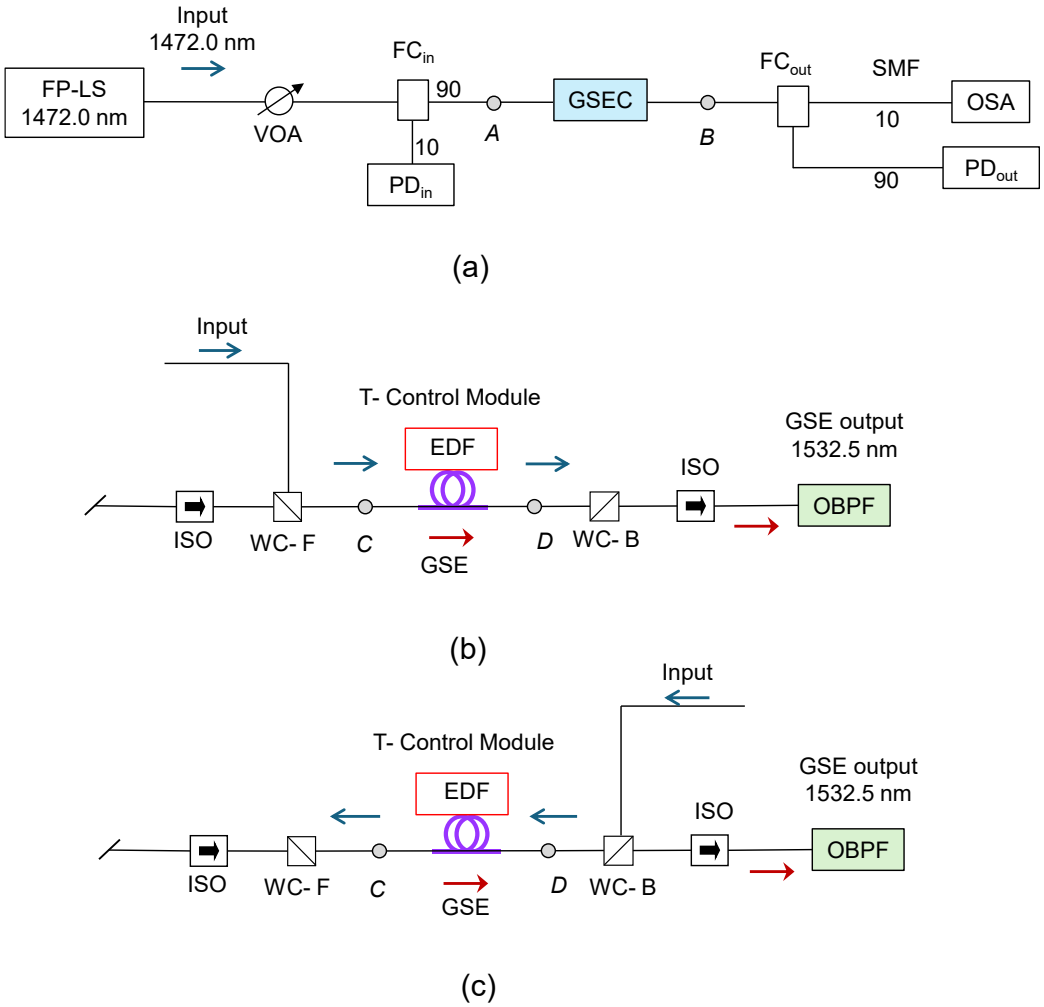

Figure 4.1. Schematic configuration of (a) measurement system and GSEC with (b) forward and (c) backward pumping**.** Referring [31].

We tested the forward and backward pumping directions, whose experimental setups using the GSEC are illustrated in **Figure 4.1 (b)** and **(c)**, respectively. The GSEC consisted of an erbium-doped fiber (EDF) as the gain medium, and a wavelength-selective coupler WC-F as the input pump light.

An additional coupler WC-B was mounted at the output to remove unwanted transmitted pump light for forward pumping. Isolators (ISOs) were set on both sides of EDF to reduce the influence of residual reflections. The input pump light was transmitted to the EDF via the WC-F for forward pumping (**Figure 4.1 (b)**). For backward pumping, the input pump light was transmitted backward to the EDF via the WC-B (**Figure 4.1 (c)**). Forward GSE emitted from the EDF passes the optical bandpass filter (OBPF), and it was then detected by an optical spectrum analyzer (OSA) and PD module PD_{out} via fiber coupler FC_{out}. PD_{in} and PD_{out} were commercial PM sensor heads (AQ2735, Ando Electric). The EDF was a 15.9 m spool with a diameter of 9.5 cm, and it was maintained within a temperature control module (T-Control Module). The ambient temperature was finely controlled at 23.0 ℃ using a temperature controller throughout the experiments.

4.3 Comparison Between Experiment and Numerical Simulation

4.3.1 Characteristics of GSEC with Forward Pumping

The output power spectra for forward pumping are shown in **Figure 4.2 (a)** at various input pump powers, P_{in}, ranging from 3.4 to 6.4 dBm with increments of 0.5 dB. The GSE spectra were measured without the OBPF in the GSEC. The optical losses between points A–C and D–B were estimated to be 0.9 dB. **Figure 4.2 (b)** shows the slope spectra obtained from the data shown in **Figure 4.2 (a)**. As shown in **Figure 2 (b)**, the slope had a maximum of approximately 1533 nm. The effective transmission bandwidth of the OBPF was estimated to be 1.0 nm.

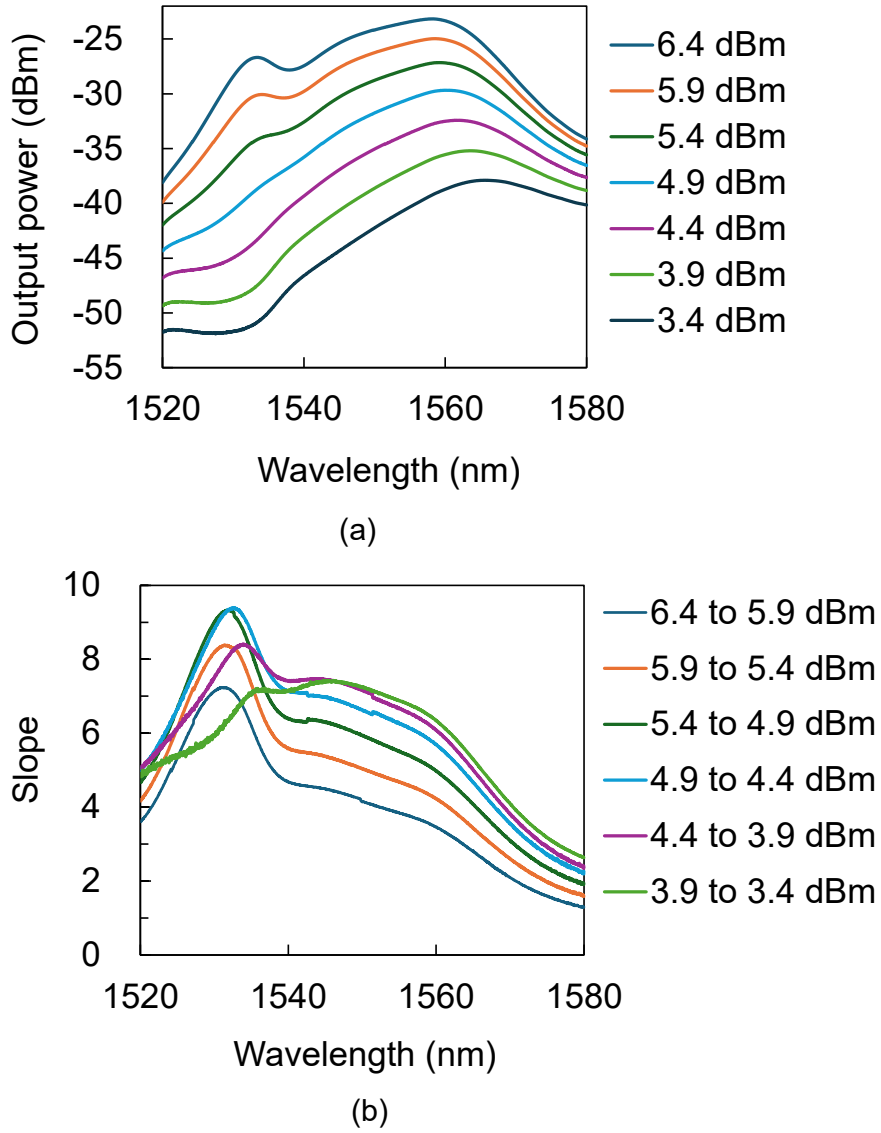

Figure 4.2. Characteristics of GSEC with forward pumping (a) output power and (b) slope spectra**.** Referring [31].

Numerical simulation utilized in several equation including a set of propagation equations describing light propagating in the EDF and a rate equation for the fractional populations of the laser energy states of $^4I_{15/2}$ and $^4I_{13/2}$ for the 1480 nm-band pumping [1,2]. For the numerical simulation based on the equations of (8) and (9), parameters needed for the simulation were derived from the measured characteristics of the 15.9 m EDF used in this study [26-29]. The parameters were the peak loss at around 1530 nm (A_{peak} in decibels), MFD, and Er-ion ratio (β).The obtained parameters were

A_{peak} = 100 dB, β = 0.015 (1.5%), and MFD of 3.5 μm. Moreover, the ratios of the output optical powers of backward to forward GSE were estimated to be 2.5 and 1/2.5 for forward and backward pumping, respectively **Figure 4.3(a)** and **(b)** show the measured and calculated values of output power P_{out} and slope S according to input power P_{in} at OBPF center wavelengths λ_c of 1533, 1540, 1550, and 1560 nm for forward pumping.

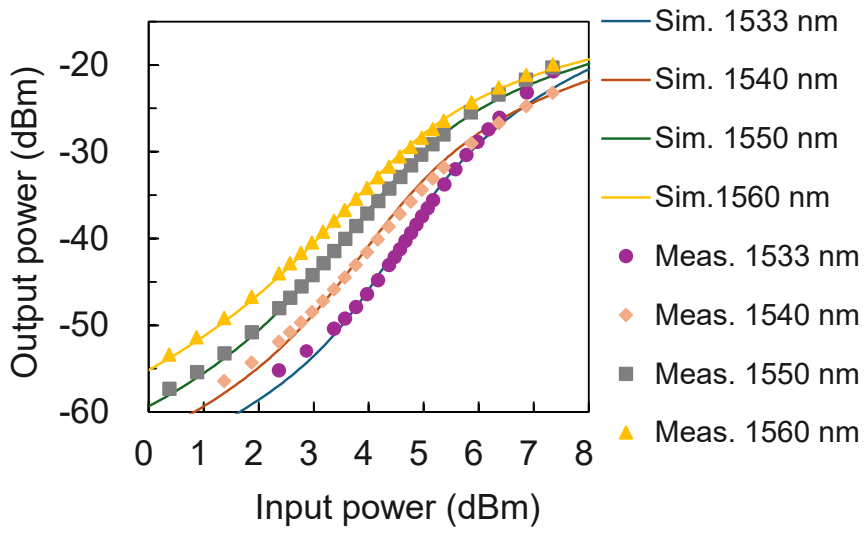

(a)

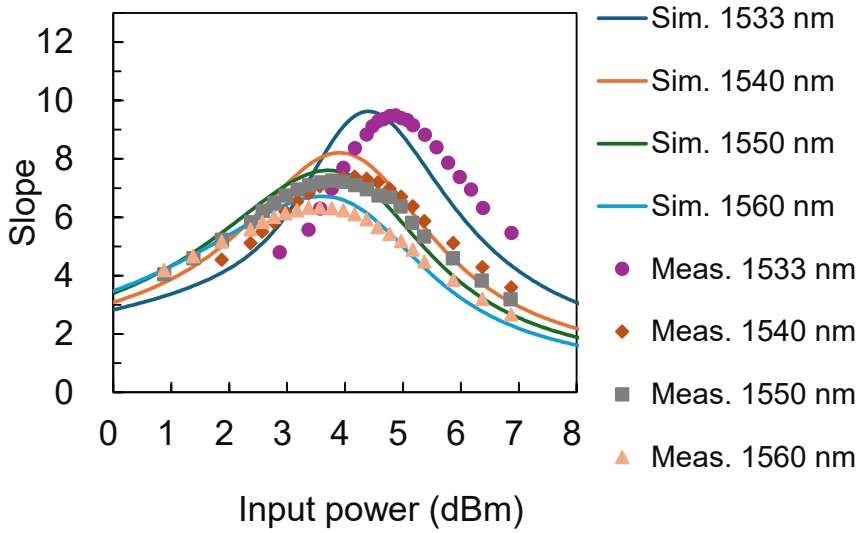

(b)

Figure 4.3. Input/output power characteristics of GSEC with forward pumping (a) output optical power and (b) slope according to input optical power. Referring [31].

Figure 4.3 (a) and **(b)** show the measured and calculated values of output power P_{out} and slope S according to input power P_{in} at OBPF center wavelengths λ_c of 1533, 1540, 1550, and 1560 nm for forward pumping. P_{in} and P_{out} were defined at the input and output of the EDF and points C and D in **Figure 4.1 (b)**, respectively. In the results shown in **Figure 4.3**, c and m represent the calculated and experimental results, respectively. A good agreement was confirmed between the calculated and experimental values. The measured and calculated P_{out} values aligned well with the measurement and calculation accuracy, which was estimated to be approximately ±0.5 dB. However, for P_{out} lower than approximately −50 dBm, a slight difference was observed between the experimental and calculated values. S_{max} was derived at each evaluated λ_c. The experimental values P_{in}, P_{out}, and S_{max} at λ_c values of 1532.5, 1540.0, 1550.0, and 1560.0 nm were (4.87 dBm, 4.17 dBm, 3.78 dBm, 3.57 dBm), (−38.40 dBm, −40.11 dBm, −38.56 dBm, −36.70 dBm), and (9.5, 7.4, 7.3, 6.3), respectively.

4.3.2 Characteristics of GSEC with Backward Pumping

Figures 4.4 (a) and **(b)** show the output power and slope spectra for backward pumping. P_{in} was varied between 3.5 and 6.5 dBm in steps of 0.5 dB. The output power spectra were different from those of forward pumping shown in **Figure 4.2 (a).** In addition, output power P_{out} was larger for backward pumping.

Figure 4.5 (a) and **(b)** show the measured and calculated values of P_{out} and S according to P_{in} at OBPF center wavelengths λ_c of 1533, 1540, 1550, and 1560 nm for backward pumping. P_{in} and P_{out} were defined at the input and output of the EDF and points D and C in **Figure 4.1 (c),** respectively. The measured and calculated P_{out} values suitably agreed within the accuracies of measurement and calculation, which were estimated to be approximately ±0.5 dB. An approximate model for backward-propagating GSE was used in the simulation. The small errors between the simulation and experimental results will be examined in future work. We derived S_{max} for each evaluated λ_c. The experimental values P_{in}, P_{out}, and S_{max} at λ_c

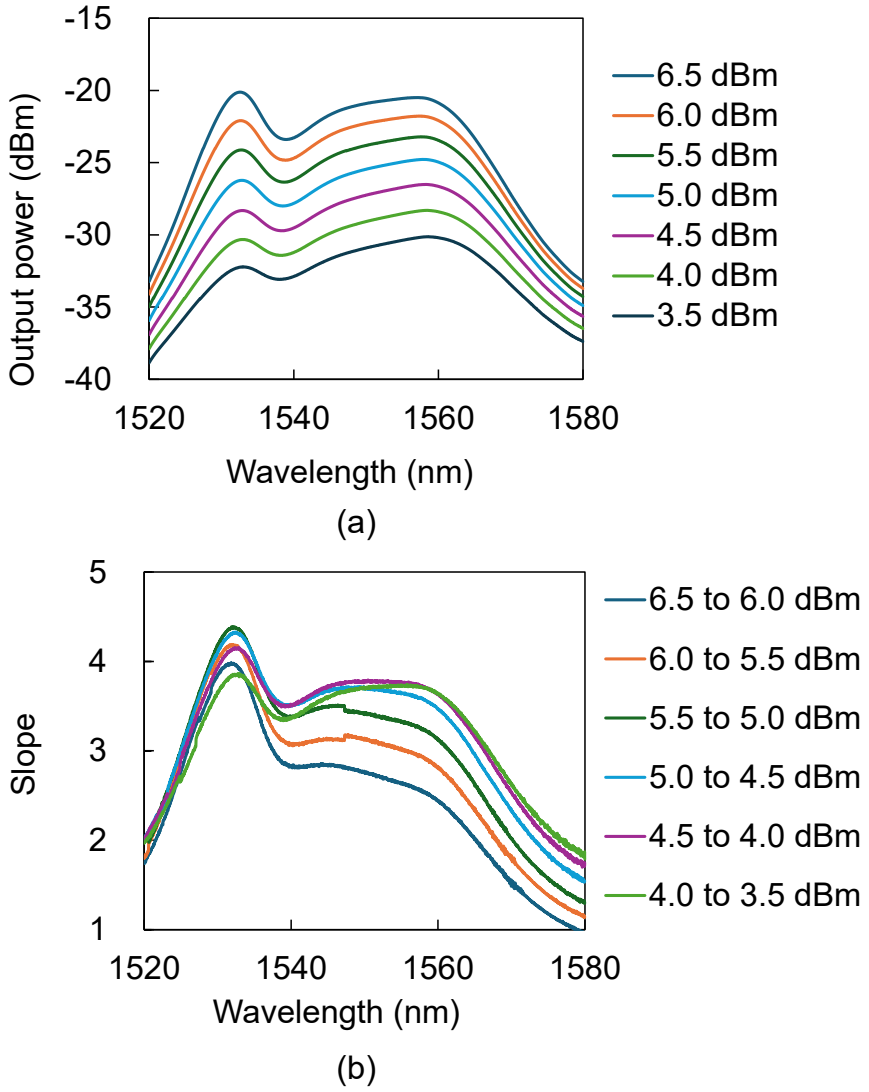

Figure 4.4. Characteristics of GSEC with forward pumping (a) output power and (b) slope spectra**.** Referring [31].

values of 1533, 1540, 1550, and 1560 nm were (5.10 dBm, 4.51 dBm, 4.32 dBm, 3.93 dBm), −25.14 dBm, −28.80 dBm, −27.26 dBm, −27.99 dBm) and (4.4, 3.5,3.8, 3.7), respectively.

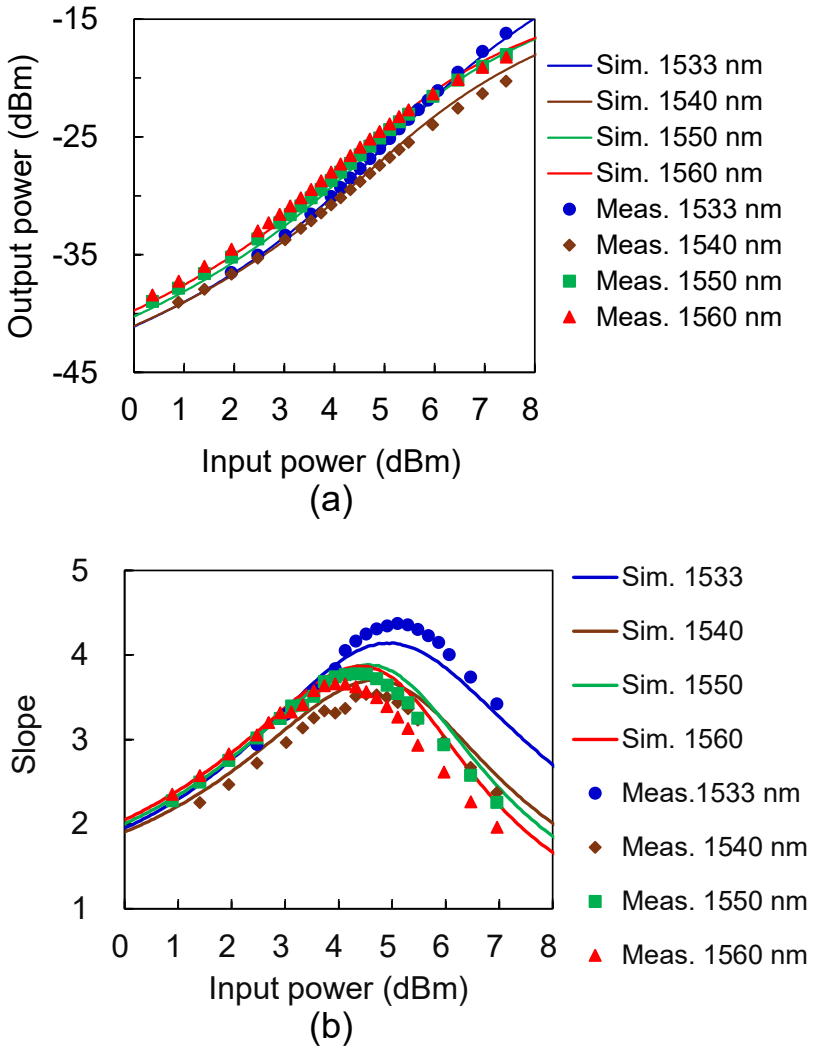

Figure 4.5. Input/output power characteristics of GSEC with backward pumping (a) output optical power and (b) slope according to input optical power. Referring [31].

4.4 Mode Field Diameter Dependence Results of Forward Pumping Based on Numerical Simulation

The simulation results of the input P_{in} and output P_{out} relation and slope S of the GSEC for forward pumping are shown in **Figure 4.6 (a), (b)**, and **Figure 4.7 (a)**, **(b)**. The MFD of the EDF was changed from 2 to 12 μm, and various wavelengths were evaluated. We derived S_{max} for each evaluated λ_c. The simulation values (P_{in}, P_{out}, S_{max}) at λ_c values of 1533, 1540, 1550, and 1560 nm for an MFD of 12 μm were (15.15 dBm, −37.42 dBm, 12.6), (15.55 dBm,

−37.64 dBm, 9.5), (15.40 dBm, −35.02 dBm, 8.5), and (15.30 dBm, −33.11 dBm, 7.4), respectively.

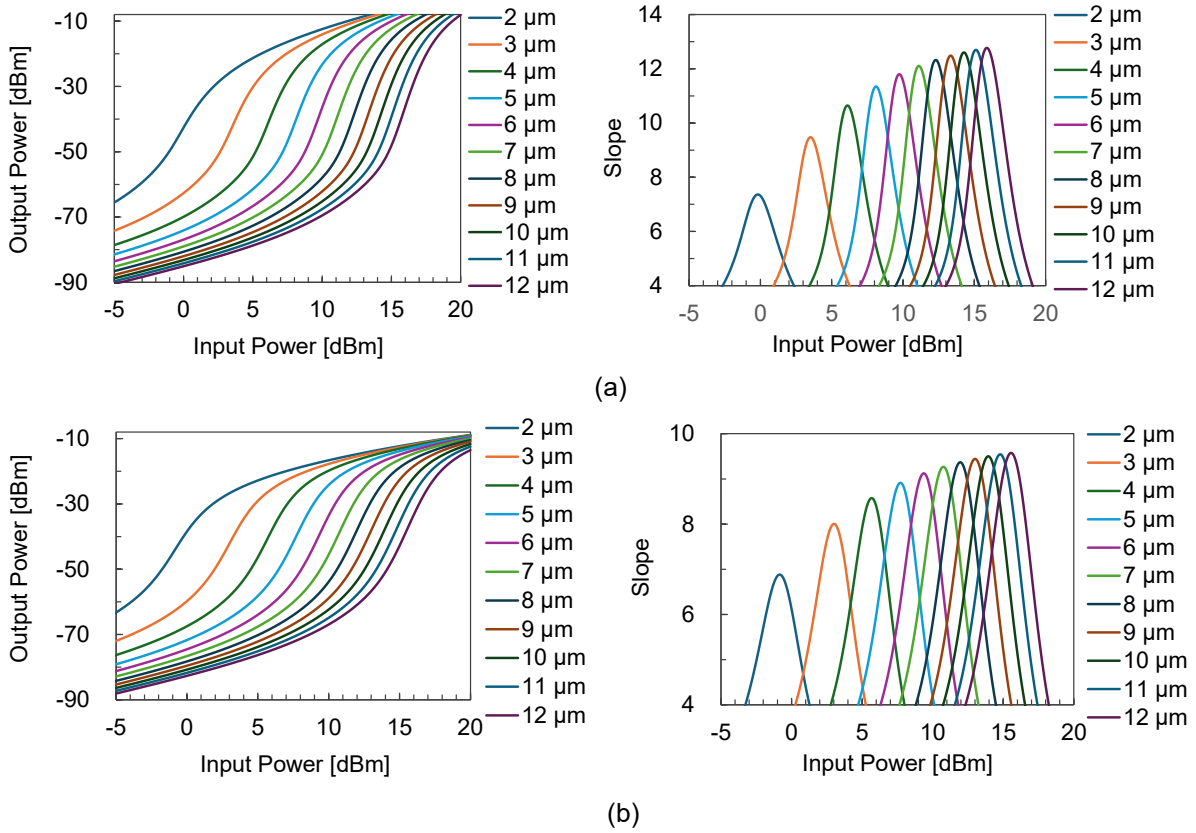

Figure 4.6. Mode Field Diameter dependence results at wavelengths of (a) 1533, (b) 1540 nm for forward pumping. The figures in the left and right columns show the output powers and slopes according to input optical power, respectively. Referring [31].

The slopes indicated that S_{max} increased with the MFD, and S_{max} reached 12.6 at λ_c = 1533 nm. At a wavelength of 1533 nm, input power P_{in} at S_{max} increased from approximately 0 to 16 dBm as the MFD increased. Therefore, a larger P_{in} was required as the MFD increased. When the MFD increased by a factor of α, the cross-sectional area of the EDF increased by α^2. As a result, the spontaneous emission of light power increased by approximately α^2. Therefore, a higher P_{in} was required to increase the spontaneous emission.

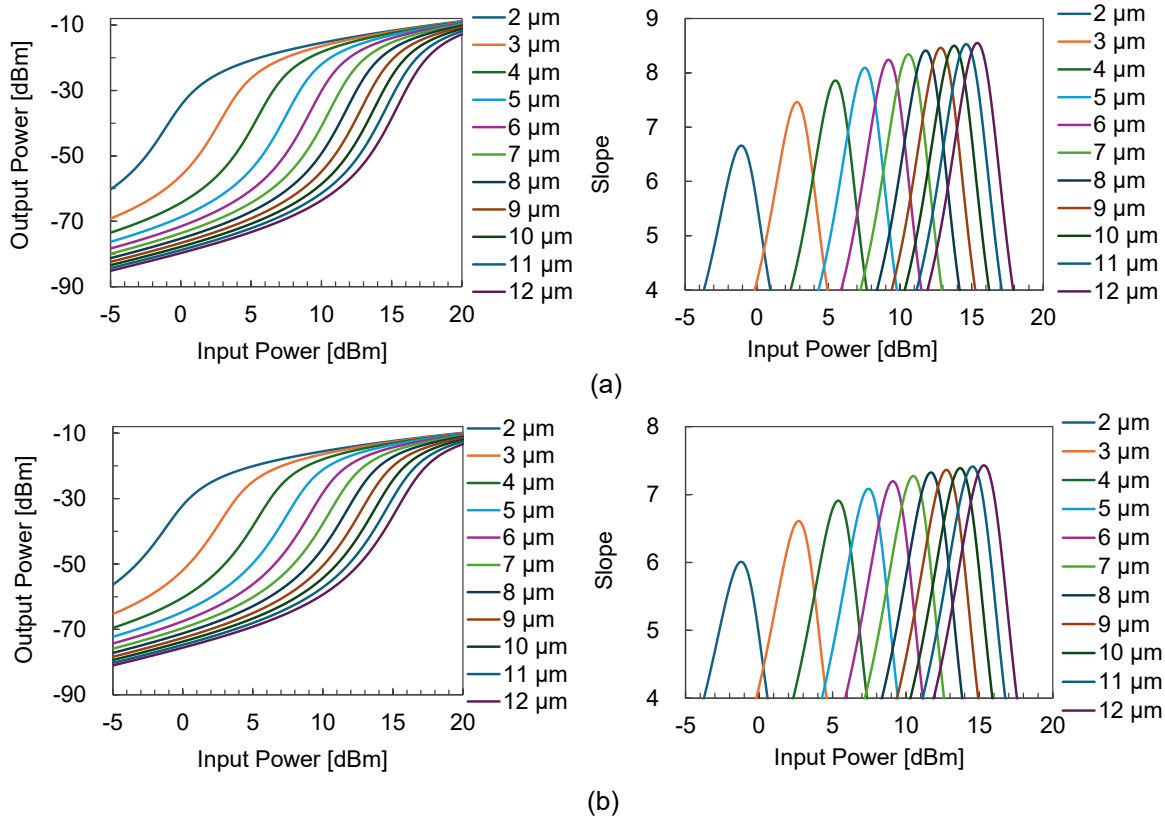

Figure 4.7. Mode Field Diameter dependence results at wavelengths of (a) 1550, (b) 1560 nm for forward pumping. The figures in the left and right columns show the output powers and slopes according to input optical power, respectively. Referring [31].

4.5 Conclusion of the Study

A numerical simulation was conducted to evaluate the performance of a GSEC that can significantly improve the OPR. Experimental results were compared and suitably agreed with the numerical simulation results. We also clarified that $S_{max,}$ which indicated the IF in OPR, was much higher for forward pumping than for backward pumping. Furthermore, we conducted a numerical simulation of the MFD dependence, observing that S_{max} increased with the MFD, and the maximum IF in OPR was achieved at wavelength λ_c of 1533 nm.

5 High Resolution Optical Power Variation Measurement to Improve the Optical Power Resolution of the Guided Spontaneous-Emission Circuit Technique

5.1 Introduction

This study proposed a novel technique called the guided spontaneous-emission circuit (GSEC) designed for precise optical power variation measurement. In principle, these two techniques, GSEC and ASEFC, are different methods for measuring optical power variation. GSEC usually consists of a spool of erbium-doped fibers (EDFs) as the gain media and does not include any feedback loop. ASEFC and GSEC exhibit a strong nonlinear relationship between P_{in} and P_{out} in the optical domain, achieving a significant improvement in OPR. The proposed method is developed on signal processing, including noise suppression similar to the reduction of thermal noise in photocurrent generation and the subsequent processing of electrical signals [34, 35]. Due to the dependence and interference, polarization noise cannot successfully enhance OPR in dB in the fundamental method. On the other hand, the GSEC method is considered a different principle and remains effective in cases where the interference and polarization noise limit the OPR in dB.

Furthermore, the conventional small-signal gain of GSECs (Gf) is less than about 5 dB, while ASEFC exceeds about 10 dB because the gain medium is required to compensate for the feedback loop losses in ASEFCs [17, 20, 23, 24]. Gf is considered imaginary because there is no input signal light in the actual GSEC. Furthermore, GSECs are different from ASE light sources (ASELS), which are used in certain fiber-optic sensing systems. [3, 21, 24]. Typical Gf values as high as about 30-40dB, which increases both output power and power density. We previously proposed our new GSEC technique, which successfully enhanced the improvement factor (IF) are approximately 22.8 [30]. However, in this study, we found that the improvement factor (IF) of GSEC can achieve approximately 30.6. The GSEC output is generated primarily by spontaneous emission, which results in a roughly flat linewidth and a lack of polarization. These characteristics reduce the interference noise and polarization

dependence of PD-PM. In contrast, ASEFC output light is partially coherent and polarization dependent. Therefore, some degree of interference noise and polarization dependence is expected in PD-PM [24]. In this experimental study, the input light wavelength was set to approximately 1470 to 1480 nm. However, numerical simulations confirmed that the input light wavelength can be extended within the 1450–1550 nm wavelength range when the output light wavelength is maintained at 1565 nm [29]. Furthermore, the input power levels can be reduced to approximately -20 dBm when we use an optical amplifier in front of the GSEC [23].

This chapter's content has already been published in the "IEICE Electronics Express", as listed on the page of Publications. (Kokoro Kitamura, **Md Golam Barkatul Abrar**, Kunihiro Tanaka, Ryuga Harada, and Hiroji Masuda, "Guided spontaneous emission circuit technique with improved optical power resolutions for optical power variation measurement," **IEICE Electronics Express**, Vol. 22, No. 10, pp. 1-6, **25 May 2025**. https://doi.org/10.1587/elex.22.20250155

5.2 Guided Spontaneous-Emission Circuit Technique

Figure 5.1 (a) shows the system configuration of our proposed method of the GSEC technique. We used a photodiode module (PDM), which comprised a photodiode followed by an electric circuit. In the setup, the guided spontaneous-emission circuit (GSEC) is placed in front of the PDM. A new type of optical power meter based on the GSEC method has been developed by cascading GSEC and PDM, which is known as GSEC-PM. Without the sensor, the system measures the optical output power of the light source. The light source used is a laser or a guided spontaneous-emission light source (GSE light source). The OPR of this PDM-type photodetector is typically limited by the known OPR interference noise and polarization dependence, which is calculated to be about 0.01 dB (relative accuracy of about 0.23%) [19, 36, 37].

Figure 5.1(b) shows the fundamental configuration of the multistage EDF-type GSEC technique. The GSEC consisted of an erbium-doped fiber (EDF) as the gain medium, and a wavelength-optical filter (OFs) as the input pump light. For simplicity, the three-stage configuration and key optical components are shown in **Figure 5.1 (b)**. The GSEC comprises three EDF spools of EDF-1, EDF-2, and EDF-3, and two optical isolators are used after EDF-1 and EDF-2. In the downstream of each of them, EDF uses three optical filters (OF-1, OF-2, and OF-3) to output GSE light (F-GSE and B-GSE) in both forward and backward pumping directions, respectively. On the other hand, in a multistage EDF configuration, the intermediate part of the B-GSE from EDF-2 to EDF-1 and from EDF-3 to EDF-2 is obstructed through ISOs. The GSEC consisted of an erbium-doped fiber as the gain medium, and a wavelength-optical filter (OFs) as the input pump light. The transmission wavelength of each optical fiber boundary, F-GSE, consists of a bandwidth-limited GSE that is subsequently generated generate the GSEC output light.

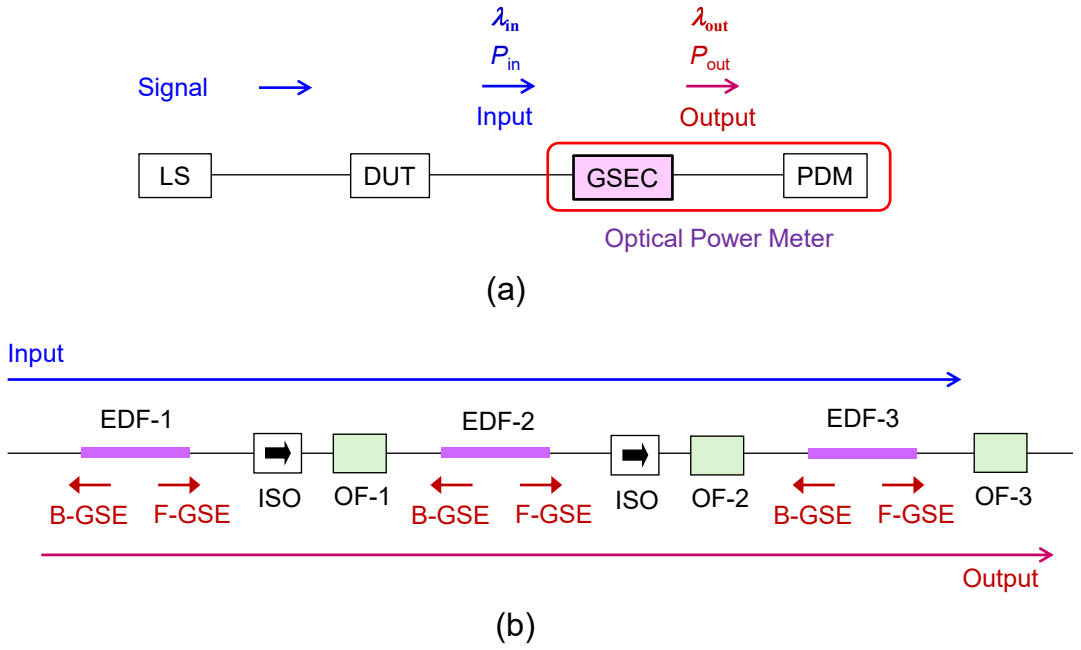

Figure 5.1. (a) System configuration of the GSEC technique, (b) basic configuration of the multistage GSEC. Referring [33].

5.3 Experimental Setup

We performed an initial numerical simulation to evaluate the performance of the two-stage EDF-type GSEC (TS-GSEC) against a single-stage GSEC (SS-GSEC).

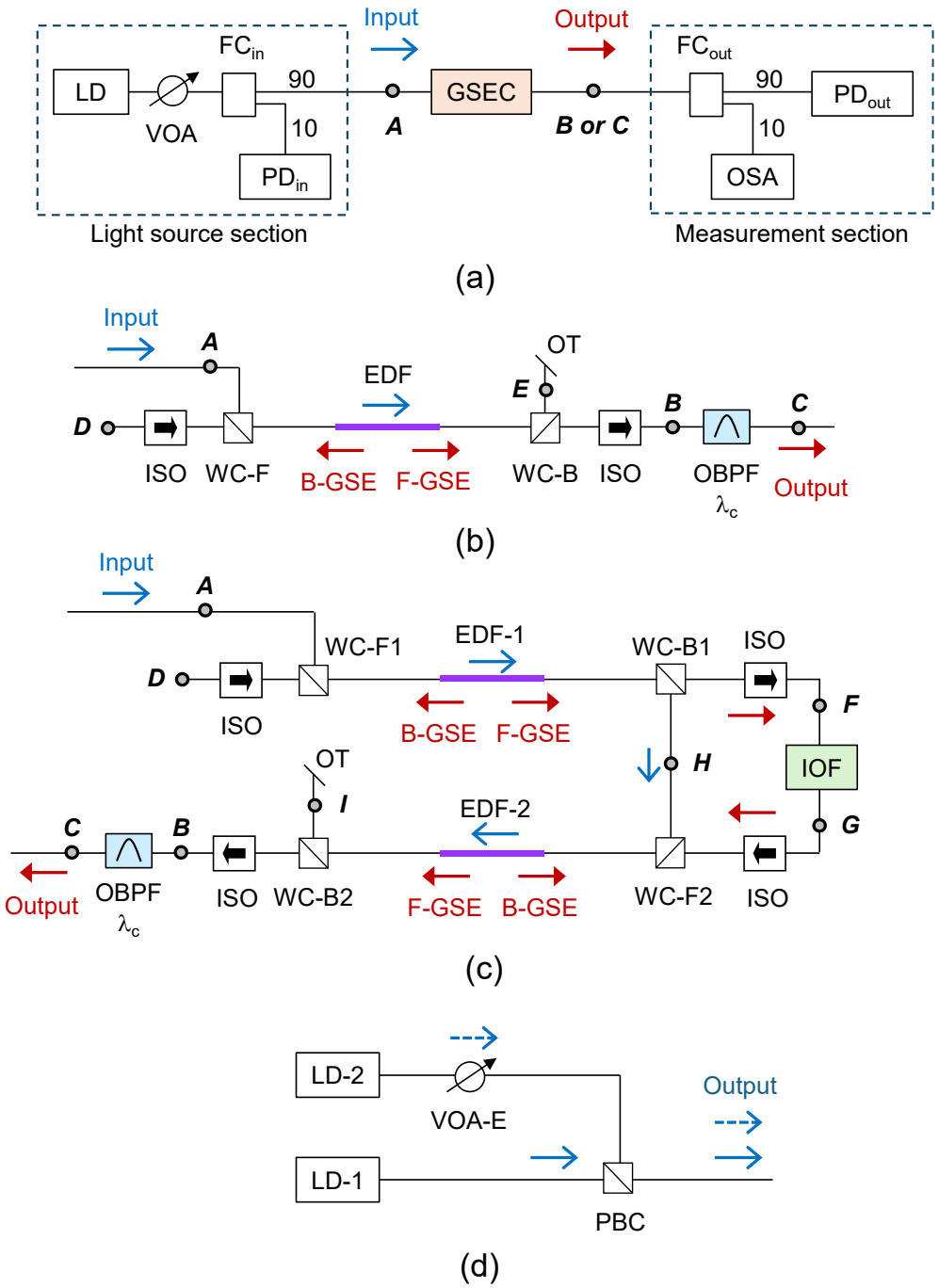

Figure 5.2. (a) Schematics of the experimental setup (a) The measurement system, (b) single-stage GSEC, (c) two-stage GSEC, and (d) emulator. Referring [33].

In this study, the details of the numerical simulation result are provided for brevity, so the TS-GSEC realized getting the higher Ifs than those of the SS-GSEC. The numerical simulation solves the differential equations for the propagation of light power in EDFs [30]. In addition, the increase in IFs from TS-GSEC to the enhancement of the three-stage GSEC was estimated to be low.

According to this result, the characteristics of the SS- and TS-GSECs were evaluated through the experiments. The experimental setup, SS-GSEC, TS-GSEC, and LS modules for simulating slight changes of input light power (emulator) are shown in **Figure 5.2**. The measurement system consists of three main components LS section, the GSEC, and the measurement section. The measurement was carried out by a Fabry–Perot laser, which is widely used in EDF applications. Two types of LDs (LD-1 and LD-2), having slightly different power-averaged center wavelengths of 1477.7 nm and 1472.1 nm, respectively, were utilizing each spectrum demonstrated multi-longitudinal mode characteristics [21]. The input light power (P_{in} in dBm) was measured using a photodiode module (PD_{in}). A variable optical attenuator (VOA) was installed after the LD to change the P_{in}, denoted as VOA_{LD}. P_{out} was measured using $PD_{out,}$ whereas P_{in} was monitored using PD_{in} through a branch located after $VOA_{LD.}$ The input power P_{in} of each sensor head was measured using a PDM (PD_{in}, Ando AQ2735), which was connected to a 10% transmission port of FC_{in}. The output optical power and output spectrum emitted from the LS section were kept at constant values by regulating the drive current and temperature of each LD at 500 mA and 25°C, respectively. The output optical power launched into the GSEC, P_{out}, is monitored using an independent photodiode module (PD_{out}, Ando AQ2735, or Yokogawa AQ2200-212) and an optical spectrum analyzer (OSA, Anritsu MS9740A) through another FC (FC_{out}). **Figure 5.2 (a)–(c)** depicts the optical splicing points, labeled from Point A to Point I, which explain the experimental configuration. At Points A and B or C, we defined the P_{in} and $P_{out,}$ including the optical spectra. The value

is determined based on measurements obtained using PD_{in}, PD_{out}, and OSA, calculating the amount of connection loss between different points and devices.

The experimental setup shows an example of a single-stage (SS-GSEC) of the system shown in **Figure 5.2 (b)**. The single-stage GSEC (SS-GSEC) consists of a spool of EDF, two isolators (ISOs), two wavelength-selective couplers (WCs) used for forward pumping and backward pumping, denoted as (WC-F and WC-B, respectively), an optical terminator (OT), and a tunable optical bandpass filter with low polarization dependence (OBPF, Santec OTF320) with a center transmission wavelength of λ_c. The GSEC consisted of an erbium-doped fiber (EDF) as the gain medium, and a wavelength-selective coupler WC-F as the input pump light. Additional coupler WC-B was mounted at the output to remove unwanted transmitted pump light for forward pumping. Isolators (ISOs) were set on both sides of EDF to reduce the influence of residual reflections. The input pump light was transmitted to the EDF via the WC-F for forward pumping. The F-GSE light generated in the EDF was emitted through the OBPF with a bandwidth of ~0.87 nm.

As shown in **Figure 5.2 (c)** example of a two-stage (TS-GSEC) configuration comprised of multiple cascaded EDF stages, denoted as EDF-1 and EDF-2. From point A to G, the first stage EDF-1 consists of a spool of EDF-1, two wavelength-selective couplers for forward and backward pumping (WC-F1 and WC-B1), and an intermediate optical filter (IOF). The second stage of EDF-2 comprises a spool, two wavelength-selective couplers for forward and backward pumping (WC-F2 and WC B2), the center wavelength of the OBPF, and an optical terminator (OT) from Point G to C. Either a short-wavelength pass filter (SWPF) or another optical bandpass filter (OBPF) of the same model used in the SS-GSEC is used as the IOF. A significant portion of the input light is absorbed by EDF-1, and the remaining light is transmitted to the second stage (EDF-2) through the WC-B1, point H, and WC-F2. We used three different EDF lengths (L_EDF) of 15.9, 18.0, and 20.4 m. The erbium-doped fiber (EDF)

exhibited a peak absorption coefficient at a wavelength of about 1530 nm, which was determined to be 6.3 dB/m. **Figure 5.2 (d),** the emulator consisted of LD-1 and LD-2, a polarization beam combiner (PBC), and a variable optical attenuator (VOA-E) after LD-2. In the LS section of **Figure 5.2 (a),** the emulator replaced the LDs, and the GSEC was used as a TS-GSEC, as detailed in Section 5.6.

5.4 Characteristics of Single-Stage GSEC

The single-stage GSEC (SS-GSEC) with a spool length of EDF 15.9 m or 20.4 m was investigated for the nonlinear relation between the input and output powers, P_{in} and P_{out}. The ambient temperature of the EDFs was finely maintained at a constant temperature of 25.0 ℃ by a temperature controller during the experiment. **Figure 5.2 (a)** shows a laser diode (LD) with λ_{in} of 1472.1 nm, which was employed as the input LS. The nonlinear input-output characteristics were obtained as the differential coefficient of P_{out} with respect to P_{in} in dBm, as follows [20,23,24].

$$S = \frac{dP_{out}}{dP_{in}} \cong \frac{\Delta P_{out}}{\Delta P_{in}} \tag{6}$$

Where ΔP_{in} and ΔP_{out} measurements are used to represent the incremental difference between P_{in} and P_{out}. The GSEC-strategy improvement factor (IF) measures the slope S, where the OPR can be improved or reduced by the slope (S).

Figure 5.3 shows the characteristics of experimental results obtained using a 15.9-m EDF. At point C, the output power (Pout) was measured using the OBPF shown in **Figure 5.2 (b)**. The optical bandpass filter (OBPF) center wavelength λ_c, was set wavelength of 1532.5, 1540, 1550, and 1560 nm, which aligned the output wavelength λ_{out} of the GSE light. The slope maximum (S_{max}) was achieved at the wavelength of 1532.5 nm [30]. The experimental results for the input power (P_{in}) were well fitted using fifth-order polynomial functions of output power (P_{out}) in the P_{in} vs. P_{out} plots, following the same approach as the ASEFC method [23,24]. Calculated and measured values of the output power (P_{out})

and slope (S) as a function of input power (P_{in}) at wavelength $\lambda_{c,}$ are shown by solid and dotted lines in **Figures 5.3 to 5.5**.

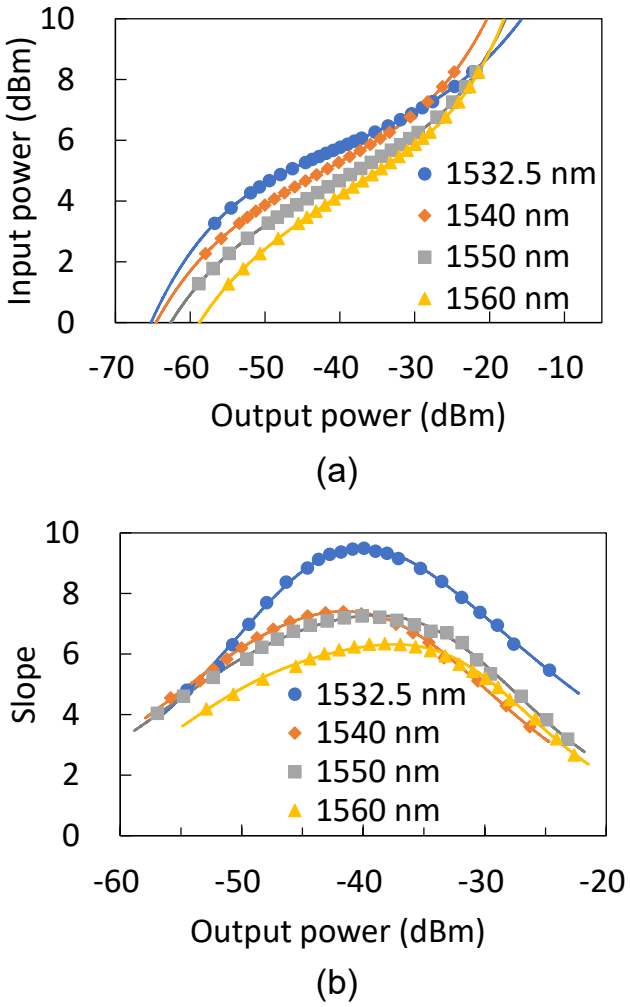

Figure 5.3. Input-output characteristics of the SS-GSEC with a 15.9-m EDF at the output wavelengths of 1532.5, 1540, 1550, and 1560 nm. (a) Input powers and (b) slopes as a function of the output power. Referring [33].

Using the data in **Figure 5.3 (a)** and Eq. (5), the measured and calculated values of slope (S) as a function of output power (P_{out}) are shown in **Figure 5.3 (b)**. The values of P_{in} and P_{out} in dBm at S_{max} are denoted as $P_{in\text{-}0}$ and $P_{out\text{-}0}$, respectively. The experimental values P_{in}, P_{out}, and S_{max} at λ_c values of 1532.5, 1540.0, 1550.0, and 1560.0 nm were (5.75 dBm, 5.08 dBm, 4.83 dBm, 4.60 dBm), (−40.12 dBm, −41.55 dBm, −38.99 dBm, −37.44 dBm), and (9.5, 7.4, 7.3, 6.3), respectively. Furthermore, we investigated the effects of using a 20.4-m EDF rather

than the 15.9 m EDF. Therefore, the maximum slope (S_{max}) at 1532.5 nm of approximately 11.9 was the maximum value of λ_{out} [30].

5.5 Characteristics of Dual-Stage GSEC

Based on the numerical simulation results, the maximum slope (S_{max}) was estimated to be limited to under approximately 15, despite increasing the EDF length the L_{EDF} of SS-GSEC is increased. However, by narrowing the transmission bandwidth of the IOF, the total length of EDF-1 and EDF-2 (L_{tot}=L_1+L_2) has increased. The maximum slope S_{max} TS-GSEC configuration values could be increased by more than about 20. As shown in **Figure 5.2 (c)**, the IOF was implemented using either a short-wavelength pass filter (SWPF) or another OBPF with a 3 dB transmission bandwidth of 0.87 nm, which was used as an OBPF set after point B. The transmitted wavelength through the SWPF was below approximately 1544 nm. Based on this investigation, four TS-GSEC configurations (TS1-TS-4) are tested TS-1, -2, -3, and -4. The detailed configuration were assigned by (L_1, L_2, L_{tot}; IOF) of (18.0m, 15.9m, 33.9m; with SWPF for TS-1), (18.0 m, 15.9m, 33.9m; without IOF for TS-2), (20.4m, 15.9m, 36.3m), and (15.9m, 20.4m, 36.3m), with OBPF for TS-3 and TS-4, respectively.

The output wavelengths λ_{out} were set to the center wavelength of 1532.5 nm. Only an EDF-1 and EDF-2 for TS-1 and TS-2, and TS-3 and TS-4 were implemented within the temperature-control module, which was maintained at 25.0°C and 20.0°C. LD-1 was used for TS-3 and TS-4 with 1477.7 nm, whereas LD-2 was used for TS-1 and TS-2 with 1472.1 nm. The input-output characteristics of TS-1 are experimentally obtained in [30]. The obtained values for $P_{in\text{-}0}$, $P_{out\text{-}0,}$ and S_{max} values of the TS-1 configuration with the values were 13.15 dBm, −44.40 dBm, and 22.8, respectively. On the other hand, for TS-2 without the SWPF, the measured values were 10.62 dBm, −57.46 dBm, and 8.0, respectively. Therefore, the result indicates that the maximum slope (S_{max}) value significantly increases from approximately 8.0 to 22.8.

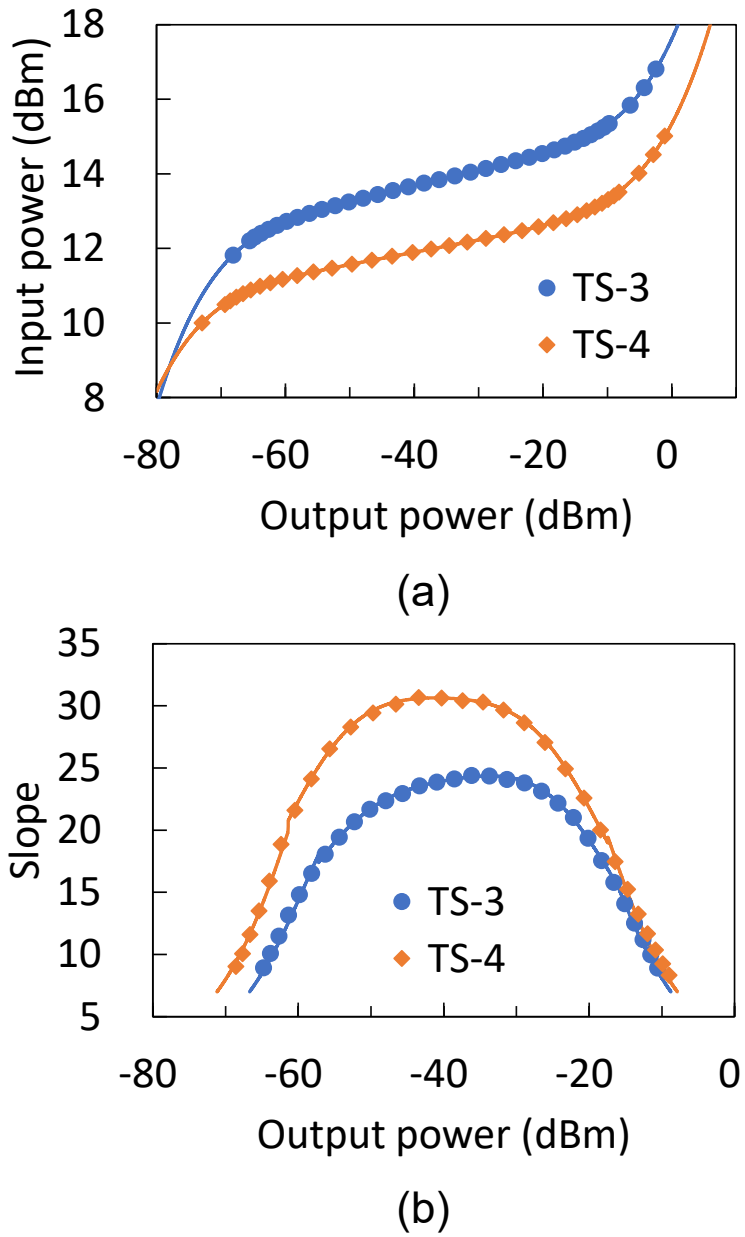

Figure 5.4. (a) Input powers and (b) slopes as a function of the output power for TS-3 and -4. function of the output power. Referring [33].

Figure 5.4 (a) and **(b)** show the input power (P_{in}) and slope (S) as a function of output power (P_{out}) for TS-3 and TS-4, respectively. For TS-3, the corresponding values for $P_{in\text{-}0}$, $P_{out\text{-}0}$, and S_{max} were 13.95 dBm, -33.62 dBm, and 22.4, respectively. In the case of TS-4 where the values were 11.86 dBm, −41.13 dBm, and 30.6, respectively. Furthermore, for TS-4, the LD-2 (λ_{in} = 1472.1 nm) was utilized instead of LD-1 (λ_{in} = 1477.7 nm), which became 11.86

dBm, −40.45 dBm, and 29.0, respectively. The input-output characteristics of the bidirectional pumping cases for TS-4 were also investigated.

The input optical signal emitted through WC-B1 from Point H was launched into Point I of WC-B2. The measured values of input optical power ($P_{\text{in-0}}$), output optical power ($P_{\text{out-0}}$), and slope maximum ($S_{\max}$) were 12.92 dBm, −19.97 dBm, and 17.7, respectively. Figure 5.4(b), the maximum slope ($S_{\max}$) of the forward pumping case is significantly higher than that of the bidirectional pumping condition. In particular, the forward-pumped TS-4 employing LD-1 at an input wavelength (λ_{in}) of 1477.7 nm achieved the maximum slope ($S_{\max}$) among all measured and calculated cases. The optimized TS-4 configuration employing LD-1 demonstrated stable input-output power repeatability during the 50-minute period, which was consistent with the case of ASEFC [23,24]. **Figure 5.5** shows the output pump powers at Points H and I of **Figure 5.2 (c)** (P_{p1} and P_{p2}, respectively) as functions of the input pump power at Point A, P_{in}, in the case of TS-4 with 15.9- and 20.4-m EDFs connected in series. The slope (S) from **Figure 5.4** were also shown as a function of P_{in} in **Figure 5.5**. Each of the two outputs, power P_{p1} and P_{p2}, increases when increasing P_{in}, with P_{p1} ranging from 3.3 to 7.0 dBm and P_{p2} ranging from −27.9 to −10.5 dBm when slope S is greater than 10.

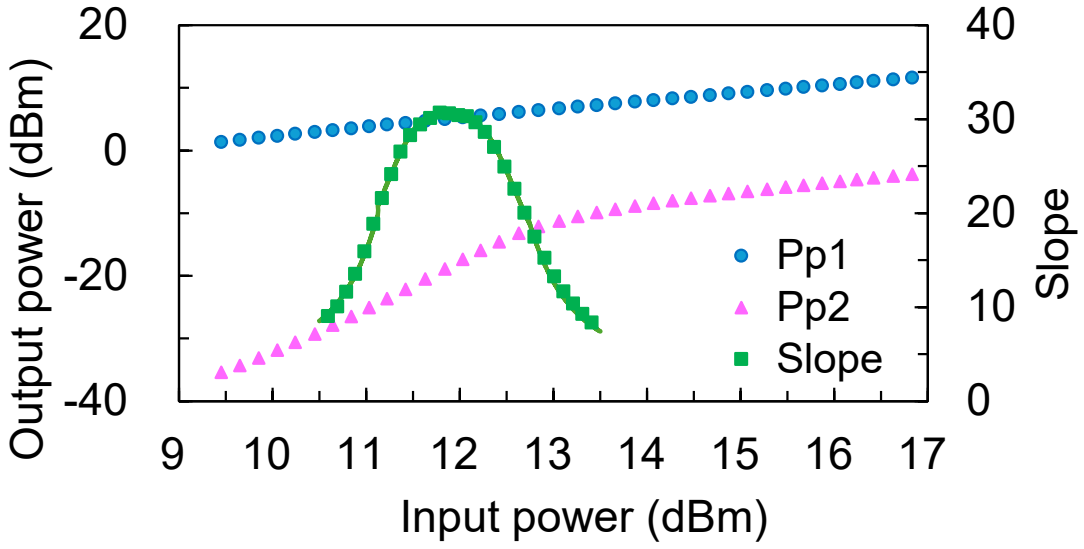

Figure 5.5. Output powers of the pump as a function of the input power

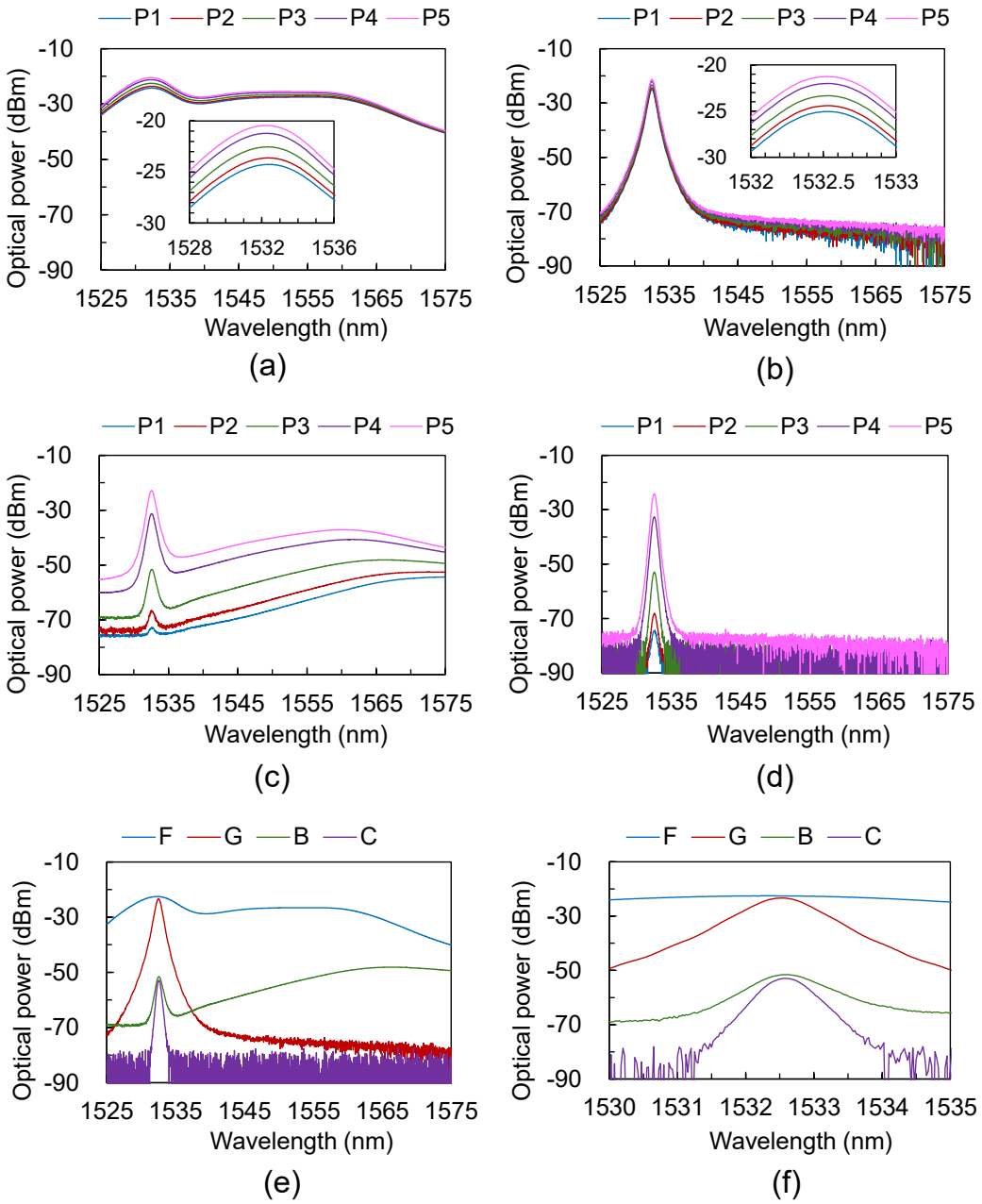

Figure 5.6. (a) Output spectra at points F, G, B, and C of TS-4 in (a), (b), (c), and (d), respectively. (e) Output spectra at operating point P3, and (f) detailed parts of (e) around 1532.5 nm. Referring [33].

Five sets of experimental operating condition values (P_{in}, S) are denoted as P1-P5, where the experimental values of slope S were approximately 15, 25, 30.6 (peak value), 25, and 15 for the five points, respectively.

The output power spectra of TS-4 at operating points P1 to P5 were measured by OSA and are shown in **Figure 5.6**. The optical spectra measured at Points in **Figure 5.2 (c) F, G, B,** and **C** are shown in **Figure 5.6 (a), (b), (c),** and **(d)**, respectively. **Figure 5.6 (e)** shows the optical spectra measured at Points F, G, B, and C at the operating point P3, where S corresponds to the maximum value, and insets highlighting finer spectral details.

Furthermore, **Figure 6 (f)** provides a detailed view of the spectra of **Figure 5.6 (e)** around the peak wavelength of 1532.5 nm, highlighting the differences among operating points P2 to P4. In **Figure 5.6 (c)**, in contrast, at the same wavelength, the corresponding power difference was approximately 36 dB. As shown in **Figure 5.6 (f)**, at Point B, we found the measured output power at 1532.5 nm approximately 28 dB lower than that at Point G. This indicates that the optical power at Point G was substantially attained at the level observed at Point B within the second EDF of 20.4 m. The 3-dB bandwidth of the output at Point C was determined to be 0.59 nm in wavelength ($\Delta\lambda$3dB) or 75 GHz in frequency ($\Delta\nu$3dB). The small-signal gain (Gf) of TS-4 at 1532.5 nm an input optical power of approximately −45 dBm. The measured fictitious gain (G_f) values were 28.5, −25.4, and 3.1 dB, from Point D to G, Point G to C, and Point D to C.

5.6 OPR Improvement Characteristics

The emitted optical power from the emulator (P_e), mW, can be mathematically expressed as $P_e = P_1 + LP_2$, where L represents the linear loss of VOA-E, not including insertion loss. The corresponding loss L, expressed in decibels (dB), is given by $10\cdot\log_{10}(L)$. In other words, L quantitatively represents the proportion of optical power transmitted through the VOA-E after experiencing controlled attenuation. The optical powers of the light emitted from LD-1 and LD-2 are denoted by the parameters P_1 and P_2, respectively, when $L = 1$ at the emulator output. The total emitted optical power from the emulator, represented by ΔP_e with the reference power of Pe when $L = 1$ ($P_{e0} \equiv P_1 + P_2$), is expressed as follows:

$$\Delta P_e = \frac{P_e}{P_{e0}} = \frac{R+L}{R+1} \tag{7}$$

In this analysis, R represents the ratio of the optical power emitted from LD-1 to that emitted from LD-2, expressed as P_1 to P_2 (R = P_1 / P_2), and was calculated value determined as (29.0 dB) in logarithmic scale. Based on the relationship described in Eq. (7), ΔPe is expressed as a linear function of the attenuation factor L. The input power, P_{in}, was observed to be lower than the emitted power, P_e, expressed in dBm ($10 \cdot \log10(P_e)$), due to the loss of approximately 8.8 dB coupling loss between the output point of the emulator and Point A of **Figure 5.2(a)**. The corresponding input power was 11.66 dBm, when $P_e = P_{e0}$

The output light from the emulator was launched into the forward-pumped TS-4. Thereafter, the attenuation factor L was adjusted through VOA-E change P_e according to Eq. (6). A fifth-order polynomial function was used to estimate the input optical power P_{in}, which could be calculated from P_{out}. Based on this investigation, P_e and ΔP_e could be determined as L varied. TS-4 was carefully operated around the maximum slope, with S calculated from the polynomial fitting, which was approximately 30.6.

The variation of ΔP_e as a function of L is shown in **Figure 5.7 (a)**. In the figure, the symbols and straight line in the figure represent the measured values ($\Delta P_{e\text{-}m}$), while the solid line represents the values calculated ($\Delta P_{e\text{-}c}$) using Eq. (6). **Figure 5.7 (b)** shows the correlation between the experimentally measured variations ΔPe-m as a function of $\Delta P_{e\text{-}c}$ for the three steps of the attenuation factor L. In the ideal case, where the measured variations $\Delta P_{e\text{-}m}$ equals $\Delta P_{e\text{-}c}$. The slope and intercept of the straight line representing the relationship would theoretically have a slope of 1 and an intercept of 0. As shown in **Figure 5.7 (b)**, the slope and intercept in the obtained fitting results were 1.004 and 1.007x10-3 milli dB (mdB),

respectively. In addition, the standard deviation of the differences between the measured (ΔPe-m) and calculated $\Delta P_{e\text{-}c}$ values is approximately 0.091 mdB.

Upon detailed observation, the output power (P_{out}) exhibited minor temporal fluctuation, although the light exhibited a significant Δv3dB of 75 GHz, with no polarization as previously described. The output optical power (P_{out}) was used to measure PD_{out} with an average time of

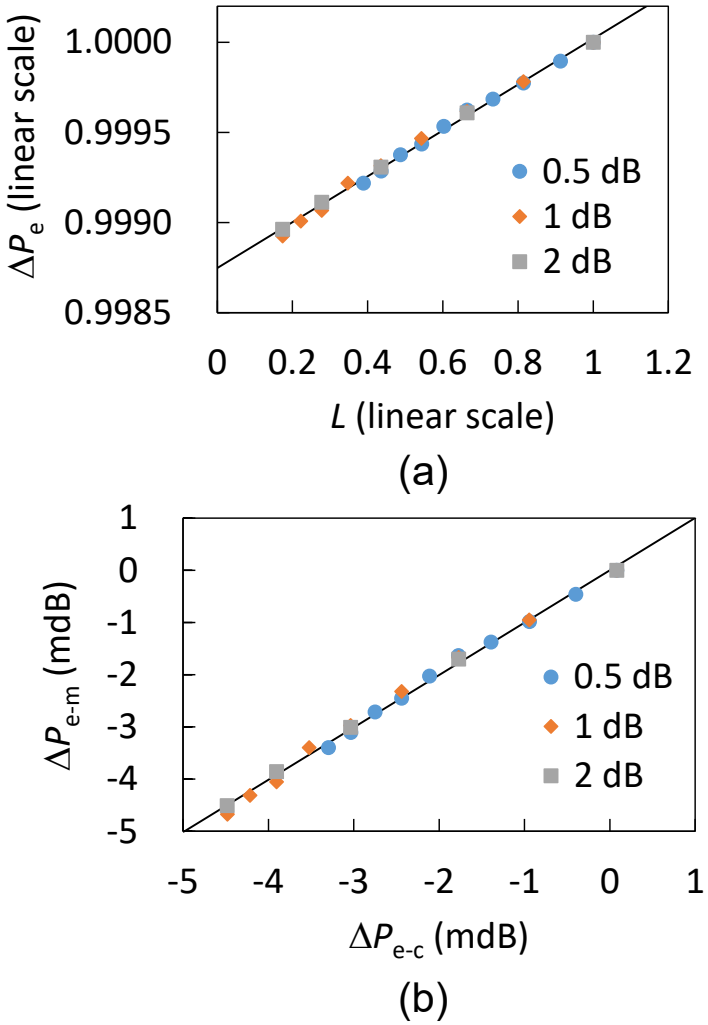

Figure 5.6. (a) Variations in the output power from the emulator (ΔPe) as a function of the loss of VOA-E (L), and (b) the measured power variation (ΔPe-m) as a function of the calculated power variation (ΔPe-c). Referring [33].

5s to minimize fluctuation and improve measurement stability. The output power P_{out}exhibited a peak-to-peak time variation of approximately 10 mdB, with the corresponding

width of $\Delta P_{\text{out-T}}$ over a measurement of approximately 1 min. This fluctuation was mainly caused by time-dependent variations in the emulator output power (P_{out}), defined as ($\Delta P_{\text{e-T}}$), and amplified by TS-4 by slope (S) of approximately 30.6, leading to an estimated value of $\Delta P_{\text{e-T}}$ of approximately 0.33 mdB. The emulator employed two Fabry–Perot laser diodes, LD-1 and LD-2, their output powers were expected a minimal degree of temporal variation in their output powers. Based on the measured value of $\Delta P_{\text{out-T}}$ (approximately 10 mdB) and considering that this value was evaluated against the typical OPR offered by conventional power meters, as discussed in Section 1, the OPR achieved by utilizing the forward-pumping cases of TS-4 was approximately 0.33 mdB.

5.7 Conclusion of the Study

This study proposed a novel guided spontaneous-emission (GSEC) technique to significantly improve the OPR in the optical power variation measurement system. Experimental results were conducted on both SS-GSEC and TS-GSEC, with particular emphasis on analyzing their optical input-output and slope characteristics. We significantly achieved the maximum slopes (S_{max}) at output wavelength λ_{out} of 1532.5 nm under a forward pumping configuration, which indicates OPR enhancement. The SS-GSEC with a 20.4-m EDF achieved a maximum slope (S_{max}) of approximately 11.9. On the other hand, compared to the SS-GSEC, the TS-GSEC achieved a significantly higher maximum slope (S_{max}) value of approximately 30.6, with a total EDF length (L_{tol}) of 36.3 m. Moreover, to achieve accurate spectral control in the experiment, the intermediate optical filter (IOF) was realized using the OBPF with a 3-dB bandwidth of 0.87 nm, with an input light wavelength λ_{in} of 1477.7 nm. Furthermore, to evaluate the effectiveness of the performance of the proposed GSEC technique, the OPR improvement characteristics were used as an emulator to simulate small variations in input power. The results confirm an improved OPR of approximately 0.33 mdB, based on an initial OPR of 10 mdB for the PDM set following TS-4.

6 Investigation of the Guided Spontaneous-Emission Circuit Using Numerical Simulation

6.1 Theory of the GSEC

Figure 6.1 shows the basic configuration of the GSEC technique. **Figure 6.1 (a)** configuration using a single-stage EDF (single-stage EDF configuration). **Figure 6.1 (b)** shows a dual-stage configuration with an optical filter between two EDFs (dual-stage EDF configuration). The GSEC consisted of an erbium-doped fiber (EDF) as the gain medium, and a wavelength-selective coupler WC-F as the input pump light. Forward- and backward-.

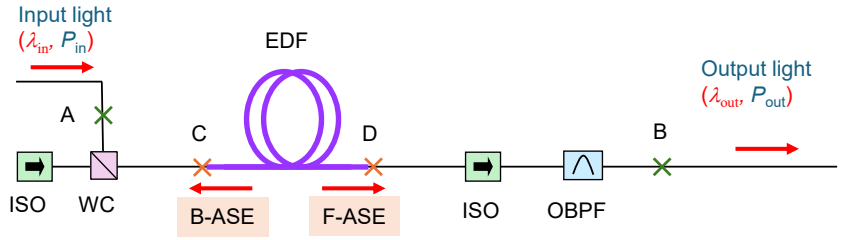

(a)

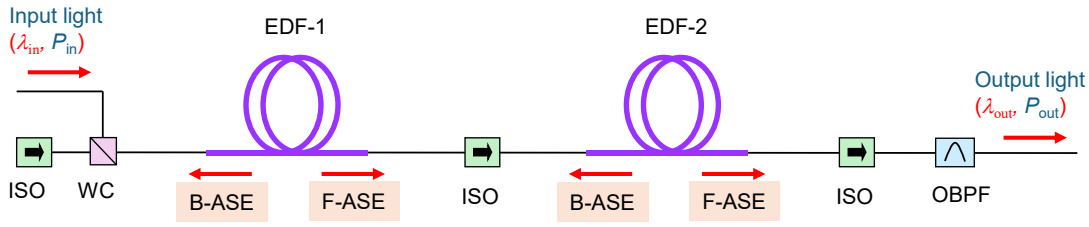

(b)

Figure 6.1. Basic configuration of a Guided Spontaneous-Emission Circuit (a) single-stage EDF configuration (b) dual-stage EDF configuration. Referring [33].

Pumping cases of (F-GSE and B-GSE, respectively) are formed within EDF. The input pump light was transmitted to the EDF via the WC-F for forward pumping. The F-GSE is output via a forward optical isolator (ISO) and a narrowband optical filter (OBPF). Forward GSE emitted from the EDF passes the optical bandpass filter (OBPF). On the other hand, the dual-stage EDF configuration, the pump light moves through the first EDF (EDF-1) and pumps the second EDF (EDF-2) via the WC-F. For the investigation of numerical simulation,

calculations were performed using the configuration in the dual-stage EDF shown in **Figure 6.1 (b)**. The backward pumping case (B-GSE) from the second EDF stage (EDF-2) is blocked by an optical isolator (ISO) installed in the middle stage, suppressing the growth of the backward pumping (B-GSE) in the first EDF stage (EDF-1). Here, the input pump power is (P_{in}) and the output pump power is (P_{out}).

6.2 Numerical Simulation Results of the 1st study

The simulation results are shown below. In this numerical study report, the approximate model shown in **Figure 6.1** uses an optical input wavelength λ_{in} of approximately 1470, 1480, 1490, 1510, 1520, 1530, 1540, and 1550 nm and an optical output wavelength λ_{out} of 1560 nm. **Figure 6.2 (a)** and **(b)** shows the dependence of output optical power and slope on input optical power for the case where λ_{in} = 1470 and 1480 nm and λ_{out} = 1560nm.

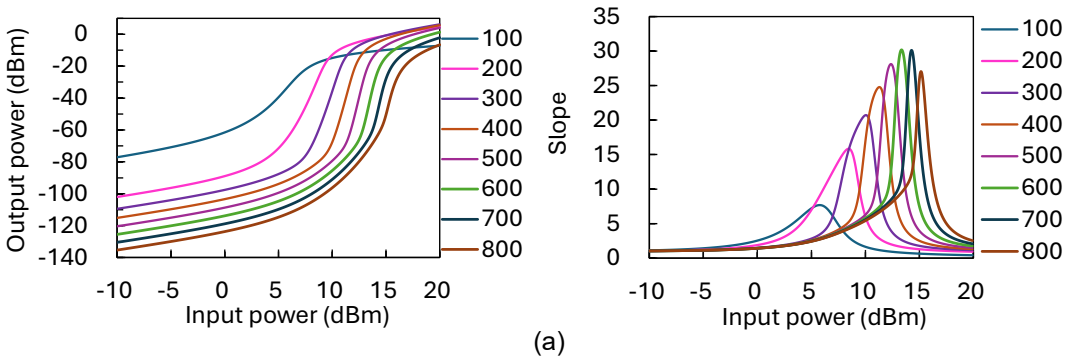

(a)

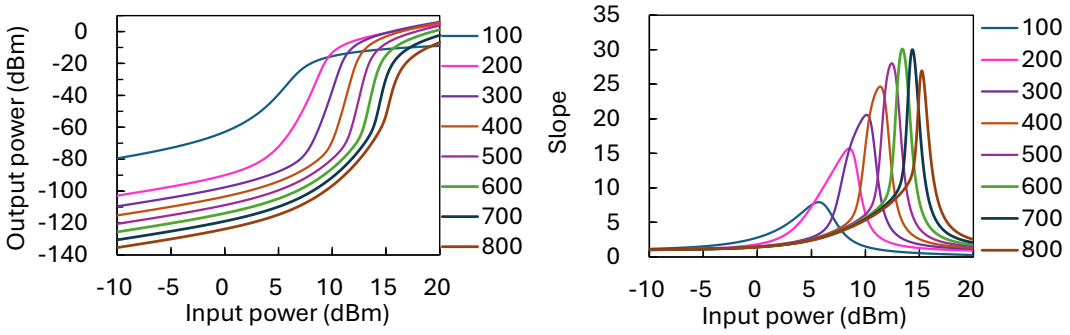

(b)

Figure 6.2. Input/output optical power characteristics at λ_{out} = 1560nm and λ_{in} = (a) 1470 nm, (b) 1480 nm. The figures in the left and right columns show the output powers and slopes according to the input optical power.

The peak loss A_{peak} value varied from 100 to 800 dB separation of 100 dB. From the dependence of the maximum slope (S_{max}) on A_{peak}, we derived S_{max} for each evaluated λ_c. The simulation values (P_{in}, P_{out}, S_{max}) at λ_c values of 1470, and 1480 nm were (13.40 dBm, −44.36 dBm, 30.18), (13.50 dBm, −43.67 dBm, 30.09).

Figure 6.3 (a), (b), and **(c)** show the dependence of output optical power and slope on input optical power for the case where λ_{in} = 1490, 1510, and 1520 nm and λ_{out} = 1560nm. The peak loss A_{peak} value varied from 100 to 800 dB separation of 100 dB.

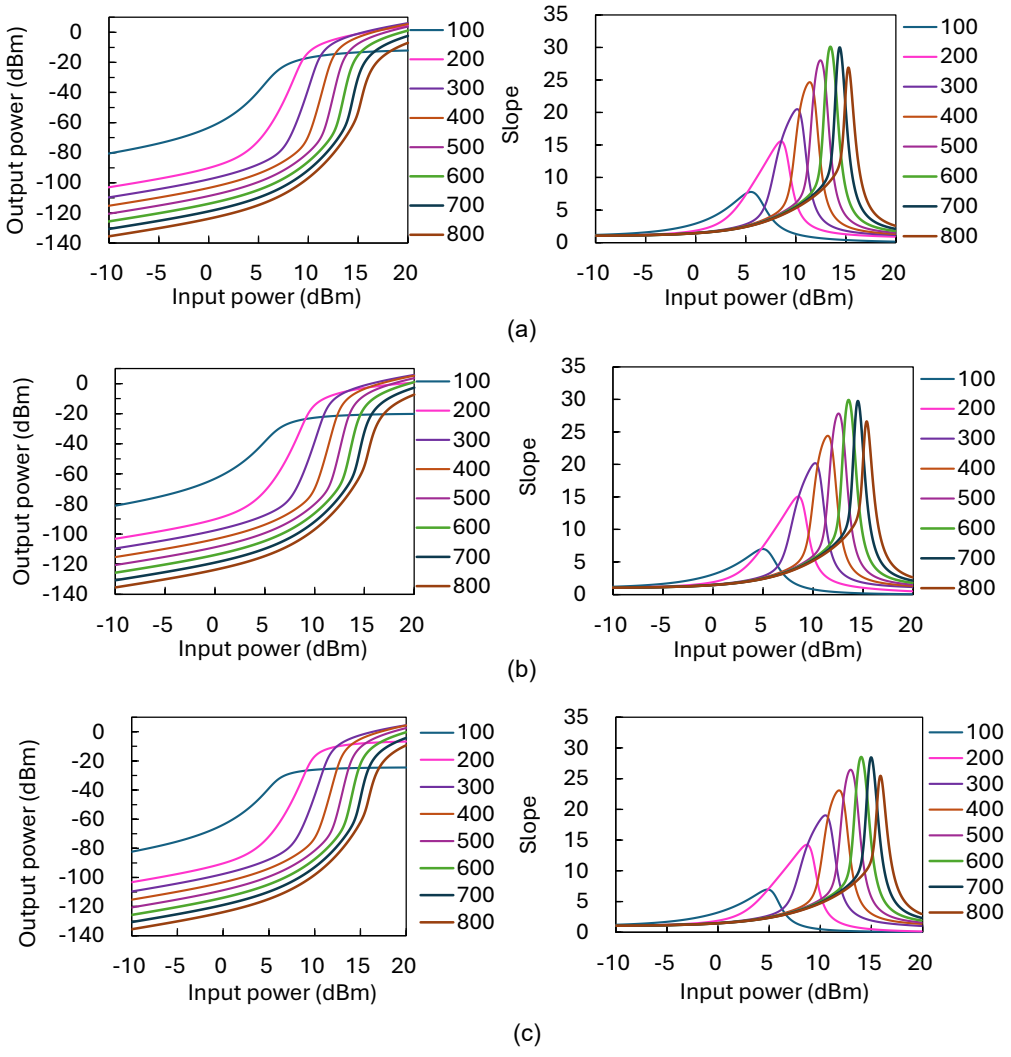

Figure 6.3. Input/output optical power characteristics at λ_{out} = 1560nm and λ_{in} = (a) 1490 nm, (b) 1510 nm, (c) 1520 nm. The figures in the left and right columns show the output powers and slopes according to the input optical power.

From the dependence of the maximum slope (S_{max}) on A_{peak}, we derived S_{max} for each evaluated λ_c. The experimental values (P_{in}, P_{out}, S_{max}) at λ_c values of 1490, 1510, and 1520 nm were (13.50 dBm, −44.58 dBm, 30.10), (13.60 dBm, −44.01 dBm, 29.09), and (14.10 dBm, −44.56 dBm, 28.53). **Figure 6.4 (a), (b),** and **(c)** shows the dependence of output optical power and slope on input optical power for the case where λ_{in} = 1530, 1540, and 1550 nm and λ_{out} = 1560 nm. The peak loss A_{peak} value varied from 100 to 800 dB separation of 100 dB.

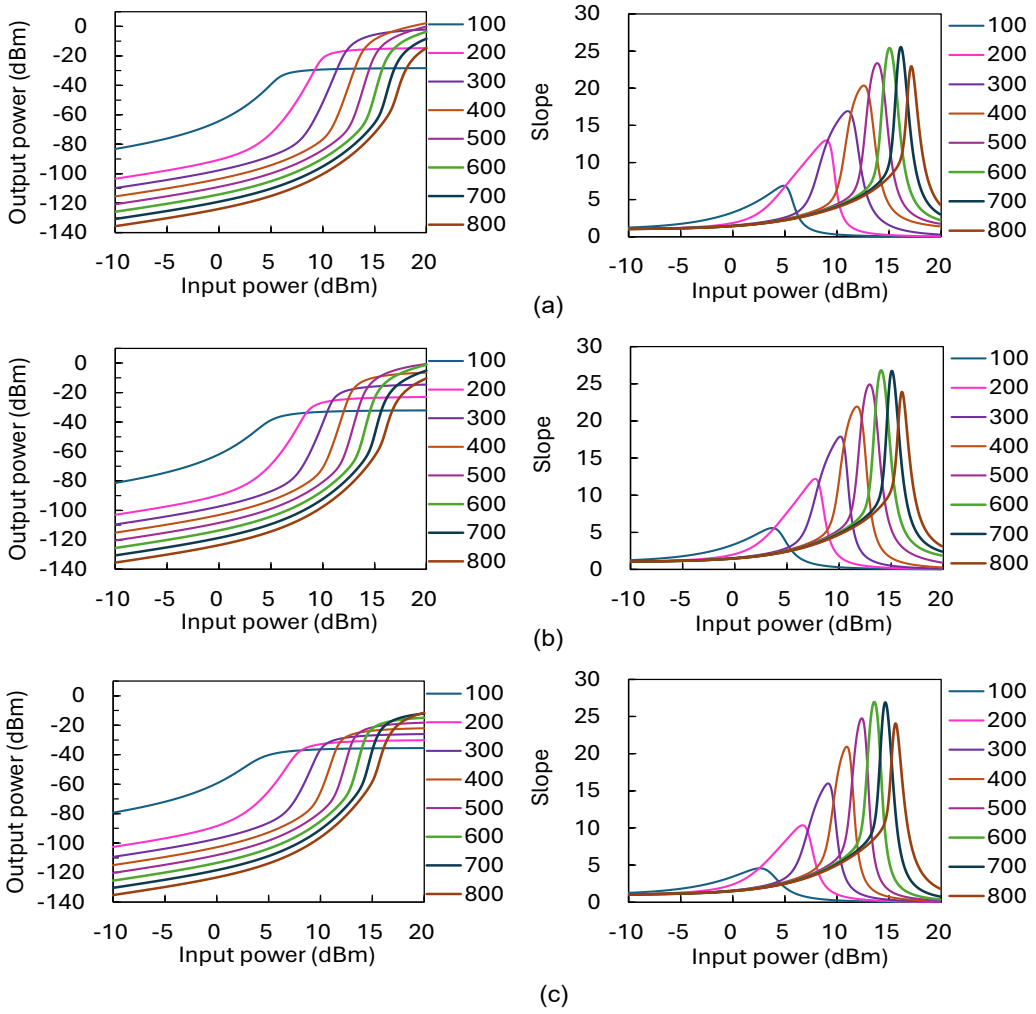

Figure 6.4. Input/output optical power characteristics at λ_{out} = 1560 nm and λ_{in} = (a) 1530 nm, (b) 1540 nm, (c) 1550 nm. The figures in the left and right columns show the output powers and slopes according to the input optical power.

From the dependence of the maximum slope (S_{max}) on A_{peak}, we derived S_{max} for each evaluated λ_c. The experimental values (P_{in}, P_{out}, S_{max}) at λ_c values of 1530, 1540, and 1550 nm

were (16.20 dBm, −21.51 dBm, 25.52), (14.10 dBm, −44.30 dBm, 26.80), and (13.65.10 dBm, −44.58 dBm, 26.95).

6.3 Numerical Simulation Results of the 2nd study

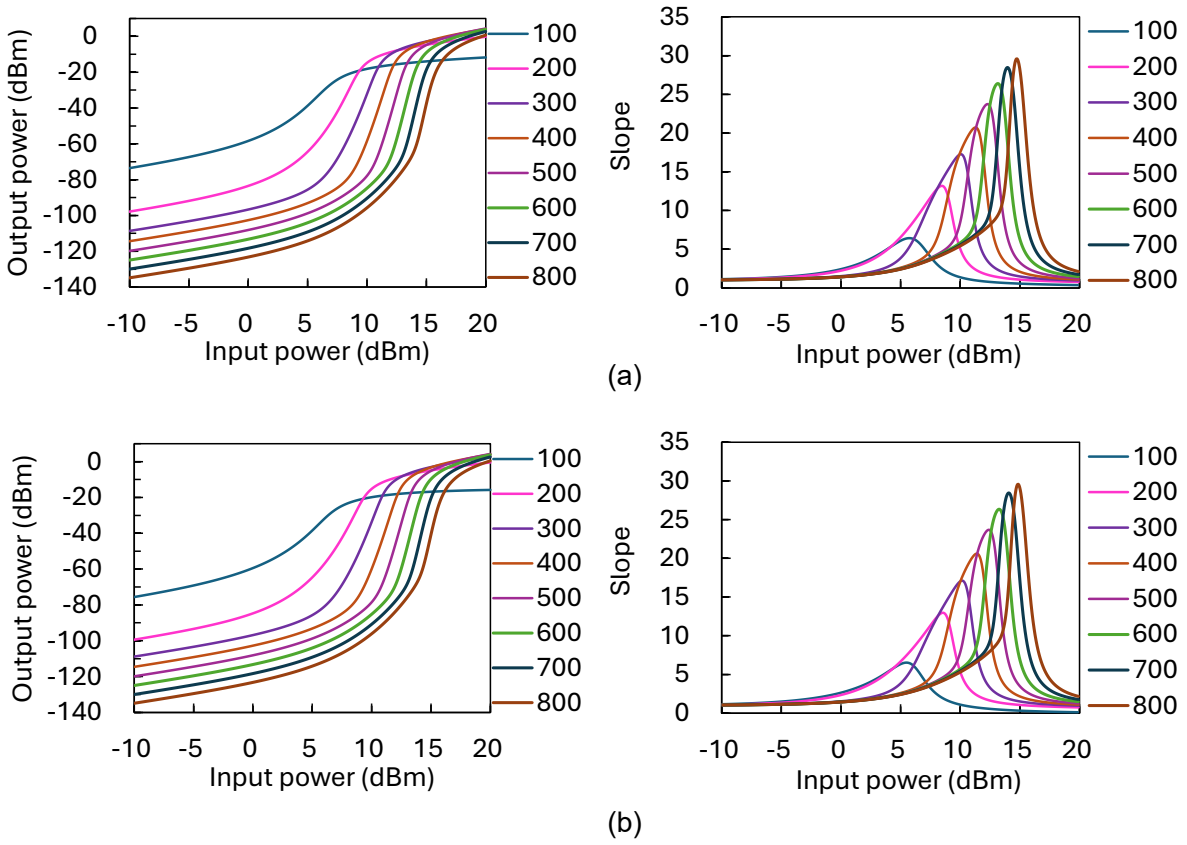

Figure 6.5. Input/output optical power characteristics at λ_{out} = 1565 nm and λ_{in} = (a) 1470 nm, (b) 1480 nm. The figures in the left and right columns show the output powers and slopes according to the input optical power.

The simulation results are shown below. In this numerical study reports, the approximate model shown in **Figure 6.1** uses an optical input wavelength λ_{in} of approximately 1470, 1480, 1490, 1510, 1520, 1530, 1540, and 1550 nm and an optical output wavelength λ_{out} of 1560 nm. **Figure 6.5 (a)**, and **(b)** shows the dependence of output optical power and slope on input optical power for the case where λ_{in} = 1470 and 1480 nm and λ_{out} = 1565nm. The peak loss A_{peak} value varied from 100 to 800 dB separation of 100 dB. From the dependence of the maximum slope (S_{max}) on A_{peak}, we derived S_{max} for each evaluated λ_c. The simulation values

(P_{in}, P_{out}, S_{max}) at λ_c values of 1470 and 1480 nm were (14.80 dBm, −43.58 dBm, 29.58), (14.85 dBm, −44.43 dBm, 29.53).

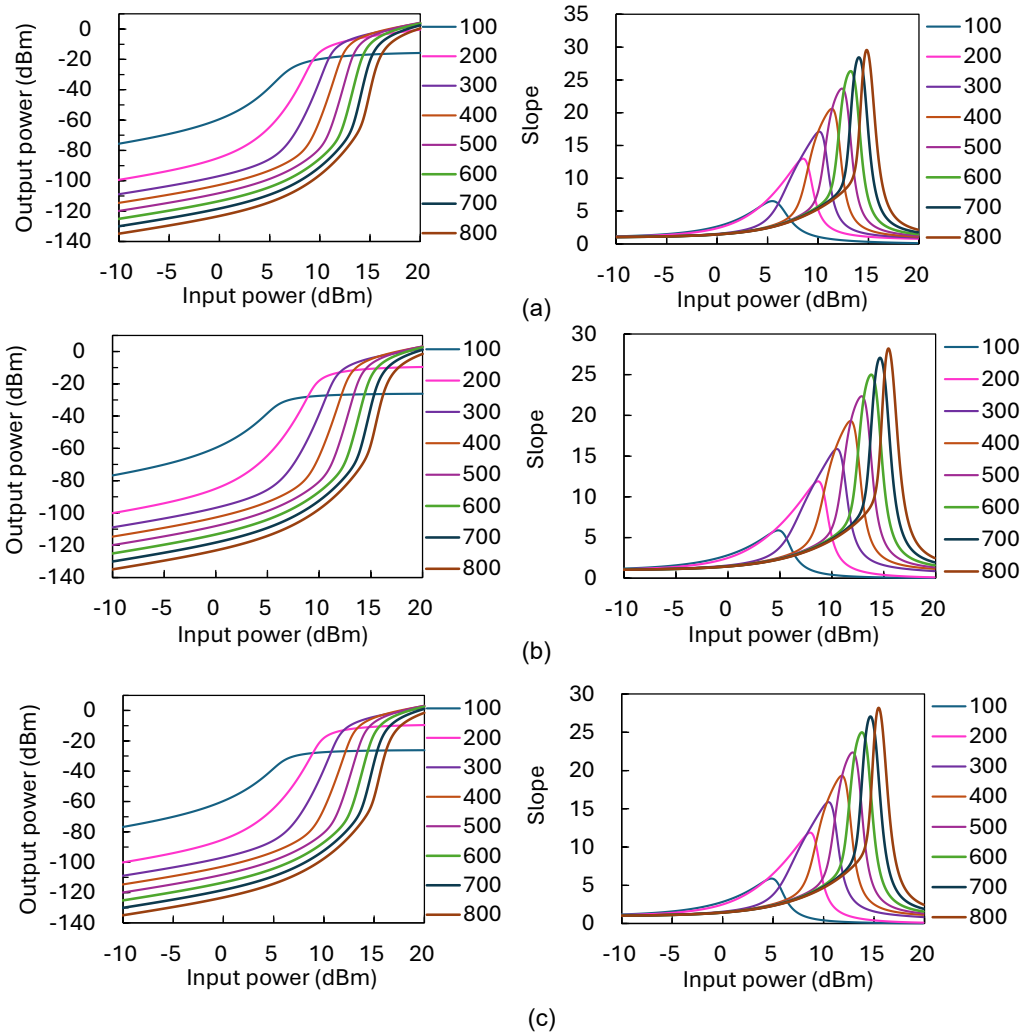

Figure 6.6. Input/output optical power characteristics at λ_{out} = 1565 nm and λ_{in} = (a) 1490 nm, (b) 1510 nm, (c) 1520 nm. The figures in the left and right columns show the output powers and slopes according to the input optical power.

Figure 6.6 (a), (b), and **(c)** shows the dependence of output optical power and slope on input optical power for the case where λ_{in} = 1490, 1510, and 1520 nm and λ_{out} = 1565nm. The peak loss A_{peak} value varied from 100 to 800 dB separation of 100 dB. From the dependence of the maximum slope (S_{max}) on A_{peak}, we derived S_{max} for each evaluated λ_c. The experimental

values (P_{in}, P_{out}, S_{max}) at λ_c values of 1490, 1510 and 1520 nm were (14.90 dBm, −43.78 dBm, 29.54), (14.95 dBm, −44.78 dBm, 29.28) and (15.50 dBm, −44.14 dBm, 28.02).

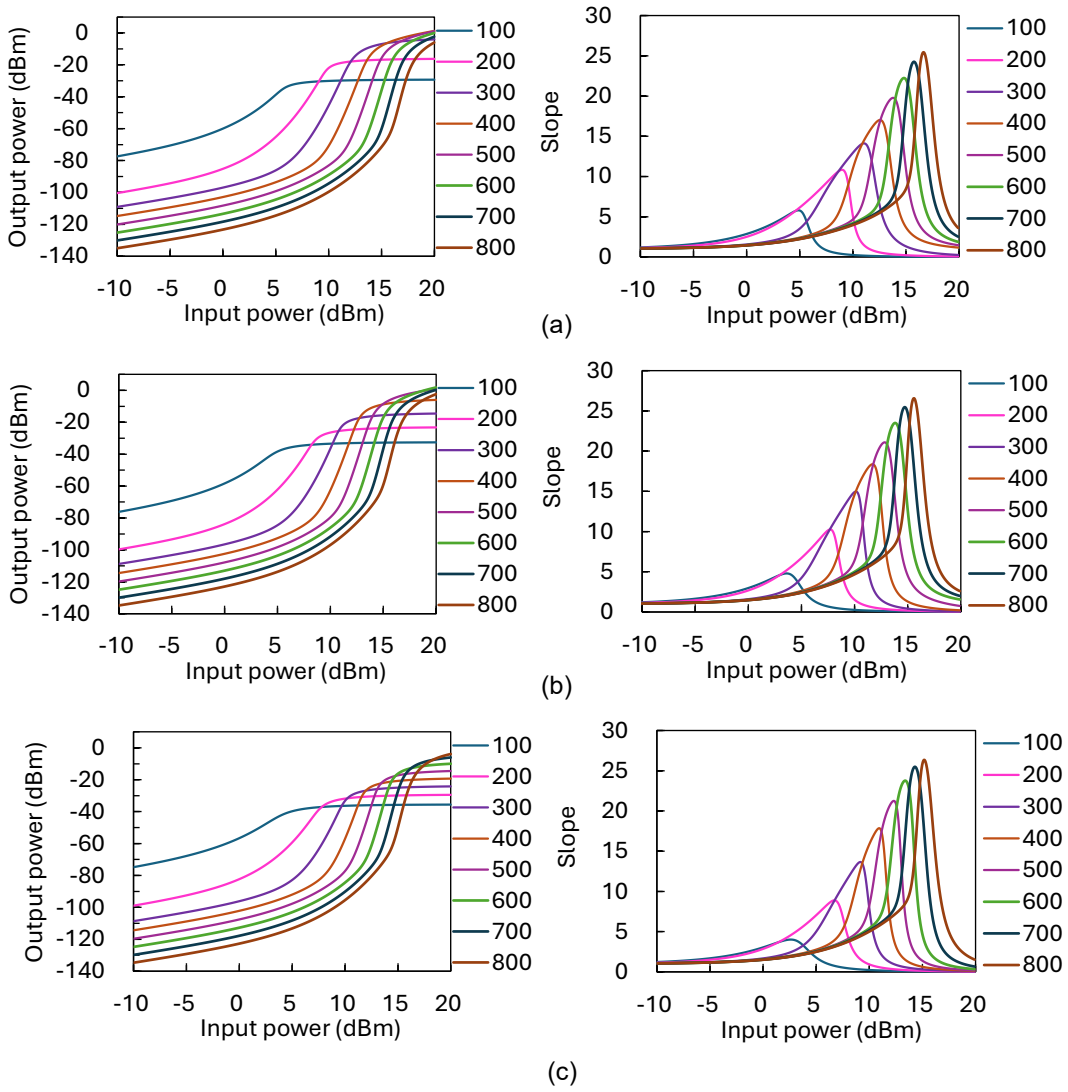

Figure 6.7. Input/output optical power characteristics at λ_{out} = 1565 nm and λ_{in} = (a) 1530 nm, (b) 1540 nm, (c) 1550 nm. The figures in the left and right columns show the output powers and slopes according to the input optical power.

Figure 6.7 (a), (b), and **(c)** shows the dependence of output optical power and slope on input optical power for the case where λ_{in} = 1530, 1540, and 1550 nm and λ_{out} = 1565nm. The peak loss A_{peak} value varied from 100 to 800 dB separation of 100 dB. From the dependence of the maximum slope (S_{max}) on A_{peak}, we derived S_{max} for each evaluated λ_c. The experimental

values (P_{in}, P_{out}, S_{max}) at λ_c values of 1530, 1540, and 1550 nm were (16.17 dBm, −43.88 dBm, 25.43), (14.10 dBm, −43.61 dBm, 15.65), and (15.25 dBm, −43.36 dBm, 26.33).

6.4 Wavelength-Dependence Performance Characteristics of the GSEC

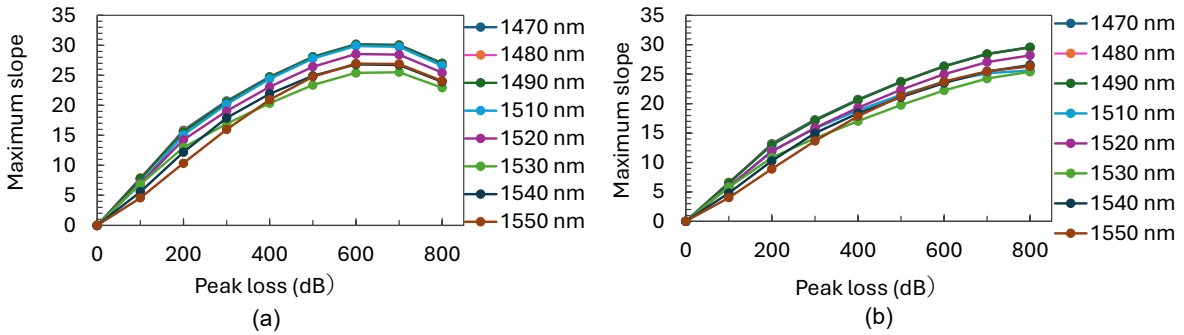

Figure 6.8 Peak loss Dependence of Maximum Slope Condition (a) λ_{out} = 1560 nm (b) λ_{out} = 1565 nm.

Figure 6.8 (a), (b) shows the calculation results on the peak loss dependence of the maximum slope for output wavelength of 1560 and 1565 nm corresponding to the results in **Figures 6.2-6.7**. At output wavelengths of 1560 nm and 1565 nm, the maximum slope reaches 30.18, 29.58, when the A_{peak} value of 600 and 800 dB, which is the S band. Meanwhile, at 1540 and 1550 nm, in the latter half of the C-band, in λ_{out} at 1560 nm, S_{max} values are 26.8 and 26.95, respectively, which are lower than the S-band. Similarly, in the case of the λ_{out} at 1565 nm, Smax values are 26.57 and 26.34, respectively, which are also lower than the S-band. Furthermore, unlike the other wavelengths, the case of 1530 nm exhibits the lowest S_{max} value above 300 dB, demonstrating poor performance.

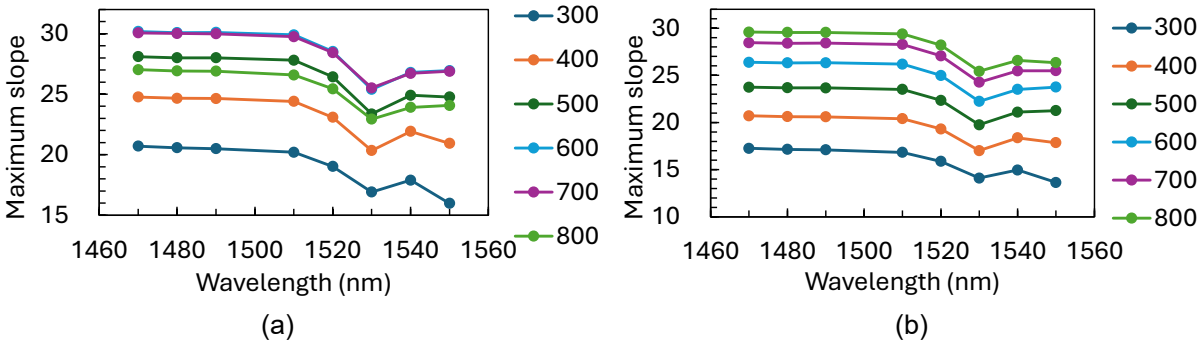

Figure 6.9. Peak loss Dependence on Input Wavelength Under the Maximum Slope Condition (a) λ_{out} = 1560 nm (b) λ_{out} = 1565 nm.

Figure 6.9 (a), **(b)** shows the calculation results on the Peak loss dependence on input wavelength under the Maximum Slope Condition at output wavelength of 1560 and 1565 nm, corresponding to the results in **Figure 6.2- 8.7**. These figures are constructed based on **Figure 6.8 (a)** and **(b)** using Apeak values excluding 100 and 200 dB. The results indicate that the maximum slope (S_{max}) begins to decrease at A_{peak} values of 700 and 800 dB for input wavelengths of 1520 and 1540 nm in both cases. These changes are considered to be a significant change in the cross-section peak. The S_{max} value is lower than the values observed below 1520 nm between 1540 and 1560 nm range in **Figure 6.9 (a)** and **(b)**. Across a broad wavelength range S_{max} value changed with minor wavelength dependence, except in the region around 1530 nm. This suggests that pumping wavelengths other than the conventional 1480 nm band used for EDFs could also be feasible. Overall, the results demonstrate that the output wavelength 1565 nm is considered the maximum slope, more stable, and significantly improves the optical power resolution.

6.5 Conclusion of the Study

This study presented the numerical simulation results of the guided spontaneous emission circuit (GSEC) and clarified the input wavelength dependency characteristics. This numerical simulation was conducted with the input wavelength in the S band and lower C band (1470–1550 nm), employing output wavelengths at 1560 nm and 1565 nm. We considered variations of the peak loss (A_{peak} = 100-800 dB) in 100 dB increments. We evaluate the system performance on the maximum slope (S_{max}) and output power (P_{out}) under different excitation conditions of the GSEC. The numerical results demonstrated that for output wavelength at 1560 nm increase the maximum slope increases by 28-30 and 25-27 at input wavelength (1470-1490) and (1530-1550). In contrast, the output wavelength at 1565 nm maximum slope

slightly lower than 1560 nm. These behaviors are affected by the spectral overlap because of the absorption cross-section and the stimulated emission cross-section, indicating reduced pumping efficiency at longer wavelengths. The output wavelength of 1560 nm achieved high performance at lower input power, whereas 1565 nm demonstrated enhanced stability of output power across a broader input wavelength range. Therefore, the output wavelength of 1565 nm enhanced optical power resolution and enhanced stability of the output power.

7 Pumping Direction Dependence of the Guided Spontaneous-Emission Circuit

7.1 Introduction

In this study, we have proposed and investigated an optical power measurement technique that can significantly improve the OPR, where the technique implements an amplified-spontaneous-emission feedback circuit (ASEFC) placed in front of the PM and called the ASEFC technique [13, 14, 15, 18, 20, 23, 24, 25]. Improvement factors (IFs) in the OPR up to 23 were experimentally confirmed, so that the resultant OPRs of the technique are estimated to be 0.44 mdB (0.00044 dB) and 0.044 mdB when we assume the resolutions of the PM equal 10 mdB and 1 mdB, respectively, for example.

In this paper, we investigate the pumping direction dependence on the performance of the GSEC for the first time. Experimental results are successful compared with the numerical simulation results. We also clarify that the IFs, the slope in the input and output optical power relation of the GSEC, are much higher for the forward pumping configuration than for the backward pumping configuration.

7.2 System Configuration

The experimental setup of the forward and backward pumping cases of the GSEC technique is schematically shown in **Figure 7.1 (a)** and **(b)**. The setup consists of a light source (LS), the GSEC, and a measurement section. We used a Fabry-Perot pump diode module as the LS.

The input and output points of the GSEC are labeled as points A and B, respectively. The power-averaged wavelength of the LS was 1472.0 nm. The lights propagating in the EDF are the input and output signal lights, the input and output pump lights, and the forward and backward GSE lights (F-GSE and B-GSE). Moreover, we consider the spontaneous emission light laterally emitted from the EDF for the numerical simulation. The light emitted from the LS was launched into the GSEC via a variable optical attenuator (VOA) and fiber coupler

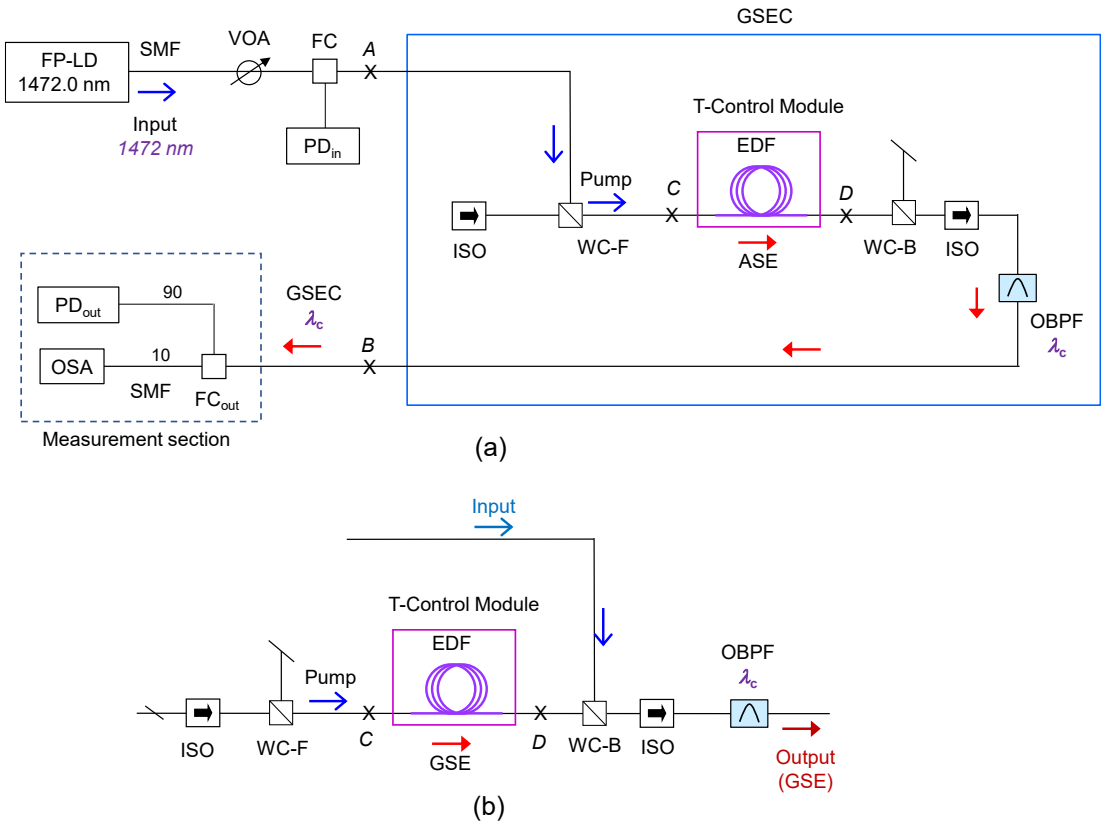

Figure 7.1. Schematics of experimental setup for (a) the forward pumping and (b) backward pumping. Referring [29].

(FC_{in}) on the input side of the GSEC. The input light power (P_{in} in dBm) is monitored using a photodiode module (PD_{in}), which is connected to the 10% branching port of FC_{in}. The GSEC circuit consists of an EDF as the gain medium and a wavelength-selective coupler for the input pump light (WC-F). Another coupler is set at the output point to remove the unwanted transmitted pump light (WC-B). The GSEC also comprises two optical isolators (ISOs) and a tunable optical bandpass filter (OBPF) with a center transmission wavelength of λ_c.

We tested two pumping directions in terms of the F-GSE propagation direction: forward and backward pumping directions. The input pump light was launched into the EDF via WC-F in the case of the forward pumping **(Figure 7.1 (a))**. On the other hand, the input pump light is backward launched into the EDF via WC-B. F-GSE emits from the EDF and passes the OBPF and is then detected by the optical spectrum analyzer (OSA) and a PD module (PD_{out})

via an FC (FC_{out}). PD_{in} and PD_{out} are commercial power meter sensor heads (Ando Electric Co. (AQ2735)). The EDF was a 15.9-m spool with a diameter of 9.5 cm and was implemented within a temperature control module (T-Control). The ambient temperature was finely maintained at 23.0 ℃ by a temperature controller during the experiment.

7.3 Modeling the GSEC for Numerical Simulation

We used several equations for the numerical simulation, which are a set of propagation equations for the lights propagating in the EDF, and a rate equation for the fractional populations of the laser energy state of $^4I_{15/2}$ and $^4I_{13/2}$ for the 1480-nm band pumping [1,2]. The propagation equations are given by the following equations for the pump and GSE lights (F-GSE and B-GSE), where the position in the EDF is denoted by *z*,

$$\frac{d}{z}P_k(z) = \pm\eta\rho\sigma_{abs}(\lambda_k)\{[(1+R(\lambda_k))(1-\beta)N_2(z)-1]P_k(z) + 2q_kR(\lambda_k)h\nu_k(\Delta\nu)_k(1-\beta)N_2(z)\}$$

$$q_k = 0(if\ k = s,\ p),\ 1(if\ k = n) \tag{8}$$

where P_p and P_n are the pump and GSE light power in the SI units of [W] or equivalently [mW]. Note that Eq. (7) includes signal light power for convenience, although there is no signal light propagation in the EDF of the GSEC in this study. η, ρ are the overlap factor between the optical mode and the doped region, and the erbium ion (Er^+) concentration, respectively. σ_{abs} (λ_k) and σ_{emi} (λ_k) are the absorption and emission cross-sections, respectively, and R is the ratio of the cross-sections: $R=\sigma_{emi}/\sigma_{abs}$. N_2 (*z)* is the fractional population of the upper state Er^{3+} ($^4I_{13/2}$), h is Planck's constant, λ and ν are the optical wavelength and frequency, respectively. Moreover, β the existing ratio of the heavily deexcited Er ions is caused by the inhomogeneous cooperative upconversion [1, 2].

Next, the local fractional population $N_2(z)$ is derived by solving the rate equation in the steady state as in the following,

$$N_2(z) = \frac{\eta^* \sum_k X_k}{1+\eta^* \sum_k X_k \left(1+R(\lambda_k)\right)}$$

$$k = s,\ p,\ n(\mathrm{ASE})$$

$$X_k \equiv \frac{P_k(z)}{P_{ch-k}}, \quad P_{ch-k} \equiv \frac{h\nu_k A_{21} \pi \omega^2}{\sigma_{abs}(\lambda_k)};$$

$$\eta^* \equiv \eta \left(\frac{\omega}{r_{Er}}\right)^2 \tag{9}$$

where X_k and η^* are the normalized optical power and normalized overlap factors, respectively. A_{21} and ω are the spontaneous emission rate and the mode intensity radius, respectively. $P_{\text{ch-}k}$ is the characteristic or saturation optical power.

7.4 Comparison Between Experimental and Theoretical Results

The spectra of the GSE output from the 15.9-m EDF in the forward pumping case are shown in Figure 7.2 (a) at several input pump powers, P_{in} from 3.4 to 6.4 dBm, with a step of 0.5 dB. P_{in} and P_{out} values are defined at the input and output points of the EDF, the points C and D in Figure 7.1 in this study. The optical losses between points A to C, and D to B were estimated to be 0.9 dB in both cases. Figure 7.2 (b) shows the power differences per 0.5 dB (ΔP) for the data of Figure 7.2 (a). From Figure 7.2 (b), we can find that (ΔP) has maximum values around 1532.5 nm. The effective transmission bandwidth of the OBPF was estimated to be 1.0 nm.

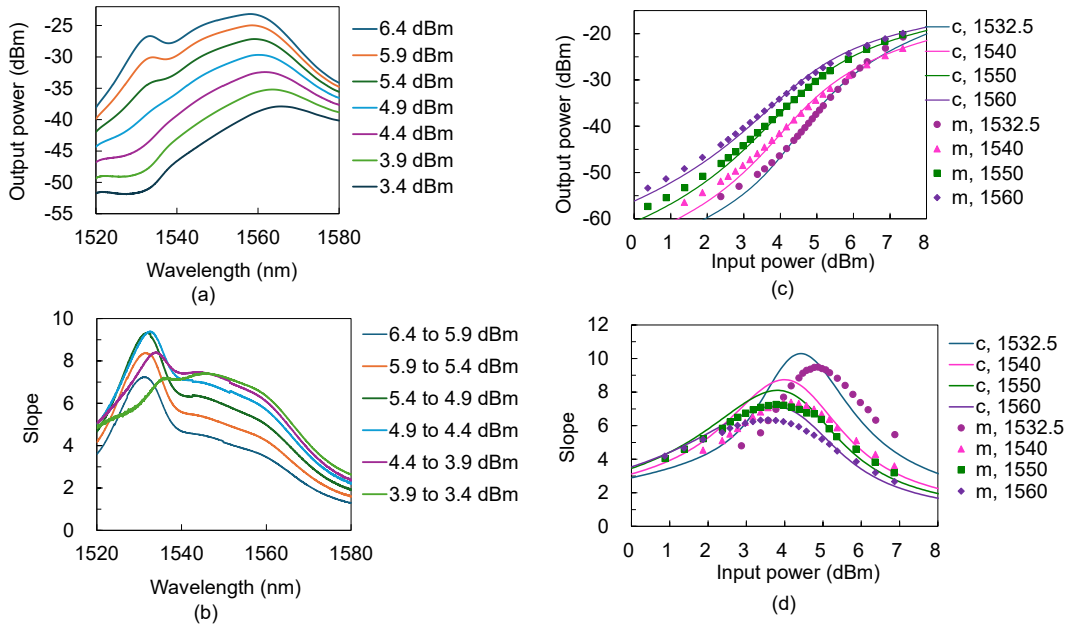

Figure 7.2. Input and output characteristics of the GSEC with 15.9-m EDF in the forward pumping configuration. (a) output power and (b) slope spectra, (c) input and output power characteristics, and (d) slope characteristics. Referring [29].

Figure 7.2 (c) shows the measured P_{out} as a function of P_{in} at the OBPF center wavelength λ_c of 1532.5, 1540, 1550, and 1560 nm. Moreover, **Figure 7.2 (d)** shows the slopes (S) of the input and output relations of **Figure 7.2 (c)**.

For the numerical simulation based on the equations of Eqs. (8) and (9), parameters needed for the simulation were derived from some measured characteristics for the 15.9-m EDF used in this study [16, 17]. The parameters are the peak loss at around 1530 nm (A_{peak} [dB]), mode field diameter (MFD), and Er-ion ratio β. The MFD is $2\sqrt{2}$ times the mode intensity radius w. Note that A_{peak} is proportional to the EDF length. The parameters derived are A_{peak} = 100 [dB], β = 0.015 (1.5%), and MFD = 3.5 mm. Moreover, the ratios of the output optical powers of B-ASE to F-GSE (R_{GSE}) were estimated to be 2.5 and 1/2.5 for the cases of the forward and backward pumping, respectively.

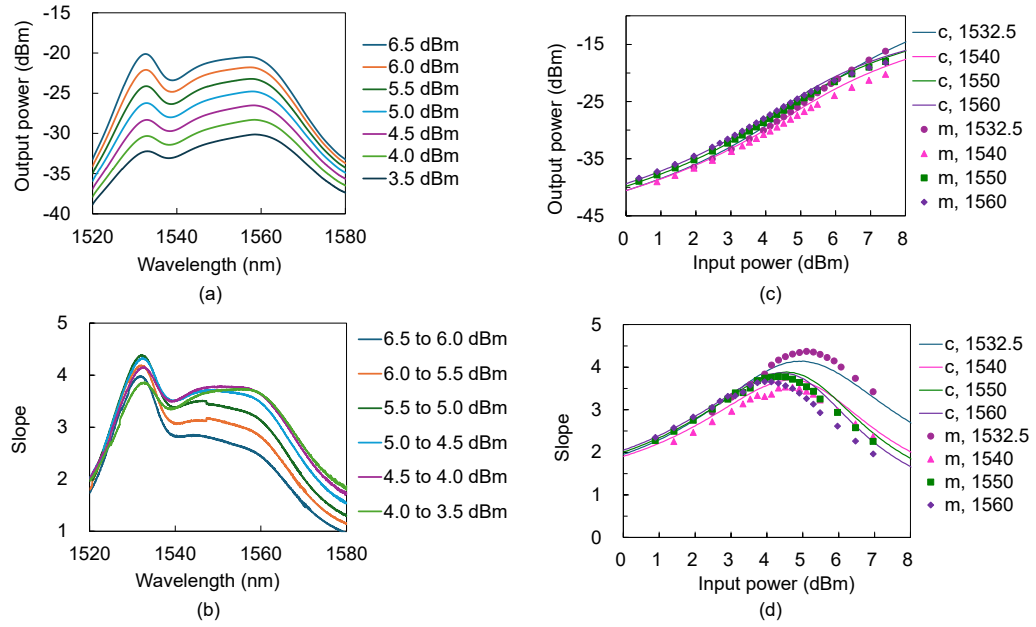

Figure 7.3. Input and output characteristics of the GSEC with 15.9-m EDF in the backward pumping configuration. (a) output power and (b) slope spectra, (c) input and output power characteristics, and (d) slope characteristics. Referring [29].

Calculated P_{out} and S as a function of P_{in} at λ_c of 1532.5, 1540, 1550, and 1560 nm are shown by solid lines in **Figure 7.2 (c)** and **(d)**, respectively. The measured and calculated P_{out} coincide well within the accuracies of the measurement and calculation, which are estimated to be approximately ±0.5 dB, except for the P_{out} region lower than approximately −50 dBm. From Fig. 2(d), we derived the maximum slope (S_{max}) at each λ_c. The sets of values (P_{in} [dBm], P_{out} [dBm], S_{max}) at λ_c of 1532.5, 1540, 1550, and 1560 nm were (4.87, −38.40, 9.5), (4.17, −40.11, 7.4), (3.78, −38.56, 7.3), and (3.57, -36.70, 6.3), respectively.

The measured and calculated values of P_{out} and S as a function of P_{in} for the backward pumping case are shown in **Figure 7.3**, as in the case of forward pumping. The measured and calculated P_{out} coincide well within the accuracies of the measurement and calculation, which are estimated to be approximately ±0.5 dB. From **Figure 7.3 (d)**, we derived the maximum S (S_{max}) at each λ_c. c 1550, and 1560 nm were (5.10, −25.14, 4.4), (4.51, −28.80, 3.5), (4.32, −27.26, 3.8), and (3.93, −27.99, 3.7), respectively. Therefore, S_{max} for the forward and

backward pumping cases are 9.5 and 4.4, respectively, at l_c of 1532.5 nm: the former is more than two times larger than the latter.

7.5 Numerical Simulation

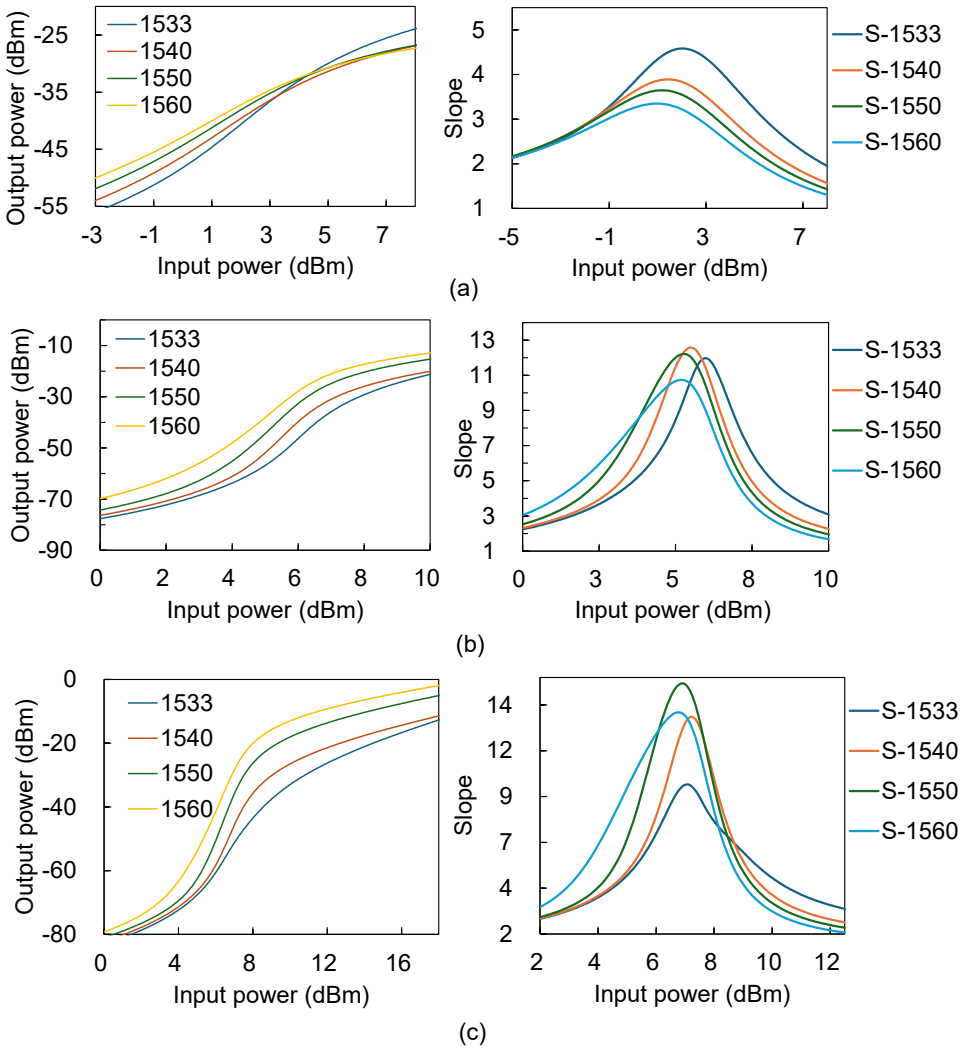

Figure 7.4. Calculated input and output characteristics at the peak loss of (a) 50, (b) 150, and (c) 200 dB for the forward pumping. Left and right-side figures show the output powers and slopes as a function of the input power, respectively. Referring [29].

As is described in the previous section 6.4, the numerical calculation is effective in evaluating the performance of the GSEC at other lengths of EDF or other values of A_{peak} in dB. Then, we calculated the input vs. output relation and the slope characteristics. **Figure 6.4** shows the numerical simulation results at A_{peak} of 50, 150, and 200 dB in addition to the case

100 dB of Fig. 2. It can be seen from **Figure 7.4 (a)**, **(b)**, and **(c)** that P_{out} decreases when A_{peak} increases from 100 dB at the operation conditions of S_{max}. On the other hand, the operation region of nonlinearity in P_{in} shifts to the right when A_{peak} increases. As for the case of the backward pumping configuration, **Figure 7.5** shows the numerical simulation results at A_{peak} of 50, 150, and 200 dB in addition of the case 100 dB of **Figure 7.3**.

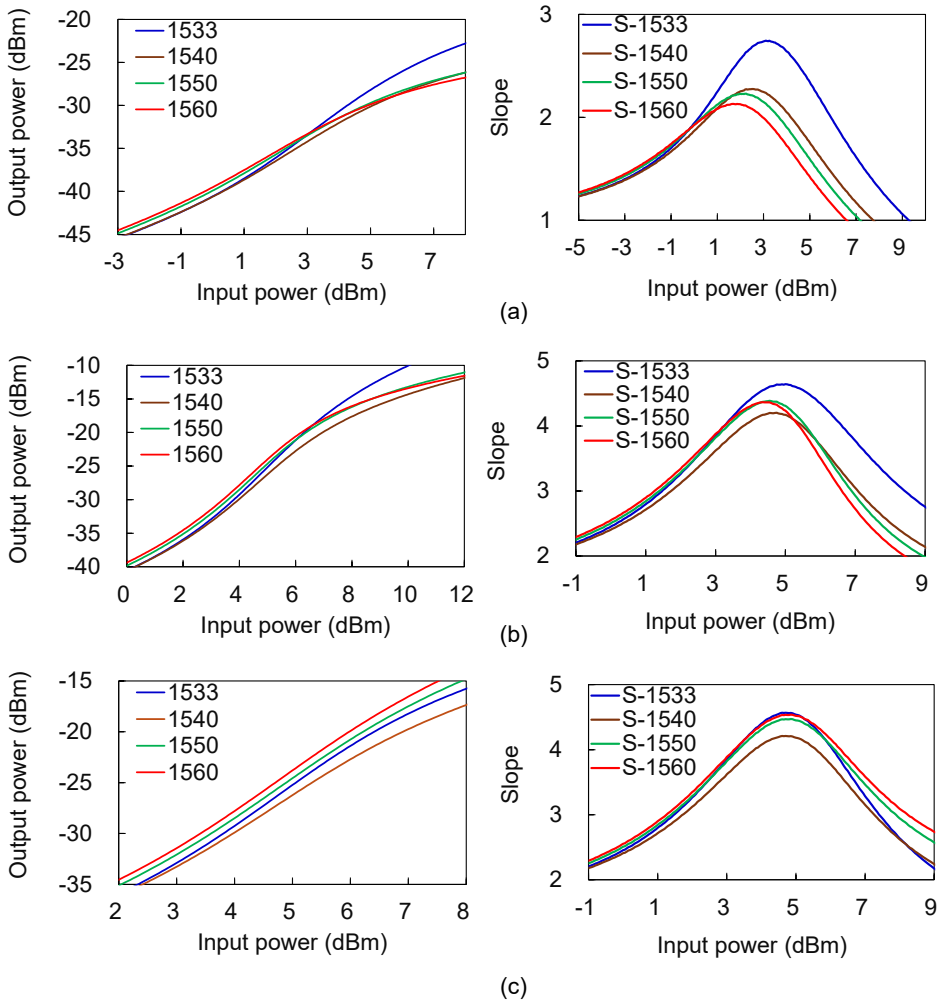

Figure 7.5. Calculated input and output characteristics at the peak loss of (a) 50, (b) 150, and (c) 200 dB for the backward pumping. Left and right-side figures show the output powers and slopes as a function of the input power, respectively. Referring [29].

It can be seen from **Figure 7.5 (a), (b)**, and **(c)** that P_{out} changes little when A_{peak} increases from 100 dB at the operation conditions of S_{max}. On the other hand, the operation region of nonlinearity in P_{in} shifts to the right when A_{peak} increases. **Figure 7.6 (a)** and **(b)** show S_{max}

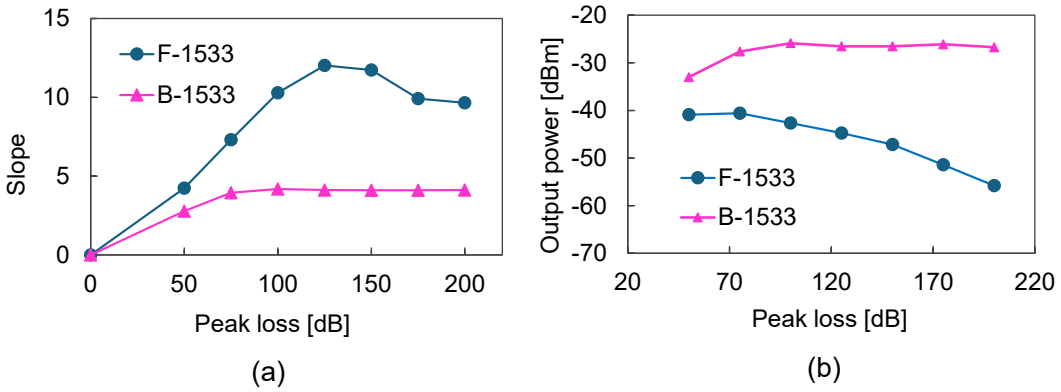

Figure 7.6 (a) The maximum slopes and (b) output powers as a function of the peak loss. Referring [29].

and the P_{out} at S_{max} ($P_{out\text{-}max}$) as a function of A_{peak}, respectively, for the forward and backward pumping configurations.

7.6 Conclusion of the Study

We proposed a technique that places a novel optical circuit called a guided spontaneous-emission circuit (GSEC) that can significantly improve the OPR in optical measurement systems. Experimental results were successfully compared with the numerical simulation results. We also clarified that the improvement factors in the OPR, the slope in the input and output optical power relation of the GSEC, are much higher for the forward pumping case than the backward pumping case. The maximum slopes of the forward pumping were larger by two times or more than those of the backward pumping in the peal loss region larger than or equal to 100 dB.

8 Application of Multicore-Fiber Sensing in Amplified Spontaneous Emission Feedback Circuit

8.1 Introduction

Optical fiber sensing techniques using multicore fibers have attracted considerable interest in the case of multicore-fiber communication technologies [4,5,6,7,8,9,10,11]. We reported some research results on a novel fiber-optic sensing technique using an ASEFC, called the "ASEFC technique," which can significantly improve the OPR in optical power measurement/sensing [20,23]. In this paper, we report experimental investigations on the parameter dependence of the OPR characteristics of the ASEFC technique.

8.2 Multicore-Fiber Sensing System

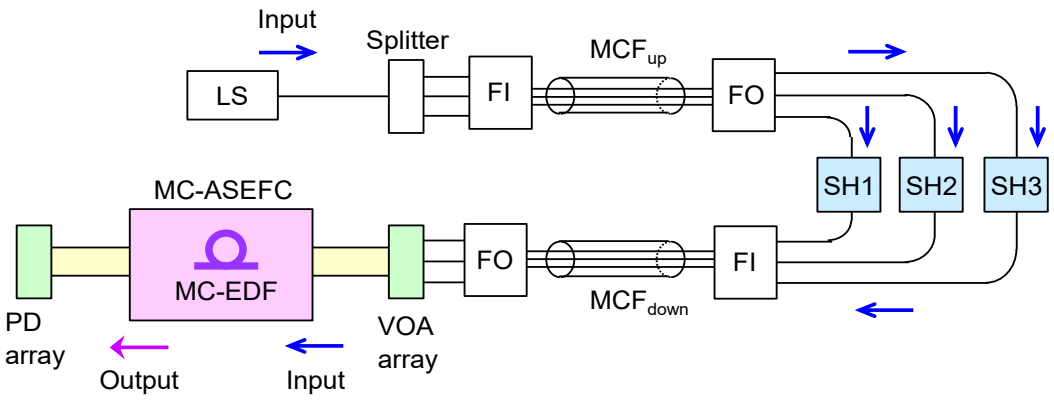

Figure 8.1. System Configuration. Referring [25].

Figure 8.1 shows the system configuration of the proposed ASEFC technique for multi-point sensing applications. The system consists of a multicore-fiber module (MCFM) based ASEFC at the detection section (MC-ASEFC), which has a multicore EDF (MC-EDF) and an MCFM-based feedback loop [39]. The system also consists of a light source (LS), sensing heads (SH*i*), multicore transmission fibers (MCF), fan-in (FI), fan-out (FO), variable attenuator (VOA) array, and a photodiode (PD) array. The case of three fiber cores is depicted for simplicity. The input light emitted from LS is split by a splitter and introduced into SH*i*

and then launched into MC-ASEFC for optical-loss sensing with high OPRs. The output lights from MC-ASEFC are launched into the photodiode (PD) array.

8.3 Experimental Setup

The setup was constructed using single-mode fiber-based components instead of multicore fiber-based components for simplicity, as shown in **Figure 8.2**. The input light for the ASEFC has a center wavelength of 1472.0 nm and operates as a pump light of an erbium-doped fiber (EDF) set in the ASEFC. The ASEFC consists of the EDF as a gain medium and a feedback fiber loop. The laser feedback loop comprises an optical bandpass filter (OBPF), a VOA (VOA_{Loop}), and optical isolators (ISO).

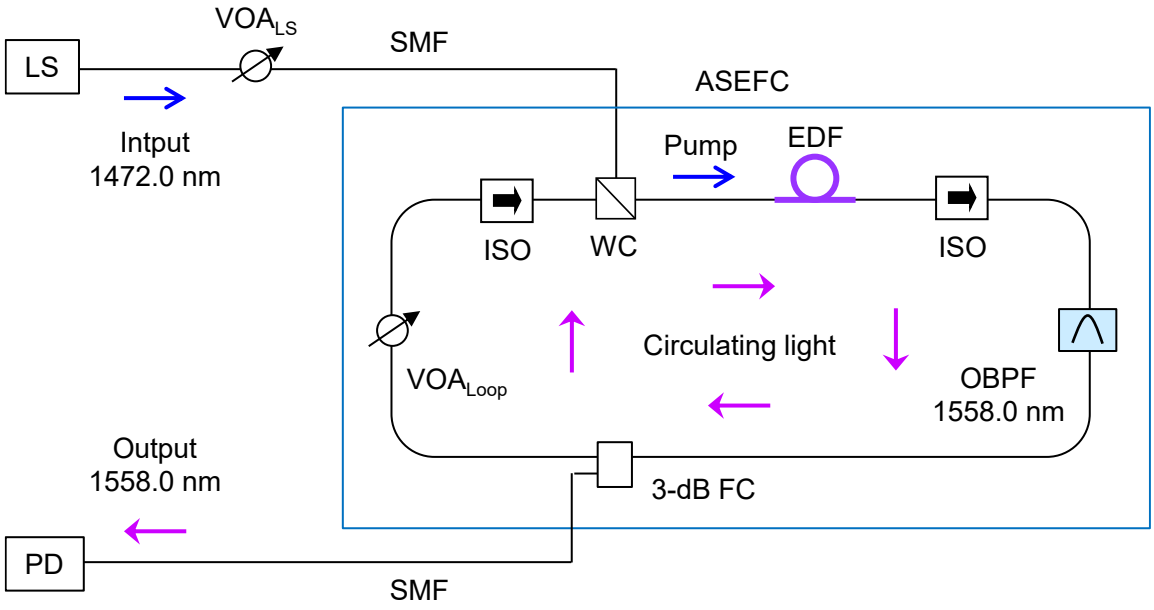

Figure 8.2. Experimental Configuration. Referring [25].

The temperature of the EDF was kept constant at 23.0 ℃ [23]. The ASEFC operates near the lasing threshold of the loop. We found that the relation between the input and light powers (P_{in} and P_{out}) was able to be changed by adjusting the loss of VOA_{Loop} (L_{VOA}). The center wavelengths of the OBPF and the output light were both 1558.0 nm. P_{out} was measured by a PD set downward of the ASEFC. P_{in} was simultaneously measured by another PD, which is not shown in **Figure 8.2**, for simplicity.

Figure 8.3(a) shows P_{in} as a function of P_{out} in dBm at L_{VOA} of 5, 6, 7, 8, and 9 dB. We can see some nonlinear relations between P_{in} and P_{out} in **Figure 8.3(a)** [20,23]. We defined a factor called "slope S" for the nonlinear relation: $S \equiv dP_{out}/dP_{in}$, which is an improvement factor (IF) thanks to using the ASEFC technique. We can calculate P_{in} from the measured value of P_{out} using a fitting function between P_{out} and P_{in} [20,23]. **Figure 8.3 (b)** shows S as a function of P_{out}. From **Figure 8.3 (b)**, the maximum values of S (S_{max}) decrease with L_{VOA} from 137 to 75 at L_{VOA} of 5 and 9 dB, respectively. These results mean the IF can be set at ~100, and the OPR can be significantly improved [3, 4]. On the other hand, P_{out} at the operating condition of S_{max} increases from −24.4 to −21.7 dBm, and P_{in} increases from 6.1 to 6.8 dBm, at L_{VOA} of 5 and 9 dB, respectively.

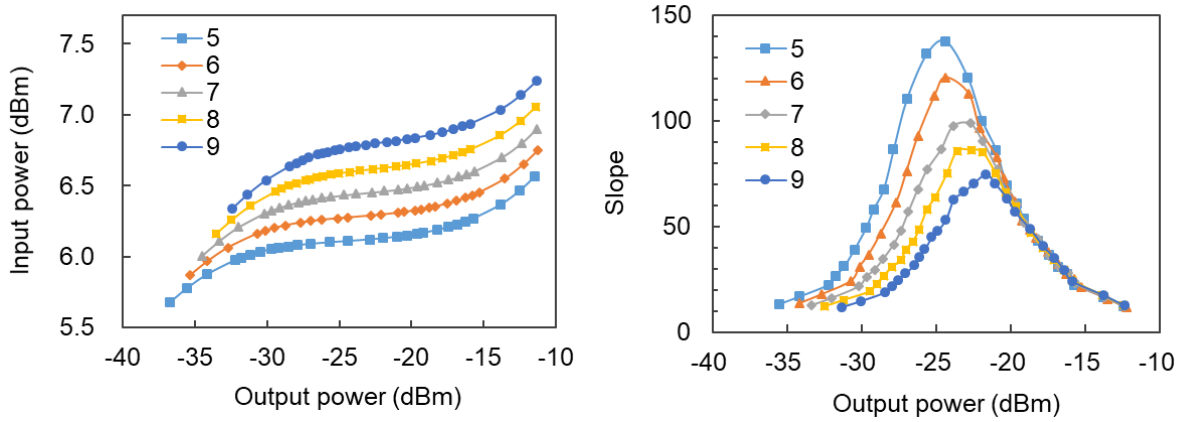

Figure 8.3. (a) The input power and (b) the slope as a function of the output power. Referring [25].

8.4 Conclusion of the Study

We investigated the loop-loss dependence of the IF characteristics of the ASEFC. The output-input relation and the IF S were successfully changed from 75 to 137 by adjusting the loop loss of the feedback loop of the ASEFC from 9 to 5 dB, respectively.

9 Summary

Optical fiber sensing (OFS) has attracted attention for various applications, such as industrial, environmental, long-distance, and wide-area sensing. An optical power meter (PM) is considered an important parameter that directly affects the accuracy of the OFS measurement system**.** This study focuses on advanced optical circuit techniques to improve optical power resolution (OPR) in optical power measurement systems. The conventional method of saturation gain and nonlinear distortion reduces the accuracy and stability of an optical power measurement. In this study, to overcome the limitation, we proposed a nonlinear EDF-based optical circuit technique that is identical throughout this study, initially known as the amplified-spontaneous-emission non-linear circuit (ASENLC) and subsequently referred to as the guided spontaneous emission circuit (GSEC). In this study, these terms (ASENLC and GSEC) are used to denote the same circuit, respectively.

We observed the OPR enhancement factors of dual stages, with the maximum slope (Smax) values of 22.8 for the forward pumping case of wavelength at 1532.5 nm. The slope maximum value (S_{max}) is 2.4 times larger than that in the case of the single-stage GSEC with 15.9 m EDF.

Through comprehensive experimental investigations and numerical simulations, to evaluate the performance of a guided spontaneous-emission circuit (GSEC) to significantly improve the optical power resolution (OPR). The Experimental investigation suitably agrees with numerical simulation results, and the maximum slopes, for forward and backward pumping, are 9.5 and 4.4, respectively, at an output wavelength of 1533 nm according to the experimental results. In addition, a numerical simulation of the mode field diameter (MFD) dependence reveals that the maximum slope increases with increasing MFD, and the largest maximum slope is 12.6 at the wavelength of 1533 nm. Finally, we proposed an optical power variation measurement technique called the guided spontaneous-emission circuit (GSEC) to

enhance the optical power resolution. We experimentally demonstrate the characteristics of both single-stage (SS-GSEC) and two-stage (TS-GSEC) configurations. The maximum slopes for the SS-GSEC are approximately 11.9 was achieved using the 20.4-m EDF. On the other hand, for the TS-GSEC, the maximum slope was achieved using the TS-4, approximately 30.6, which consisted of two EDFs with total length (15.9 m for EDF-1 and 20.4 m for EDF-2). The proposed two-stage GSEC configuration can significantly improve the OPR.

In general, the present research work has significantly improved the OPR compared with that of a conventional PM. The motivation and methodological details were presented comprehensively and systematically. This research offers new practical knowledge and relevant technology. The results may aid in the development of future technologies, as well as the potential for various applications, including industrial, environmental, long-distance, and wide-area sensing.

The future tasks for our research group are listed in the following

1. It requires developing the three-stage GSEC and experimentally and numerically investigating to enhance the optical power resolution.
2. Increase the EDF length ratio (L_1, L_2, L_3) and investigation difference between previous EDF length.
3. Using another type of optical filter, excluding OBPF and SWPF.
4. It will need to investigate the input and output power levels to improve the dynamic range characteristics for wider operational conditions.
5. Theoretically and experimentally investigate the L-band operation for system optimization.
6. Investigate the temperature sensing characteristics in variable temperature environments and extend the stability test.

Reference

[1] H. Masuda: "Local fractional population measurement of the upper state 4I13/2 of an erbium-doped fiber amplifier," *J. Lightw. Technol.*, vol. 10, pp. 1540–1543, Nov. 1992. DOI: 10.1109/50.184891.

[2] H. Masuda, A. Takada, and K. Aida: "Modeling the gain degradation of high concentration erbium-doped fiber amplifiers by introducing inhomogeneous cooperative up-conversion," *J. Lightw. Technol.*, vol. 10, pp. 1789–1799, Dec. 1992. DOI: 10.1109/50.202830.

[3] H. Masuda, et al.: "1.65 μm band fibre Raman amplifier pumped by wavelength-tunable amplified spontaneous emission light source," *Electron. Lett.* 34 (1998) 2339. DOI: 10.1049/el:19981543.

[4] A. D. Kersey: "A review of recent developments in fiber optic sensor technology," *Optical Fiber Technol.* 2 (1996) 291. DOI: 10.1006/ofte.1996.0036.

[5] A. C. Garcia and J. E. A. Cuenca: in *Handbook of Optical Fiber Sensing Technology* (John Wiley & Sons, Inc., New Jersey, 2002), ed. J. M. Lopez-Higuera, p. 209.

[6] B. Culshaw and A. Kersey: "Fiber-optic sensing: a historical perspective," *J. Lightw. Technol.* 26 (2008) 1064. DOI: 10.1109/JLT.0082.921915.

[7] K. Nakazawa, et al.: "Technologies for checking outside optical distribution equipment," *NTT Technical Review* 7 (2009) 1. [Online]. Available: https://www.ntt-review.jp/archive/ntttechnical.php?contents=ntr200911le2.html

[8] X. G. Huang, et al.: "A quasi-distributed fiber-optic temperature sensor with a resolution of 0.07 °C based on Fresnel reflection," *J. Lightw. Technol.* 27 (2009) 2583. DOI: 10.1109/JLT.2009.2012411.

[9] J.-R. Zhao, et al.: "High-resolution and temperature-insensitive fiber optic refractive index sensor based on Fresnel reflection modulated by Fabry–Perot interference," *J. Lightw. Technol.* 28 (2010) 2799. DOI: 10.1109/JLT.2010.2065215.

[10] Z. Yin, et al.: "Fiber ring laser sensor for temperature measurement," *J. Lightw. Technol.* 28 (2010) 3403. DOI: 10.1109/JLT.2010.2086046.

[11] G. Liu, et al.: "High-resolution and fast-response fiber-optic temperature sensor using silicon Fabry-Pérot cavity," *Opt. Express* 23 (2015) 7237. DOI: 10.1364/OE.23.007237.

[12] Y. Mizuno, et al.: "Pilot demonstration of refractive index sensing using polymer optical fiber crushed with slotted screwdriver," *IEICE Electron. Express* 14 (2017) 20170962. DOI: 10.1587/elex.14.20170962.

[13] H. Masuda and K. Kitamura: "Highly sensitive optical sensing scheme using erbium-doped fiber ring circuit," *The 7th Asia-Pacific Optical Sensors Conf.* (2018) Wed-6.

[14] K. Kitamura and H. Masuda: "Nonlinear characteristics of a fiber ring circuit with a semiconductor optical amplifier for sensing applications," *The 23rd OECC* (2018) 3C1-3. DOI: 10.1109/OECC.2018.8730129.

[15] H. Masuda, et al.: "Optically amplified feedback circuit with high improvements in optical power resolution," *The 24th OECC* (2019) MC2-5. DOI: 10.23919/PS.2019.8817895.

[16] J. Shi, et al.: "High-resolution temperature sensor based on intracavity sensing of fiber ring laser," *J. Lightw. Technol.* 38 (2020) 2010. DOI: 10.1109/JLT.2019.2954117.

[17] H. Masuda and K. Kitamura: *Japan Patent* 6660977 (2020).

[18] H. Masuda and B. Biswas: "Highly sensitive and stable temperature sensing method using amplified-spontaneous-emission feedback circuit," *26th Microoptics Conf.* (2021) MC2-5. DOI: 10.23919/MOC52031.2021.9598083.

[19] S. Donati: *Photodetectors – Devices, Circuits and Applications* – (John Wiley & Sons, Inc., New Jersey, 2021) 2nd ed., pp. 103–173.

[20] H. Masuda, et al.: "Amplified-spontaneous-emission feedback circuit scheme for optical measurement with improved optical power resolutions," *IEICE Comm. Express* 11 (2022) 46. DOI: 10.1587/comex.2021XBL0189.

[21] H. Masuda, et al.: "Fiber-optic temperature sensing with high resolution and stability by detecting amplified spontaneous emission," *OECC* (2022) TuP-C-1. DOI: 10.23919/OECC/PSC53152.2022.9850201.

[22] K. Fukushima, et al.: "EDF laser displacement sensor based on bending characteristics of polarization-independent double-pass cascaded-chirped long-period fiber grating," *IEICE Electron. Express* 20 (2023) 20220496. DOI: 10.1587/elex.19.20220496.

[23] B. Biswas, et al.: "High-resolution and stable optical power measurement using a temperature-controlled amplified-spontaneous-emission feedback circuit," *IEICE Comm. Express* 12 (2023) 230. DOI: 10.1587/comex.2023XBL0014.

[24] B. Biswas, et al.: "Amplified-spontaneous-emission feedback circuit with wide operating bandwidth and dynamic range," *IEICE Electron. Express* 20 (2023) 20230229. DOI: 10.1587/elex.20.20230229.

[25] M. G. B. Abrar, B. Biswas, T. Tanaka, R. Harada, K. Kitamura, and H. Masuda: "Amplified-spontaneous-emission feedback circuit technique with high optical power resolutions for multicore-fiber sensing," International Symposium EXAT 2023, P-27, p. 60, May 2023.

[26] K. Kitamura, M. G. B. Abrar, K. Tanaka, R. Harada, and H. Masuda: "Proposal of an optical input and output nonlinear circuit technique and investigation of the characteristics of improvements in the optical power resolution," *IEICE Tech. Rep.*, vol. 123, no. OFT2023-45, pp. 115–118, Oct. 2023.

[27] H. Masuda, K. Kitamura, M. G. B. Abrar, K. Tanaka, and R. Harada: "Design of a guided spontaneous-emission type of the optical input-output nonlinear circuit," *IEICE Tech. Rep.*, vol. 123, no. OFT2023-50, pp. 13–18, Nov. 2023.

[28] K. Tanaka, R. Harada, M. G. B. Abrar, K. Kitamura, and H. Masuda: "Proposal and simulation characteristics of an amplified-spontaneous-emission nonlinear circuit technique for high-resolution optical power measurement," *HISS 2023*, TP-A-7, pp. 27–30, Nov. 2023.

[29] M. G. B. Abrar, K. Tanaka, R. Harada, K. Kitamura, and H. Masuda: "Pumping direction dependence of the performance of amplified-spontaneous-emission nonlinear circuits," *HISS 2023*, TP-B-8, pp. 184–187, Nov. 2023.

[30] K. Kitamura, et al.: "Amplified-spontaneous-emission nonlinear circuit technique with improved optical power resolution," *ICETC* (2023) O1-4. DOI: 10.34385/proc.79.O1-4.

[31] Md Golam Barkatul Abrar, Kokoro Kitamura, Hiroji Masuda: "Performance Evaluation Based on Numerical Simulation of Novel Guided Spontaneous Emission Circuit for Improved Optical Power Resolution," *ICCT-Pacific* (30 May 2025). DOI: 10.1109/ICCT-Pacific63901.2025.11012822.

[32] R. Harada, et al.: "Optical power resolution improvements in optical input-output nonlinear circuits," *ICCT-Pacific* (2025) (accepted).

[33] Kokoro Kitamura, Md Golam Barkatul Abrar, Kunihiro Tanaka, Ryuga Harada, Hiroji Masuda: "Guided spontaneous emission circuit technique with improved optical power resolutions for optical power variation measurement," *IEICE Electron. Express* 22 (2025) 20250155. DOI: 10.1587/elex.22.20250155.

[34] B. E. A. Saleh and M. C. Teich: *Fundamentals of Photonics* (John Wiley & Sons, New Jersey, 2019) 3rd ed., Chaps. 19 and 25.

[35] S. Donati: *Photodetectors – Devices, Circuits and Applications –* (John Wiley & Sons, Inc., New Jersey, 2021) 2nd ed., Chaps. 6 and 10.

[36] https://www.keysight.com/jp/ja/assets/7018-01006/data-sheets/5988-1569.pdf

[37] https://www.graytechnos.com/60017987/wp-content/uploads/2022/12/manual_211B_212B_213B_20221219.pdf

[38] https://www.hamamatsu.com/content/dam/hamamatsu-photonics/sites/documents/99_SALES_LIBRARY/ssd/g8370-81_etc_kird1064e.pdf

[39] M. Nakazawa et al., ed., "Space-division multiplexing in optical communication systems," Springer (2023).